THIRD INTERNATIONAL SUMMER STUDENT SCHOOL

NUCLEAR PHYSICS METHODS AND ACCELERATORS IN BIOLOGY AND MEDICINE

Joint Institute for Nuclear Research
University Centre

NUCLEAR PHYSICS METHODS AND ACCELERATORS IN BIOLOGY AND MEDICINE

Third International Summer Student School

Dubna (Ratmino), June 30 – July 11, 2005

Proceedings

Dubna 2005

УДК 539.1.04(063)
ББК 28.071.25я431 + 22.381.1я431
N91

Topics

- Nuclear Medicine
- Radiation Physics in Medicine
- Fundamentals of Ionizing Radiation Dosimetry and Radiobiology
- Accelerator Complexes in Medicine
- Electron, Photon, and Hadron Radiotherapy
- Modern Imaging Technologies for Medicine
- Ionizing Radiation in Medicine and Other Applied Fields

The contributions are reproduced directly
from the originals presented by the Organizing Committee.

Nuclear Physics Methods and Accelerators in Biology and Medicine: Proc. of the Third Intern. Summer
N91 Student School (Dubna, June 30 – July 11, 2005). — Dubna: JINR, 2005. — 173 p.

ISBN 5-9530-0101-0

The collection includes the lecture abstracts and the students' reports presented at the Third International Summer Student School «Nuclear Physics Methods and Accelerators in Biology and Medicine» held in Dubna (Ratmino), Moscow Region, Russia, June 30 – July 11, 2005.

Ядерно-физические методы и ускорители в биологии и медицине: Труды Третьей Международной летней студенческой школы (Дубна, 30 июня–11 июля 2005 г.). — Дубна: ОИЯИ, 2005. — 173 с.

ISBN 5-9530-0101-0

В сборник включены аннотации лекций и студенческие доклады, представленные на Третьей Международной летней студенческой школе «Ядерно-физические методы и ускорители в биологии и медицине», проходившей с 30 июня по 11 июля 2005 г. в Дубне (Ратмино).

УДК 539.1.04(063)
ББК 28.071.25я431 + 22.381.1я431

ISBN 5-9530-0101-0

Contents

Introduction

Acad. V.G. Kadyshevsky noted in his School opening speech that in recent time medicine attaches increasingly great importance to the use of achievements of physics, especially nuclear physics. The wide medical use of ionizing and non-ionizing radiation, radionuclides, gamma sources, electron and proton accelerators, and computer tomographs has turned medical physics into a strategic weapon of medicine.

Prof. W.Nawrocik, Chairman of the JINR Programme Advisory Committee on Condensed Matter Physics, a permanent member of the School's Organizing Committee, and Chair of the Organizing Committee of the Second School (Poznan, Poland), welcomed the participants of the School. The School's traditional organizers are the JINR University Centre, Adam Mickiewicz University (Poznan, Poland), the Czech Technical University in Prague, and Moscow State University (MSU). The School's students came from Belarus, Bulgaria, the Czech Republic, Poland, Romania, Russia (MSU, MEPI, and Novosibirsk Institute of Nuclear Physics), Slovakia, and the JINR University Centre. The first two schools were held in 2001 and 2003; they were highly appraised by students and postgraduates; so there was an influx of applications for attending the Third School. The most numerous delegations came from Poland, the Czech Republic, and MSU. New to the School were its participants from Bulgaria and Slovakia. The audience numbered 75 in all; there were 21 lecturers.

The experience of the previous Schools and active work of the Organizing Committee members (first of all, Prof. G. Beyer) resulted in the notably well-balanced programme of the Third School. And, of course, the lecture cycle of the School was successful to the most extent thanks to highly skilled specialists of different countries.

For the School participants' further work at their home institutions, most of the lectures, with the lecturers' kind permission, have been put up at the School's Internet site, http://uc.jinr.ru/3SummerSchool/lecture.html .

Following the School tradition, students presented their research at the Student Sessions. This School had the greatest number of student reports. At the first School (2001), 12 reports were made; at the second (2003), 31; this time, the School audience members made 42 reports within the School subjects. By tradition, the best reports were selected by the audience themselves. The student reports will be published in the Proceedings of the School.

In the School participants' opinion, its programme was elaborated quite good. They found most of the lectures absorbing and useful. In their own words, they got a more

generalized idea of the world and began to understand what, and for whom, is being done in this area of knowledge. To the organizers of the School, its most important result is its participants' intention to attend further schools and, which is yet more important, to come to JINR for practice and performing their diploma and dissertation theses.

In conclusion, the School organizers express their deep gratitude to the Plenipotentiaries of Belarus, Bulgaria, the Czech Republic, Poland, Romania, and Slovakia at JINR, who allotted special grants for the organization of the School. The School was also supported by a grant from the Russian Foundation for Basic Research.

S.P. Ivanova
T.A. Strizh

Device for the Proton Beam Energy Control for Radiotherapy

A.V. Agapov

Dzhelepov Laboratory of Nuclear Problems, JINR

In our days protons take a special place in radiotherapy.

The proton beams have radical advantages of dose distributions in comparison with conventional kinds of radiation, such as electron beams and photons. Dose distribution of protons allows one to reduce radiation dose to healthy tissues and to deliver higher dose to a tumor.

Unlike the electron-photon radiation, proton beams undergo significantly weaker scattering as they penetrate in tissues. They have well defined range, linear energy transfers (LET) of these particles increase with the penetration depth forming the so-called "Bragg peak" at the end of the range.

But the Bragg peak of monoenergetic is very narrow for irradiation of large targets. To increase the width of the maximum dose region, a nonmonochromatic beam with a specially selected spectrum is used, which is equivalent to superposition of several Bragg curves of different ranges. It can be made with a help of an energy degrader of variable thickness (DVT) installed on a proton beam up-stream the patient (Fig.1).

Two Plexiglas wedges are the most important components of DVT. Big wedge can move across the proton beam axis with the stepper motor and the worm-gear. The total thickness of material will vary and change the mean energy of the proton beam during the treatment procedure. A computerized system automatically adjusts the thickness of material (and the beam energy) such a way that the Bragg peak always coincides with the tumour for any beam direction of irradiation.

To measure the current position the wedge two sensors are used.

Construction of DVT is the first step in creation of a compact system for proton beam dynamic irradiation. The dynamic irradiation is conformal irradiation of the targets with the hardware-software complex including the device for proton beam energy degrader (DVT), computer control multileaf collimator (MLC) and the specialized software. During irradiation DVT changes energy of the proton beam step-by-step, at the same time MLC changes aperture according to the calculation treatment plan. This method is similar to the beam

scanning technique, but does not use a pencil beam and scanning magnets. Tumor received dose layer-by-layer.

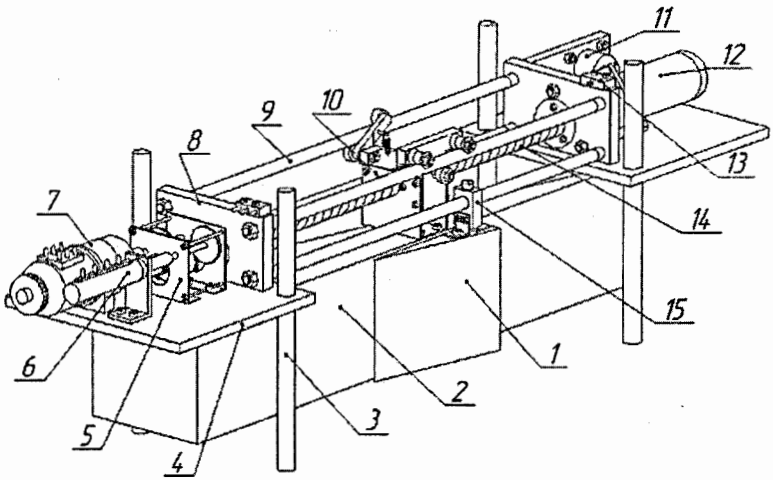

Fig.1. Energy degrader of variable thickness (DVT): 1-small wedge; 2-big wedge; 3-rack; 4-platform; 5-reducer; 6-first sensor (linear potentiometer); 7-second sensor (phase changer); 8- cheek; 9- director; 10-carriage; 11-sockets; 12-stepper motor; 13-microswitch; 14- worm-gear; 15-clamp of a small wedge

To see the influence of DVT to the proton beam characteristics some measurement were performed. Depth-dose distributions and horizontal profiles of the beam behind the DVT were measurement with miniature semiconductor detector for different values of DVT thicknesses: 0 mm waters (the device is removed from a working zone); 35 mm waters; 70 mm waters and 105 mm waters. The results are presented in Fig.2. As one can see both parameters are almost independent of DVT thicknesses.

DVT has been constructed and put into operation in the Medical-Technical Facility for hadron radiotherapy based on Joint Institute of Nuclear Reaction phasotron (Dubna, Russia). The constructed device use for the proton beam energy control and measurement of depth-dose curve in a treatment room and in the further it will be used in a technique of a dynamic irradiation.

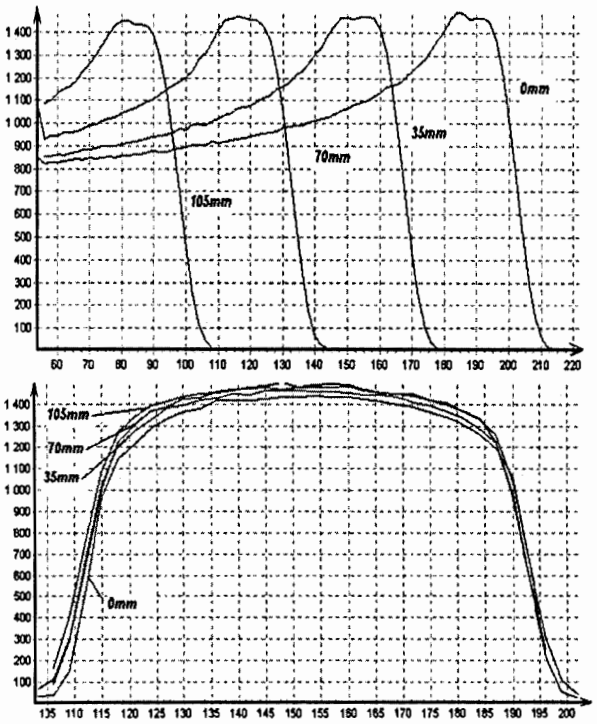

Fig.2. Proton beam depth-dose curves (on the left) and lateral penumbra (on the right). (AxisX-depth in water; AxisY- relative dose)

Tritium: Sources, Levels of Pollution

Julia Aleksiayenak

International Enviromental Sacharov University

Minsk, Republic of Belarus

e-mail: beataa@gmail.com

Tritium is a radioactive element. The radioactive decay product of tritium is a low energy beta that cannot penetrate the outer dead layer of human skin. Therefore, the main hazard associated with tritium is internal exposure. In addition, due to the relatively long half life and short biological half life, tritium must be ingested in large amounts to pose a significant health risk. In keeping with the philosophy of ALARA, internal exposure should be kept as low as practical.

The main tritium sources are:

- Cosmic rays
- Nuclear testing
- Reactors
- Fuel reprocessing plants

Tritium, as a form of Hydrogen, is found naturally in air and water. In nature, it is produced by cosmic rays in two source terms:

$$^{14}N + {}^{1}n \rightarrow {}^{3}H + {}^{12}C$$

and

$$^{2}H + {}^{2}H \rightarrow {}^{3}H + {}^{1}H$$

Cosmic rays interact with nitrogen (^{14}N) or with deuterium (^{2}H) and form tritium and carbon (^{12}C). These are primarily interactions that happen in the upper atmosphere and the tritium falls to earth as rain. The unit curie is a measure of an amount of radioactivity. A curie (Ci) is the amount of a radioactive substance that has 3.7×10^{10} decays per second. The world wide production of tritium from natural sources is 4×10^{6} curies per year with a steady state inventory of about 70×10^{6} curies. Human-made tritium is generated by bombarding hydrogen with neutrons in a nuclear reactor or an accelerator

Tritium distribution in theenvironment

- Stratosphere 6.8%
- Troposphere 0.4%
- Biosphere 27.8%
- Ocean 65%

All atoms are composed of a center nucleus surrounded by shells of electrons. The tritium atom (^3H) is unstable because it has two extra neutrons in its nucleus. These neutrons give tritium an excess amount of energy. Because of this, the atom will undergo a nuclear transformation or radioactive decay. In this, the atom emits two radiations: a beta particle (β^-), which is similar to an electron, and an anti-neutrino.

$$^3H \rightarrow {}^3He + \beta^- + \text{anti-neutrino}$$

This reduces the energy in the nucleus and the atom, now a helium atom (^3He), is left more stable. The anti-neutrino is of no biological significance because it does not interact with matter.

The beta is non-penetrating with a maximum energy of 18.6 keV and an average of 5.7 keV. This is a low energy beta compared to most radioactive beta emitters and it can be easily shielded. The outer layer of dead skin is enough to stop all of the beta external of the body. Only if tritium is taken into the body can it produce a significant dose.

Tritium has a single electron the same as the more abundant forms of hydrogen. This causes tritium to react chemically to form compounds in the same manner as hydrogen. The two primary forms that personnel will likely to be exposed to are HT (which is similar to hydrogen gas) or HTO (tritiated or heavy water). Of these two forms, the HTO is the only form that is a significant exposure hazard. HT gas is inhaled and exhaled with only of 0.005% of the activity being deposited in the lungs. The uptake of HTO vapor is near 100% for inhalation and ingestion. Tritium can also enter the body by absorption through the skin or open wounds. Skin contact should always be minimized to prevent absorption. Tritium will also be absorbed into materials such as gloves, clothing and metal. If not properly controlled, these contaminated materials can present an additional exposure source by releasing tritium when in contact with skin.

HTO is in the form of water, so one to two hours after an uptake, it will be evenly distributed through out the body's fluids. The amount of time it takes for half of the activity to be physically removed form the body is the biological half life. The biological half life of tritium varies significantly because of variations in bodily excretion rates, temperature dependence and fluid intake. Biological half-life of tritium is about 9.4 days, often rounded to 10 days. This can be shortened to 2-3 days (Fig 1) with ten fold increase of liquid intake (2 liters to 20 liters), or in serve cases to 4-8 hours by using dialysis machines.

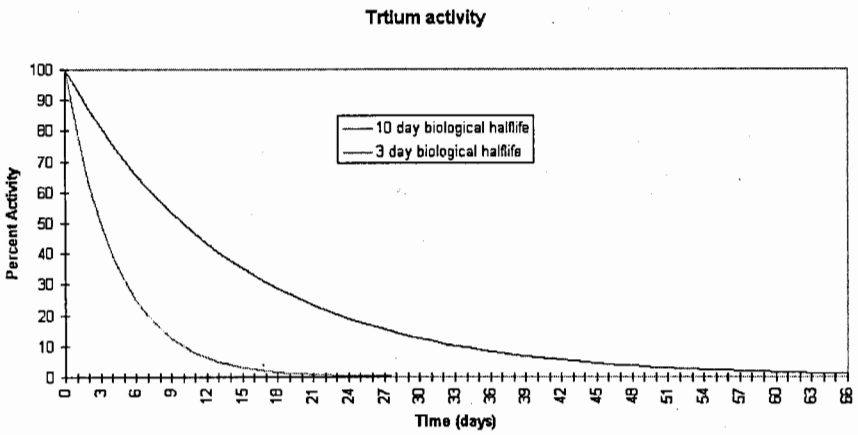

Fig. 1. The percent of tritium left in a human based on removal half-life of 10 day (average for humans) and 3 days (based on increased water intake)

Methods of reduction of tritium in the body must be weighed against the potential harm that the tritium will cause. Any treatment should be based on known levels of uptake and made in consultation with medical personnel.

№	City	Country	C [T], Bq/l
1	Minsk	Belarus	41
2	Minsk	Belarus	46.6
3	Minsk	Belarus	40.2
4	Kiev	Ukraine	39.3
5	Obuhov	Ukraine	39.7
6	Carpatian Mountains	Ukraine	38.2
7	Tiraspol	Moldova	39.9
8	Yerevan	Armenia	38.5
9	Baku	Azerbaijan	39.2
10	Izen (r. Kura)	Azerbaijan	41.7
11	Vulcano source	Azerbaijan	39.7
12	Tashkent	Uzbekistan	40.4
13	Tashkent	Uzbekistan	44.7
14	Dushanbe	Tadjikistan	41.4
15	Alma-Ata	Kazahstan	37.3

In the previous table are shown the results of the research of tritium concentration in the rain water. This results are lower then established levels in 17 times, but in 10 times exceeded natural concentration before nuclear testing. In our republic main contribution of tritium in the environment made nuclear testing, because in our country there's no reactors and reprocessing plants.

Applications of Exogenous Sensitizers in Photodiagnosis, Photodynamic Therapy, Radiation Therapy, and Boron Neutron Capture Therapy – Short Survey

Ekaterina Borisova, Latchezar Avramov

Institute of Electronics, Bulgarian Academy of Sciences

72, Tsarigradsko Chaussee Blvd., 1784 Sofia, Bulgaria

e-mail: borisova@ie.bas.bg

Cancer is the second most common cause of death. An ideal therapy for cancer would be one whereby all tumor cells were selectively destroyed without damaging normal tissues. Most of the cancer cells should be destroyed, either by the treatment itself or with the help from the body's immune system; otherwise the danger exists that the tumor may re-establish itself. Although today's standard treatments - surgery, radiation therapy and chemotherapy - have successfully cured many kinds of cancers, there are still many treatment failures. The promise of new experimental cancer therapies with some indication of their potential efficacy has led many scientists from around the world to work on approaches called photodynamic therapy (PDT) and boron neutron capture therapy (BNCT). PDT and BNCT are binary modalities for cancer treatment involving activation of tumor cell-localized sensitizers with light or low-energy neutrons. Both therapies allow local control with minimal side-effects common in other cancer treatments.

Exogenous sensitizers as porphyrins and porphyrin-like macrocycles have been shown to selectively localize in a wide variety of neoplastic tissues, and this property provides the basis for their use in the photodynamic therapy of tumors. PDT relies on the selective uptake of a photosensitizer in tumor tissues, followed by generation of singlet oxygen and other cytotoxic species upon irradiation with red light [1, 2], see figure 1.

In addition to necrosis (as the result of oxidative damage) it has been recently shown that some porphyrins also induce apoptosis (programmed cell death). Active research in the area of development of highly efficient PDT photosensitizers is currently underway. The promising new PDT photosensitizers in human clinical trials are porphyrin-based compounds with enhanced absorptions in the red region, as well as chlorins, benzoporphyrins, and phthalocyanines [2].

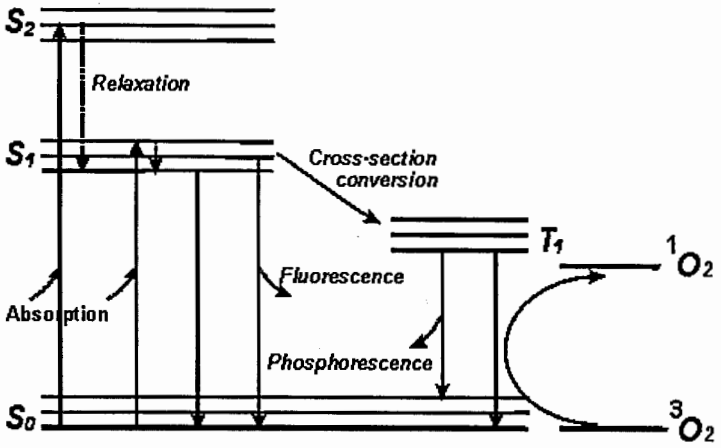

Fig. 1. Jablonsky diagram [2]

Another therapeutic modality for cancer treatment, the Boron Neutron Capture Therapy (BNCT) is based on the $^{10}B(n,^{4}He)^{7}Li$ nuclear reaction which occurs when a ^{10}B nucleus captures a reactor-generated low-energy neutron to produce cytotoxic high linear energy transfer particles ($^{4}He^{2+}$, $^{7}Li^{3+}$) [3], see figure 2. Due to their tendency to selectively accumulate in neoplastic tissue, the family of exogenous sensitizers are attractive boron carriers for BNCT [1]. There are a number of nuclides that have a high propensity for absorbing low energy or thermal neutrons. Of the various nuclides that have high neutron capture cross-sections, ^{10}B is the most attractive for the following reasons: 1) it is non radioactive and readily available, comprising approximately 20% of naturally occurring boron; 2) the particles emitted by the capture reaction $^{10}B(n, alpha)^{7}$ Li are largely high "Linear Energy Transfer", dE/dx, (LET); 3) their combined path lengths are approximately one cell diameter; i.e., about 12 microns, theoretically limiting the radiation effect to those tumor cells that have taken up a sufficient amount of ^{10}B, and simultaneously sparing normal cells; and 4) the well understood chemistry of boron allows it to be readily incorporated into a multitude of different chemical structures [3, 4].

A major advantage of a binary system is that each component can be manipulated independently of the other. With BNCT one can adjust the interval between administration of the capture agent and neutron irradiation to an optimum time when there is the highest differential ^{10}B concentrations between normal tissues and the tumor. Furthermore, the

neutron beam itself can be collimated so that the field of irradiation is circumscribed and normal tissues with high ^{10}B concentration can be excluded from the treatment volumes. Protection of normal tissues near and within the treatment volume is achieved by selective targeting of ^{10}B to the tumor [4].

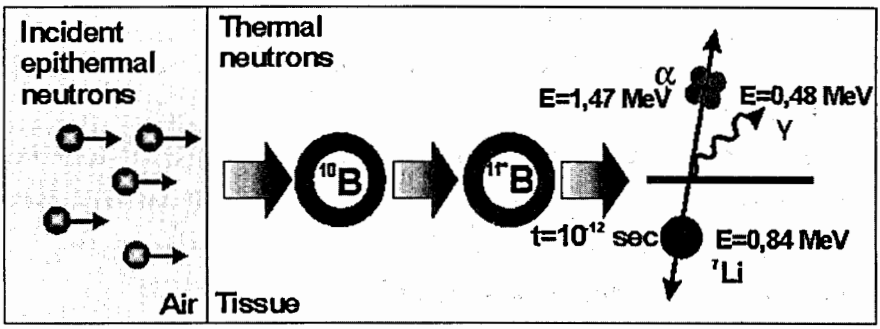

Fig. 2. Schematic view of $^{10}B(n,^{4}He)^{7}Li$ nuclear reaction in human tissues

Porphyrins and their diamagnetic metal complexes are highly fluorescent thus providing a means for the photodetection of tumor cells by their fluorescence, and could be used for an effective treatment planning. Furthermore, tumor-selective paramagnetic metal complexes of porphyrins are used as effective contrast agents for MRI. Radiolabeled derivatives of porphyrins with ^{3}H, ^{14}C, and ^{125}I are useful radiodiagnostic agents. Porphyrin complexes bearing radioisotopic metals have also been shown to retain their in vitro and in vivo localization properties in tumor cells and to be highly promising radiopharmaceuticals for tumor detection and antibody labelling [1]. Other non-cancerous therapeutic applications of porphyrins include treatment of atherosclerosis, vascular re-stenosis, age-related macular regeneration, rheumatoid arthritis and blood sterilization.

New photosensitizers for application in both BNCT and PDT are object of many investigations. The correlation of the chemical structure and biological activity of these compounds is studied. Their accumulation in tumor cells is studied by the fluorescence uptake in order to establish parameters for the successful design of effective sensitizers for cancer treatment.

References

[1] M. Vicente, Porphyrin-based sensitizers in the detection and treatment of cancer: recent progress, Curr. Med. Chem.-Anti Cancer Agents, 2001, 1 175-194.

[2] R. Bonnett, Photosensitizers of the Porphyrin and Phthalocyanine series for photodynamic therapy, Chem Soc Rev 1995; 24:19-33.

[3] S. Green, Developments in accelerator based boron neutron capture therapy, Radiat. Phys. Chem. 1998, 51:561-569.

[4] J. Burian, M. Marek, J. Rataj, S. Flibor, J. Rejchrt, L. Viererbl, F. Sus, H. Honova, L. Petruzelka, K. Prokes, F. Tovarys, V. Dbaly, V. Benes, P. Kozler, J. Honzatko, I. Tomandl, V., Mares, Report on the first patient group of the phase I BNCT trial at the LVR-15 reactor, International Congress Series 2004; 1259:27-32.

Influence of Temperature on Radiation-Induced Micronuclei in Human Peripheral Blood Lymphocytes

Kinga Brzozowska[1] and Andrzej Wojcik[1,2]

[1]*Institute of Nuclear Chemistry and Technology, Department of Radiation Biology and Health Protection, Warszawa,*

[2]*Swietokrzyska Academy, Institute of Biology, Department of Radiobiology and Immunology, Kielce, Poland*

Abstract

The level of cytogenetic damage induced by ionizing radiation under in vitro conditions in human peripheral blood lymphocytes is analyzed for the purpose of establishing calibration curves used in biological dosimetry and for assessing the intrinsic radiosensitivity of the blood donor. The irradiation of blood should be performed under strictly controlled physical conditions that allow a high reproducibility of the dose. A factor that is often not regarded is the control of blood temperature during exposure. Available data on the influence of blood temperature on the level of cytogenetic damage is scarce and somewhat contrdictory. We have, therefore, performed experiments to analyze the impact of blood temperature on the level of radiation-induced micronuclei. Blood was exposed to different doses of X-rays (200 kVp, 5 mA, 3mm Cu filter) at 0, 20 and 37^{0}C. Thereafter a standard micronucleus test was performed and micronuclei were analyzed optically on microscopic slides.

Introduction

Ionizing radiation damages all biomolecules but the most radiation-sensitive biomolecule in living tissue is DNA. DNA-damage takes place during interphase of mitosis. Fragments of damaged chromosomes form micronuclei in cells, which passed the mitosis.

Micronuclei are small, round-shaped structures that stain like the cell nucleus and contain fragments of chromosomes or whole chromosomes. They are formed during mitosis as consequence of radiation exposure of cells.

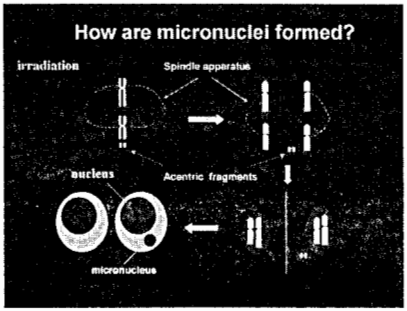

Fig.1. Forming micronuclei in daughter cell after irradiation of mother cell

Chromosome damaged may be so serious that irradiated cells die after the second, third or next mitosis. For this reason we analyze only those cells, which have completed the first division. Cells possess two independent mechanisms of nucleus division and cytoplasm division. By adding cytochalasin B to the lymphocytes culture, we inhibit the cytoplasm division. In consequence binucleated cells (BNC) are formed.

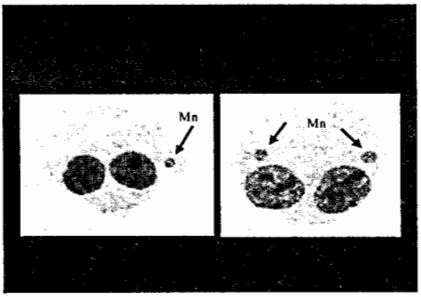

Fig.2. Binucleated cells with one and two micronuclei (Mn)

The level of radiation damaged is most often expressed through dose-effect curves. The curves can express the relationships between the dose and the number of micronuclei per 1000 binucleated cells. The frequency of micronuclei increases with dose (Fig.3).

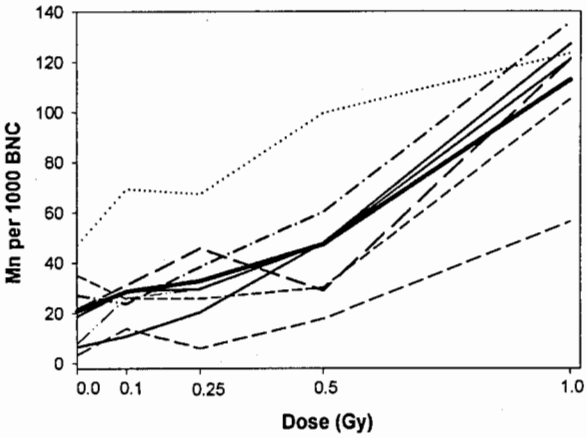

Fig.3. The dose-response curves for micronuclei in binucleated cells in lymphocytes of 7 donors. The line represents the mean (Wójcik et.al.,2000)

Not only the dose of radiation can modify the frequency of MN. We were interested in the influence of temperature on the radiation-induced level of micronuclei.

The impact of temperature on the frequency of radiation-induced chromosome aberrations in the human lymphocytes was first described by Bajerska and Liniecki (1969). We have performed experiments to analyze the impact of blood temperature at irradiation in vitro on the level of radiation-induced micronuclei.

Materials and methods

Blood samples were drawn from two healthy male donors aged 24 and 45 years and irradiated at 0°C, 20°C, 37°C with X-rays 200 kVp, 5 mA, 3mm Cu filter. The doses were:

- 0, 1 and 2 Gy for the first donor,
- 0, 1.35 and 2.7 Gy for the second donor.

Immediately before (for 20 minutes) and during irradiation blood samples were incubated at 0°C, 20°C or 37°C. After irradiation blood samples (0.5 ml) were transferred into 4.5 ml RPMI 1640 medium supplemented with 25 % calf serum, 2.5% PHA, anibiotic solution and incubated for 72 hours at 37°C, 5% CO_2.

Cytochalasin B was added to samples with 5.6 μg/ml after 44 hours after start of the cultures.

After incubation with cytochalasin B duplicated cells (after first mitosis) were harvested by applying 0.14 M KCl, methanol: 0.9% NaCl: acetic acid (12:13:3) and methanol:acetic acid (4:1). Then lymphocytes were dropped onto clean, dry slides and stained with Giemsa. On each slide 500 or 1000 binucleated cells (BNC) were count.

Results

1) For first donor

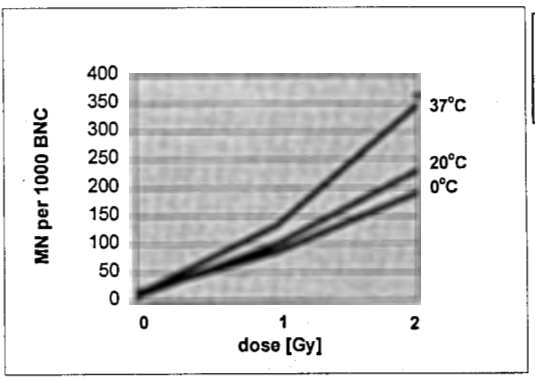

*The difference significat with $p<0.05$ (Fisher test for Poisson distribution events)

Fig.4. The dose-response curves for micronuclei in binucleated cells in lymphocytes of first donor

2) For second donor

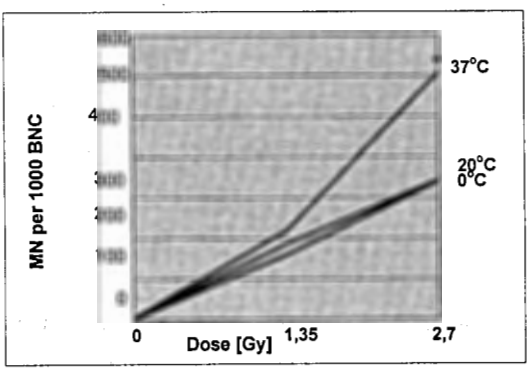

*The difference significat with $p<0.05$ (Fisher test for Poisson distribution events)

Fig.5. The dose-response curves for micronuclei in binucleated cells in lymphocytes of second donor

Conclusion

Temperature influence on the frequency of radiation-induced micronuclei in human peripheral blood lymphocytes. The highest frequency of micronuclei is observed for samples incubated in 37°C before and during irradiation in vitro with doses of 2Gy and 2.7Gy. At this stage of our research we can not explain which mechanisms are responsible for this situation.

Future plans

In the nearest future we would like:

- to irradiate isolated lymphocytes in the presence of radical scavengers like acetone or DMSO,
- to analyze chromosomal aberration after irradiation in different temperatures,
- to analyze DNA repair using Comet Assay.

References

[1] A. Bajerska, J. Liniecki, The influence of temperature at irradiation in vivo on the yield of chromosomal aberrations in peripheral blood lymphocytes. *Int. J. Radiat. Biol.*, 1969, vol. 16. No. 5, 483-493.

[2] M. Fenech, The in vivo micronucleus technique. *Mutat Res*; 455: 81-95.

[3] M. Fenech, The cytokinesis-block micronucleus technique: a detailed description of the method and its application to genotoxicity studies in human populations. *Muatation Research*, 285, 35-44, 1993.

[4] M. Fenech, A.A. Morley, Measurement of micronuclei in lymphocytes. *Mutat. Res.* 147: 29-36, 1985.

[5] M. Kirsch-Volders, M. Fenech, Inclusion of micronuclei in non divided mononuclear lymphocytes and necrosis/apoptosis may provide a more comprehensive cytokinesis block micronucleus assay for biomonitoring purposes. *Mutagenesis* 2001; 16: 51-58.

[6] A. Wójcik et. al., Validation of the micronucleus-centromere assay for biological dosimetry. Genetics and Molecular Biology, 23, 4, 1083-1085 (2000).

A System for the Proton Beam Controle During Radiotherapy

Yu.G. Budjashov, V.O. Karpunin, P.E. Kolonuto, G.V. Mytsin,
A.G. Molokanov, S.V. Shvidkij

Joint Institute for Nuclear Research, Dubna, Russia

Abstract

A system for the on-line control of the proton beam profiles and range has been designed and constructed to guarantee the quality assurance of radiotherapy carried out in a Medico-Technical Complex of the Joint Institute for Nuclear Research.

To measure horizontal and vertical profiles of the beam in the treatment room a multi-wire ionisation chamber has been designed and constructed. The chamber consists of two anode and three cathode planes. Each anode plane contains 30 wires 0.1 mm in diameter separated by 3 mm.

To control the range of the beam 4 semiconductor diodes 2D212A for radio engineering application were used. The system is installed up-stream a first collimator at a peripheral part of the beam, so it does not disturb the useful part of the beam.

Output signals from the ionisation chamber and the diodes are processed by a specially constructed electronics connected to a personal computer. It utilizes 64-inputs 16-bits charge integrators ("TERA" chip).

One-year experience of the system operation in the proton therapy treatment sessions showed its high reliability and sensibility to the proton beam parameters. The accuracy of controlling the symmetry of the beam profiles is 2 % and the range deviations - 0.2 mm of water.

Аннотация

Для обеспечения гарантии качества протонной лучевой терапии, проводимой в Медико-техническом комплексе Объединенного института ядерных исследований, была разработана и создана система контроля профилей и пробега протонного пучка, работающая в реальном масштабе времени.

Для измерения горизонтального и вертикального профилей пучка в процедурной кабине была разработана и изготовлена многопроволочная ионизационная камера. Камера включает два анодных и три катодных электрода. Каждый анодный электрод состоит из 30 проволочек диаметром 0,1 мм натянутых с шагом 3 мм.

Для контроля пробега пучка задействованы 4 промышленных диода типа 2Д212А, предназначенных для использования в радиотехнике. Система установлена перед первым коллиматором в периферической зоне пучка и не вносит искажения в его используемую часть.

Выходные сигналы с камеры и диодов оцифровываются специально разработанным блоком, связанным с персональным компьютером. В блоке использован так называемый "TERA"-чип, представляющий собой 64-канальный 16-битный преобразователь "ток-частота".

Система в течение года проработала в сеансах протонной терапии и продемонстрировала свою надежность и чувствительность к параметрам протонного пучка. Точность определения асимметрии профиля пучка составляет 2 %, а изменения пробега – 0,2 мм воды.

Введение

Пучки ускоренных протонов в лучевой терапии позволяют формировать дозные поля существенно более конформные облучаемой мишени, чем это возможно при использовании конвенционального излучения (гамма квантов, электронов). Это объясняется относительно малым боковым рассеянием протонного пучка, а также наличием в конце пробега частиц максимума ионизации - пика Брэгга, за которым доза резко спадает практически до нуля.

Протонные пространственные дозные поля характеризуются резким градиентом по краю поля – уменьшение дозы с 80% до 20% происходит на расстоянии нескольких миллиметров, что позволяет уменьшить лучевую нагрузку на окружающие мишень здоровые ткани и повысить величину поглощённой дозы в радиорезистентных опухолях.

Эти преимущества протонной лучевой терапии (ПЛТ) позволяют врачу-радиологу с помощью компьютерной программы планирования моделировать облучение мишеней, непосредственно прилегающих к радиочувствительным структурам и органам тела пациента (ствол мозга, зрительные нервы и др.)

Для прецизионного воспроизведения рассчитанных дозных полей в сеансах протонной лучевой терапии необходимо, чтобы реальные параметры протонного пучка при облучении полностью соответствовали заложенным в программу планирования. К таким параметрам, в частности, относятся: горизонтальный и вертикальный профили пучка, его глубинное дозное распределение (кривая Брэгга), величина поглощенной дозы с каждого поля облучения.

Целью настоящей работы явились разработка и создание компьютеризированной системы контроля параметров протонного пучка непосредственно при проведении ПЛТ пациентов в Медико-техническом комплексе (МТК) ДЛЯП ОИЯИ. Система включает следующие основные элементы:

- Широкоапертурная проходная ионизационная камера - монитор интенсивности пучка;
- Профилометр - установленная на входе протонного пучка в процедурную кабину многопроволочная ионизационная камера, предназначенная для контроля горизонтального и вертикального профилей пучка;
- Система полупроводниковых диодов, используемых в качестве детекторов ионизационных потерь пучка при прохождении его через вещество и позволяющих контролировать пробег пучка;
- Многоканальный блок преобразователей "ток-частота" для измерения выходных сигналов профилометра и диодов;
- Интерфейс КАМАК для передачи данных с измерительных приборов в персональный компьютер;
- Компьютерная программа обработки и визуализации получаемых данных;
- Система контроля отпуска дозы при облучении пациентов.

1. Конструкция многопроволочной ионизационной камеры

Устройство многопроволочного профилометра - ионизационной камеры (ИК) представлено на рис. 1. Она состоит из трех высоковольтных, двух сигнальных (анодных) и двух защитных электродов, разделенных диэлектрическими рамками-прокладками толщиной по 5 мм. Высоковольтные и защитные электроды выполнены из алюминиевой фольги толщиной 17 мкм и 50 мкм соответственно. Анодный электрод представляет собой рамку, изготовленную из фольгированного стеклотекстолита, на которую натянуты и распаяны 30 проволочек из бериллиевой бронзы диаметром 100 мкм с шагом 3 мм. Проволочки двух электродов ориентированны ортогонально друг другу, что позволяет независимо измерять горизонтальный и вертикальный профили протонного пучка. Сигнальные проволочки соединяются с контактами двух 32 штырьковых выходных разъемов, установленных на корпусе камеры.

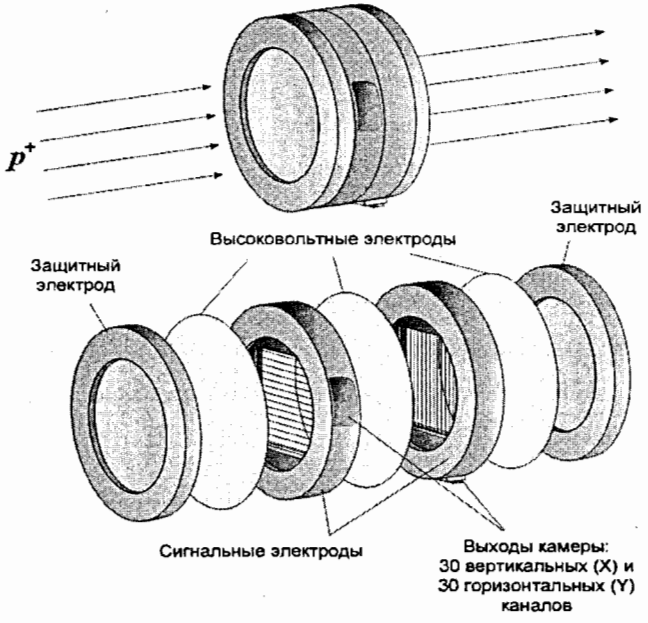

Рис. 1. Устройство многопроволочной ионизационной камеры

1 – нормальная кривая; 2 – смещённая кривая

На высоковольтные электроды от внешнего стабилизированного источника питания подается постоянное отрицательное напряжение 1000 В, обеспечивающее линейный режим работы камеры в рабочем диапазоне интенсивности протонного пучка при незначительном уровне токов утечки на сигнальные проволочки.

Конструкция ионизационной камеры - монитора интенсивности пучка - аналогична конструкции профилометра за тем исключением, что анодная плоскость выполнена так же, как катодная.

2. Контроль пробега пучка с помощью полупроводниковых диодов

Основным преимуществом протонов и других тяжёлых заряженных частиц перед другими видами излучения применительно к лучевой терапии является увеличение их ионизирующей способности по мере проникновения в вещество. Кривая глубинного дозного распределения для этих частиц имеет характерный максимум в конце пробега (пик Брэгга), за которым доза резко спадает до нуля. Величина энергии, выделяемой

протонами в пике, может в несколько раз превышать эту же величину на входе в объект. Это позволяет подвести необходимую дозу к облучаемой мишени, максимально снизив лучевую нагрузку на ткани и органы, расположенные на пути пучка, и практически не облучая область за опухолью.

Так как спад дозы от максимального до нулевого значения за пиком Брэгга происходит всего на нескольких миллиметрах воды, то даже при незначительном изменении глубины проникновения пучка в ткань пространственное распределение дозы относительно рассчитанного программой планирования может сильно исказиться. Это, в свою очередь, может привести к недооблучению опухоли или к переоблучению критических структур, непосредственно прилегающих к облучаемой мишени. Поэтому по радиологическим требованиям отклонение глубины проникновения пучка от требуемого значения не должно превышать 1 мм.

Условия формирования и транспортировки протонного пучка от фазотрона ДЛЯП ОИЯИ к процедурным кабинам МТК таковы, что средняя энергия частиц в пучке в месте облучения пациентов может варьироваться в довольно широких пределах в течение сеанса терапии. Это обусловлено, в первую очередь, наличием различного рода нестабильностей магнитного поля в поворотных магнитах тракта транспортировки пучка. Поэтому необходимо контролировать пробег протонного пучка непосредственно во время облучения пациентов.

В разработанной системе для измерения относительных значений ионизационных потерь протонов использованы промышленные радиотехнические диоды 2Д212А. Чувствительный объем диодов представляет собой диск диаметром 3 мм и толщиной около 0,2 мм, что позволяет контролировать положение пика Брэгга протонного пучка с хорошим разрешением по глубине проникновения в веществе. Кроме того, они являются достаточно радиационно-стойкими и могут использоваться без замены в течение нескольких лет работы в сеансах протонной терапии.

Как правило, при проведении сеанса терапии в процедурную кабину выводится пучок только с одной фиксированной энергией. Перед началом сеанса пробег пучка измеряется анализатором пучка с помощью миниатюрного дозиметрического кремниевого детектора, перемещаемого в водном фантоме под управлением компьютера. После этого установленное значение пробега нужно контролировать на протяжении всего сеанса терапии. Из этого следует, что к системе контроля пробега не

предъявляется требования измерения абсолютного значения пробега пучка, необходимо лишь измерять его смещение.

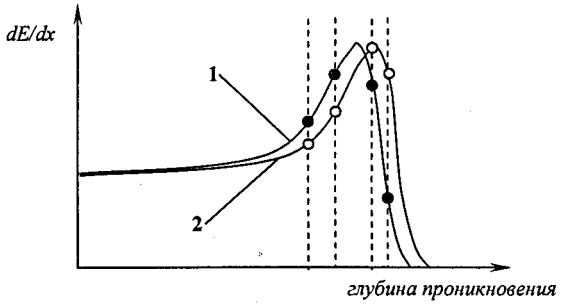

Рис. 2. Вид кривых Брэгга и выбираемое на них расположение точек контроля

Было проведено компьютерное моделирование с целью определения количества диодов, необходимого для измерения пробега пучка с заданной точностью. Оказалось, что для поставленной задачи достаточно использовать всего 4 диода, если 2 из них установить на подъеме пика Брэгга, а 2 других – на его спаде (рис.2). В этом случае при не очень больших отклонениях пробега от номинального значения (до 10 мм воды) показания диодов хорошо аппроксимируются гиперболой, и смещение пробега может быть вычислено с необходимой точностью.

Проведенные измерения кривой Брэгга с помощью диода 2Д212А показали, что изменение средней энергии пучка, при котором пробег смещается на 1 мм воды, приводит к изменению сигнала диода (в области пика на его градиентах) в среднем на 5%, что существенно превышает статистическую и аппаратурную точность измерений (около 2 %).

Аппаратная реализация этой идеи представлена на рис.3. Замедлитель и диоды установлены ниже апертуры коллиматора, расположенного на входе пучка в процедурную кабину. Таким образом, в полезную часть пучка, проходящую сквозь апертуру коллиматора и используемую для облучения пациентов, не вносится никаких дополнительных искажений.

В качестве материала замедлителя был выбран дюралюминий, но возможно также использование и других материалов, например, стали, т. к. измерения пробега пучка являются относительными. Он состоит из 3-х скрепляемых вместе деталей. Деталь 1

предназначена для учёта разностей толщин дополнительного замедлителя для каждого из диодов, а также для крепления всей конструкции и диодов к коллиматору.

Вторая часть замедлителя, легкосъёмная, предназначена для основного гашения энергии протонов. При выводе в процедурную кабину пучка с другой энергией эта деталь может быть легко заменена на другую деталь нужной толщины. Деталь 3 предназначена для окончательного подбора суммарной толщины замедлителя с помощью дюралюминиевых пластин толщиной по 1 мм.

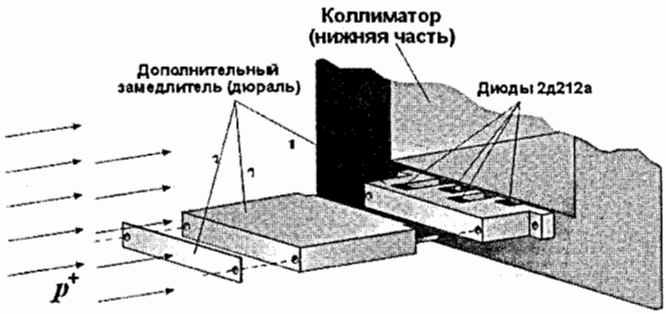

Рис. 3. Расположение диодов и дополнительного замедлителя относительно первого коллиматора и протонного пучка

3. Электроника съема информации

В рабочем режиме при прохождении через ионизационную камеру и диоды терапевтического пучка протонов с сигнальных проволочек и диодов возникает ток порядка 0.1 нА. Для измерения этих сигналов был разработан и изготовлен модуль в стандарте КАМАК на основе микросхемы TERA. Микросхема представляет собой 64 канальный 16-битный стробируемый преобразователь входного тока в пропорциональный ему цифровой код. Каждый канал состоит из двух частей: аналоговой и цифровой (рис.4). Аналоговая часть состоит из конвертера ток-частота. "Квант" тока, соответствующий одному импульсу, составляет 600 фКл, что позволяет измерять входные токи в диапазоне от 0.1 нА до 1 мкА с точностью не хуже 1 %.

Рис. 4. Блок-схема одного из каналов БИС "TERA"

Импульсы с конвертера ток-частота поступают на 16-битный счетчик и выходной буфер. Внешней командой "Latch" данные со всех счетчиков одновременно записываются в выходные буферы и затем последовательно считываются в память компьютера.

Блок преобразователей установлен в процедурной кабине в непосредственной близости от камеры и диодов, что позволяет свести к минимуму уровень внешних наведенных сигналов и кросс-токов между каналами. Для его сопряжения с компьютером используются стандартные блоки КАМАК: регистр ввода-вывода КИ015 и контроллер крейта КК009, установленные в пультовом помещении.

4. Система отпуска дозы

В состав системы отпуска дозы входят: мониторная плоскопараллельная ионизационная камера, преобразователь ток-частота, счетчик-частотомер, 6-ти разрядный десятичный установочный счетчик и управляющий блок (рис.5).

Мониторная камера установлена на входе протонного пучка в процедурную кабину (после многопроволочной камеры). Ток с анодных плоскостей камеры подается на преобразователь ток-частота, выполненный в механическом стандарте КАМАК. С выхода преобразователя импульсы поступают на счетчик-частотомер для контроля интенсивности пучка и на 6-ти разрядный десятичный установочный счетчик блока отпуска дозы.

Установочный счетчик включает в себя собственно 6-ти разрядный десятичный счетчик, 6-ти разрядный десятичный регистр с устройством ввода числа и схемы сравнения чисел. Счетчик и регистр имеют визуальную индикацию содержащихся в них значений.

При равенстве записанного в регистр числа и набранного числа импульсов счетчиком схема сравнения чисел блокирует дальнейший набор числа счетчиком и подает сигнал на управляющий блок. С управляющего блока запрещающий сигнал подается на блоки управления ускорителем для быстрого (около 50 мкс) прерывания пучка, а также дублируется на систему блокировок отключения ВЧ, системы ускорителя.

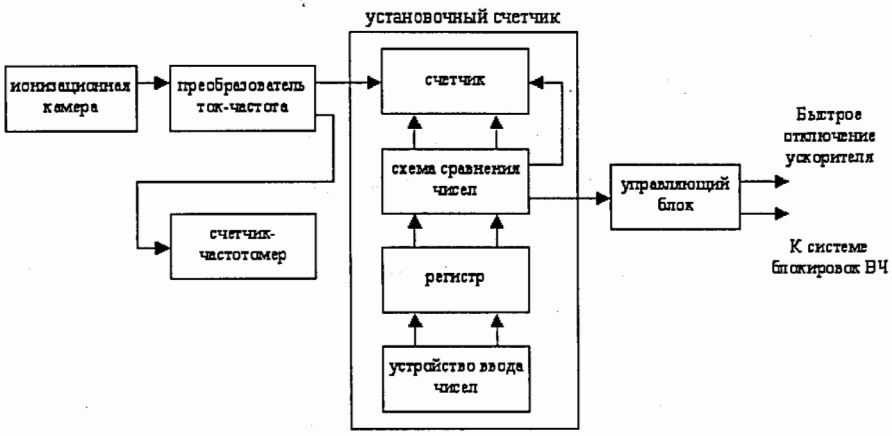

Рис 5. Блок-схема системы отпуска дозы

В начале каждого сеанса радиотерапии проводится калибровка системы отпуска дозы с помощью поверенного клинического дозиметра, устанавливаемого в месте облучения пациентов. Эти измерения дают возможность пересчитать дозу, получаемую пациентом при облучении протонным пучком, в число импульсов преобразователя ток-частота.

Перед облучением пациента в регистр установочного счетчика заносится число, соответствующее заданной врачом дозе. При включении ускорителя начинается подсчет счетчиком числа импульсов, поступающих с преобразователя ток-частота. При достижении равенства значений, содержащихся в регистре и в счетчике (заданная доза и отпущенная доза), срабатывает схема сравнения чисел и происходит отключение ускорителя.

5. Компьютерная программа управления измерениями

Для считывания, обработки и визуального представления информации с ионизационной камеры и диодов в среде "Turbo Pascal" была написана специальная компьютерная программа "Beam Control". Программа позволяет проводить измерения в различных режимах, выбираемых в зависимости от текущей задачи. Основные режимы описаны ниже.

Измерение фонового сигнала. Этот режим служит для измерения сигналов, поступающих без прохождения через детекторы протонного пучка, т.е. токов утечки, если таковые присутствуют. Измеренные данные заносятся в файл и сохраняются на жёстком диске компьютера. Затем во время измерения сигналов уже при наличии пучка эти значения вычитаются из показаний детекторов.

Режим подбора толщины дополнительного замедлителя предназначен для измерения пика Брэгга в дюралюминии с помощью диодов системы. Он позволяет подобрать суммарную толщину дополнительного замедлителя в зависимости от выбранных "реперных" точек на полученной кривой.

Режим калибровки. Как уже было сказано выше, перед началом каждого сеанса терапии профили и пробег пучка в месте облучения пациентов настраиваются с помощью специального прибора – анализатора пучка. Сразу после этого запускается режим калибровки камеры и диодов. Выходные сигналы записываются в специальный файл и в дальнейшем используются в качестве эталона для сравнения с текущими значениями.

Контроль параметров пучка. В этом режиме программа позволяет проводить как визуальное наблюдение за горизонтальным и вертикальным профилями протонного пучка и пиком Брэгга, отображаемых на мониторе компьютера в виде гистограмм, так и за числовыми значениями величин отклонения контролируемых параметров от их значений, установленных при калибровке (рис. 6). При превышении хотя бы одного из параметров заданного в программе предела, компьютер подает звуковой сигнал предупреждения и окрашивает соответствующую гистограмму в красный цвет.

Асимметрия профиля пучка относительно его оси вычисляется следующим образом. По измеренным значениям методом наименьших квадратов проводится усреднённая прямая. Угол наклона этой прямой относительно оси абсцисс

характеризует степень асимметрии пучка в соответствующем направлении. Точность контролирования этого параметра составляет около 2 %.

Для удобства визуального наблюдения за изменением пробега протонного пучка в гистограмму "BRAGG" между столбцами синего цвета, показывающими текущие сигналы с диодов, вставляются красные столбцы, показывающие "идеальные" сигналы, полученные при калибровке и считываемые из файла. Если пробег уменьшается, то 2 левых синих столбца гистограммы становятся выше "идеальных" красных, а 2 правых, соответственно, ниже. Если пробег пучка увеличивается, то всё происходит в обратном порядке.

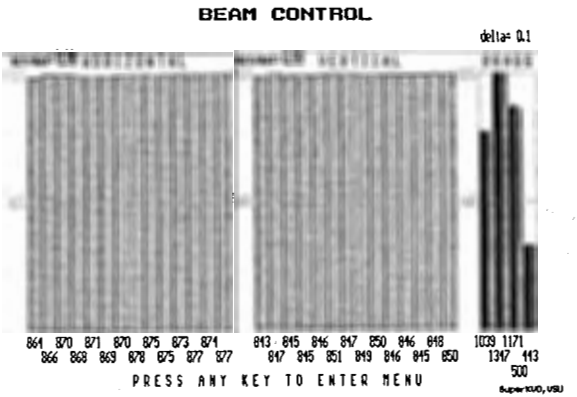

Рис. 6. Экран работы программы в режиме "контроля" при нормальных параметрах протонного пучка

Для определения количественного отклонения пробега от эталонного значения показания диодов аппроксимируются гиперболой. Смещение, выраженное в миллиметрах пробега в дюралюминии, преобразуется в соответствующее значение для воды и выводится на экран монитора ("delta"). Точность определения смещения пика составляет 0,2 мм воды.

6. Опыт эксплуатации системы

На рисунке 6 приведено изображение экрана монитора компьютера в режиме "контроля" при нормальных параметрах протонного пучка. Оба профиля, горизонтальный и вертикальный, не перекошены и представляют собой практически

прямую линию. Измеренный пик Брэгга также почти полностью совпадает с "идеальным".

На рисунке 7 представлено изображение экрана монитора в случае, когда протонный пучок с помощью отклоняющих магнитов был искусственно перекошен по горизонтали и его пробег был увеличен примерно на 2 мм воды. Одновременно с помощью анализатора пучка и миниатюрного кремниевого детектора был измерен горизонтальный профиль в месте облучения пациента (рис.8). Как можно видеть, имеется достаточно хорошее совпадение измеренных двумя приборами профилей. Некоторое возрастание интенсивности пучка по краям профиля на рис.8 обусловлено так называемым коллиматорным эффектом – вкладом рассеянных на стенках коллиматора частиц.

Система контроля параметров пучка использовалась в течение года в сеансах протонной терапии, проводимых в МТК ДЛЯП ОИЯИ, и показала свою исключительную полезность как для ускорения процесса вывода пучка в процедурную кабину, так и для обеспечения гарантии качества облучения пациентов.

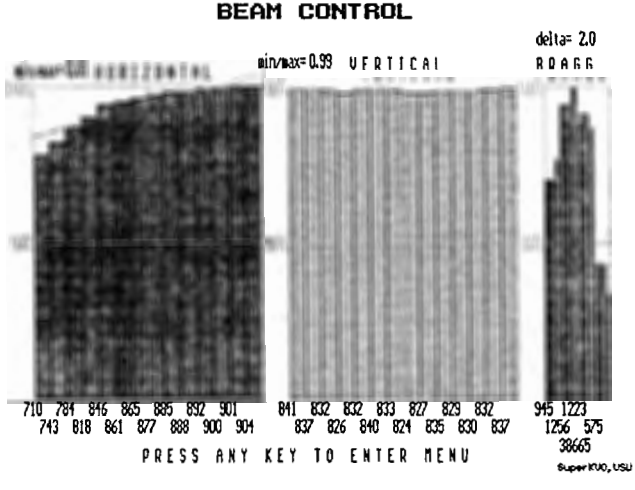

Рис. 7. Экран работы программы в режиме "контроля" при несимметричном в горизонтальном направлении профиле протонного пучка и увеличении пробега пучка на 2 мм воды

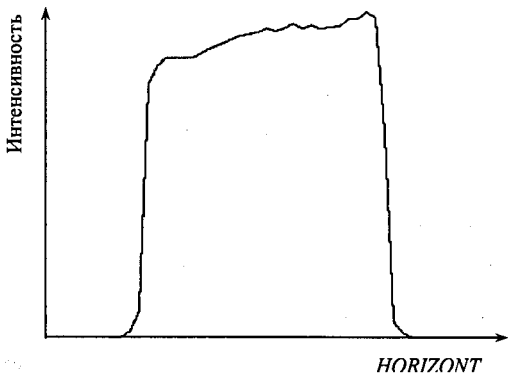

Рис. 8. Горизонтальный профиль, измеренный с помощью анализатора пучка

Список литературы

[1] Г.В. Мицын и др., Дубненский центр адронной терапии, статус и перспективы // Материалы 3-го Российского научного форума "Лучевая диагностика и лучевая терапия в клинике XXI в.", М., 2002, С.109.

[2] О.П. Григорьев и др., Диоды: Справочник, М., Радио и связь, 1990, С.48.

[3] С.А. Кутузов, Устройство для автоматизированного измерения дозных полей. Сообщение ОИЯИ Р10-89-194, Дубна, 1989.

[4] G.C. Bonazzola, M. Donetti, G. Mazza, A VLSI circuit for the charge measurement of a strip ionization chamber // 6^{th} workshop on heavy-charged particles in biology and medicine, GSI report 1997-9 (G11).

[5] В.А. Антюхов и др., Цифровые блоки в стандарте КАМАК, разработанные для исследований на синхроциклотроне. Сообщение ОИЯИ 10-11636, Дубна, 1978.

[6] В.А. Антюхов и др., Цифровые блоки в стандарте КАМАК, разработанные для исследований на синхроциклотроне. Сообщение ОИЯИ Р10-87-928, Дубна, 1987.

Principles of Thermoluminescent Dosimetry

Tomasz Cybulski, Pawel Dziepak

Faculty of Physics and Applied Computer Science

AGH University of Science and Technology, Cracow, Poland

Introduction

Everything has begun when Antoine Henri Becquerel discovered radioactivity first named Becquerel Rays after him. Than Ernest Rutherford in 1911 discovered atomic nuclei. Practically these discoveries made XX century a period of nuclear physics. A lot of different applications in nuclear and atomic radiation have been introduced to our lives and technology since that time. In the same year of the discovery of X rays by Wilhelm Conrad Roentgen (1896) first severe radiation effects on human body were notified. It appeared a significant matter to find methods for quantitative describing of radiation. This was a must due to the fact that the effects on radiation interactions with matter are closely connected with absorbed dose. Every single exposure to both directly and indirectly ionizing radiation has to be controlled. This has lead to development of a new discipline - dosimetry which main goal is to measure and decrease exposure to reasonably low level that does not affect our practice.

Thanks to our good knowledge of radiation interactions with matter several different techniques of its measurements were introduced. These are as follows:

- Ionizing
- Photometric
- Scintillation
- Semiconductor
- Luminescent

Luminescent methods are integral methods based on changes made by radiation in dielectric crystals. Effects of this exposure can give us useful information about exposure after specific stimulation by both light (radiophotoluminescence) and temperature (radiothermoluminescnce called thermoluminescence).

First thermoluminescent events were observed by Robert Boyle in 1663 while examining luminescence of diamond during heating. Further ages brought new studies on thermoluminescence for instance developed by Maria Sklodowska-Curie in her PhD thesis.

She was examining luminescence of CaF after exposure to Ra radiation. 1940s' investigations on this phenomena lead finally to the first concept of thermoluminescence which succeeded in final application of radiation quantitative measurements. Nowadays most laboratories, hospitals and other institutions in the world base their personnel dose controll on TL detectors.

TL detectors

Thermoluminescence is strongly connected with dielectric crystals. It is very convenient to show or explain this phenomena on energetic band model of solid state. In ideal crystal valence band is filled with electrons while forbidden band and conduction band are empty. Thermoluminescent processes are impossible to occur in this situation. However, there are always defects of crystal lattice such as irregularities or impurities that make this process possible. Irregularities mentioned above have very specific energetic structure similar to outer orbit electrons. They trap electrons with energy that is located in forbidden band. These centers are located in different places of f.b. and are normally separated one from another. They can either play role of the acceptor of electron or donor. The first is located near conduction band and is called electron trap. The other is located next to valence band and is called hole trap simultaneously being luminescence center. Electron traps bind electrons with different energies that are dependent on so called depth of the trap. Luminescent centers (hole traps) recombine with electrons form electron traps what results in conversion of its energy to photon. All this centers along with its specific properties result in TL pjenomena which nowadays is considered to be a two-stage process:

1. Absorption of radiation, ionization and trapping of holes and electrons.
2. Stimulation of TL material resulting in recombination of charge carriers and emission of luminescent light.

In standard dielectric crystal the forbidden band is wide enough to prevent valence electrons from being lifted to conduction band. Neither light nor mechanic or chemical stimulation of material can give enough energy for this process. Situation is different when it comes to ionizing radiation. It has enough energy to elevate these electrons to conduction band (upper energetic level). Electrons in c.b. stay there as long as they find themselves in the vicinity of the trap. When they find a trap they recombine immediately. The energy of electron in the trap is called binding energy. If we want to release electron from the trap we

have to deliver at least as much energy as is the binding energy. Holes generated in valence band also stay in it untill they find an irregularity that will be able to deliver electron to v.b. Trapping of the hole in f.b. is the end of the first stage of the thermoluminescence process. The concentration of filled traps in material is proportional to absorbed dose (dependent on radiation type).

Fig.1. LiF:Mg,Ti,Cu – TL light

"Excited"[1] state after irradiation lasts until we deliver high enough energy portion to release electrons from traps. In practice it is realized by heating the detector. Also environment conditions can deliver sufficient energy e.g. light or mechanic stress, what is very undesirable. After thermal stimulation trapped electron finds itself again in conduction band. It will stay there until it finds itself in the vicinity of the hole trap. This causes recombination which results in emission of luminescent photon. Not all traps are being empted at the same time of heating. At the beginning electrons come from those traps of the lowest binding energy. We can define function that will show us changes in number of thermally released electrons in period of time. This is as follows:

$$\frac{dn}{dt} = n \cdot s \exp(-E/kT), \qquad (1)$$

$p = s\exp(-E/kT)$ - Boltzman distribution defining probability of electron release [s^{-1}],

s - frequency parameter dependent on defect type (normally $10^6 - 10^{14}$ s^{-1}),

E – energy of trap [eV],

K - Boltzman constant [JK^{-1}],

T – temperature [K],

n – number of traps filled in the first stage.

[1] Term excited means the state after irradiation of TL detector when electrons and holes are trapped with reference to the theory above.

We can see that the higher the temperature is the more electrons are released from traps what increases the intensity of luminescent light. The increase has its critical moment when n parameter in Eq.1. starts do decrease. Due to fact that the intensity is proportional to number of traps it also starts to decrease.

Linear growth of temperature and registration of TL light leads to obtaining detector glow curve. The number of peaks and shape of glow curve depends on trap types. Fig.2 shows example glow curve of TL detector for several different types of traps. Surface under the curve is proportional to absorbed dose, that can be obtained form specific calibration of the detector.

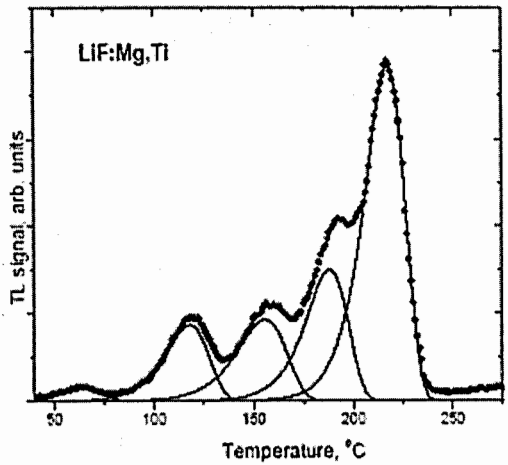

Fig. 2. TL glow curve

Very important thing in production of TL detectors is existence of reasonably deep traps with minimal number of different traps giving signal in temperatures between 180° and 250°. It is also very crucial to obtain the same parameters of read out process. Changes in temperature growth result in shift of glow peaks to higher temperatures what makes collected data useless in comparison to calibration curves. It is also very important to keep all the detectors in right conditions especially to prevent them from any surface contamination or exposure to UV light. All this factors can affect our expected to collect information spoiling reliability of detector - memorized data.

Investigation and application of TL detectors have been the main goal of the Institute of Nuclear Physics of Polish Academy of Science in Cracow, Poland. Main types of TLDs produced there are based on:

LiF:Mg,Ti (so called MTS); LiF:Mg,Cu,P (so called MCP); $Li_2B_4O_7$:Mn – under investigation.

What makes TL detectors so special?

We must remember that whenever we are investigating any single subject we cannot omit its advantages and disadvantages. Considering TL detectors it is worth mentioning that their application is very easy and wide however technological processes of their preparation and analysis are often very complicated and labor-consuming. TL dosimetry however gives us great possibility of controlling radiation exposure in very wide range of doses form 100nGy up to 1kGy. They are environment resistant what helps in their application in various conditions. It often happens that our measurement is being run in places where reach of power supply is limited. This doesn't bother TL dosimetry as it is in a group of passive detectors. Moreover absorbed dose memory of the detector is very useful when we do not have possibility of reading out detector directly at place of irradiation. Their dimensions – normally 4.5mm in diameter and ca. 2mm thickness allow us to reach places that are not available for relatively big active detectors in comparison with TLD.

The Magic World of Photosynthesis

Wojciech Giera, Wawrzyniec Kaszub, Zuzanna Pawłowska, Karolina Tomczyk

Faculty of Physics, Adam Mickiewicz University, Poznań, Poland

Abstract

Life on Earth depends on photosynthesis which converts solar energy to chemical energy by means of two large protein complexes located in the thylakoid membranes: photosystem I and photosystem II. In this paper, some basic features of photosystem I are presented: composition and architecture of photosystem I, antenna system and the electron transport chain. The main techniques applied to study dynamics of electron transfer in photosystem I are also described, including the generation ultrashort laser pulses needed to investigation fast photosynthetic processes.

1. What is a photosynthesis?

The term "photosynthesis" means literally synthesis with light, but conventionally it is used to name a particular photobiological process. Because of that a narrower definition will be adopted here:

Photosynthesis is a process in which energy of light is captured and stored by an organism, and the stored energy is used to drive cellular processes.

It should be noted that this definition is still relatively broad, because includes different forms of photosynthesis:

- a form based on chlorophyll – most common,
- a form based on bacteriorodopsin – carried out by some bacteria,
- other mechanisms, which are not discoverd yet.

In photosynthetic eukaryotic cells, photosynthesis takes place in a cellular organellum called chloroplast (Figure 1). Inside chloroplast, an extensive system of membranes can be found. These membranes are called thylakoids and bind most of chlorophylls and other photosynthetic pigments. In typical plant chloroplast most of thylakoids are organized in stacks called grana. The non-stacked ones are called stroma thylakoids. The stroma is an aqueous nonmembranous interior of chloroplast, and is the place of carbon metabolism reactions.

Photosynthesis is driven by two large pigment-protein complexes, photosystem I and photosystem II, which are embedded in the thylakoid membranes (Figure 2). These photosystems contain antenna complexes absorbing photons, the energy of which is next used to drive electron transfer across the membrane. This transport is carried out through a chain of redox cofactors, which can be found in both photosystems, and leads to transmembrane difference in electrical potential and concentration of protons H^+. The electrochemical force created in this way is next used to drive ATP synthesis and reduction of $NADP^+$ to NADPH. ATP and NADPH are used to convert CO_2 to carbohydrates in stroma by means of certain enzymes.

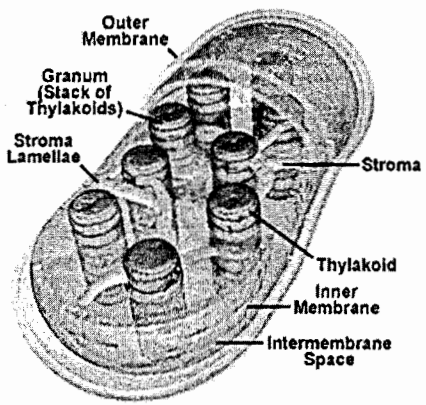

Fig. 1. Anatomy of the plant cell chloroplast [11]

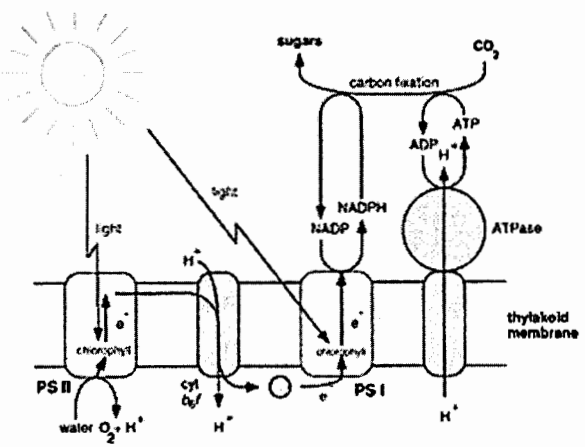

Fig. 2. Schematic presentation of photosynthetic processes which occur in plants, algae, and cyanobacteria [12]

2. Ultrashort pulses lasers

2.1. Laser – at the beginning

"Laser" is the acronym of Light Amplification by Stimulated Emission of Radiation. The first laser was made by Theodore Maiman in 1960. It was a ruby laser – the first pulse construction. After this invention, Ali Javan presented the He-Ne laser – the first construction which had a continuous beam. Next, in sixties in Bell Laboratories and all over the world many scientists developed and presented different laser constructions (e.g. a semiconductor or dye laser).

Lasers have many useful and interesting advantages. Their beam is nearly monochromatic, coherent and powerful. This last property is very important in view of non-linear optics experiments or photochemistry researches.

There are pulse and continuous lasers, working with a solid-state, semiconductor, gas or dye active medium. They are used in communication and computer technology, entertainment, medical equipment and many other areas. They are also used in laboratory researches, especially the pulse one.

At the beginning pulse ruby lasers were the most popular source of high power light pulses, giving much more possibilities than gas or semiconductor constructions. Later the dye lasers have been found to be a good source of shorter in time duration and higher in energy pulses. Nowadays instead of ruby and dyes we are using as an active material (crystal doped with) elements with Nd^{3+}:YAG and Ti:Sapphire.

2.2. Pulses lasers

The time duration of the pulses of the first laser constructions was very long (10^{-6} s). Today, in professional studies in physics, chemistry or medicine, scientist need very fast pulse lasers. The pulse duration of these systems is of about 10^{-12} to 10^{-15} s.

2.3. Frequency domain description of mode locking

The laser beam is a superposition of many electromagnetic wave, oscillating in many accidental modes. Each mode has a distinct phase. In the case of a continuous beam, the intensity of the beam show a random-value time behavior.

In ultrashort pulse lasers to reach very short pulses, we must implement mode locking. This is a process in which the relations between phases are well defined. Let's imagine 2n+1 longitudinal modes oscillating with the same amplitude (as shown in figure 3).

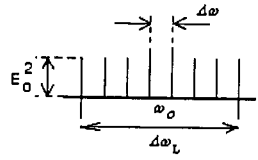

Fig. 3. 2n+1 longitudinal modes oscillating with the same amplitude

Lets imagine that due to a synchronization process, the modes present in the laser cavity satisfy the relation (2.3.1):

$$\varphi_l - \varphi_{l-1} = \varphi = \text{const}, \qquad (2.3.1.)$$

where φ_l is the l-mode phase. Then, the total electric field, which is the sum of wave's equations for different modes, can be described by formula (2.3.2):

$$E(t) = \sum_{-n}^{+n} E_o \exp\{j[(\omega_0 + l\Delta\omega)t + l\varphi]\}. \qquad (2.3.2.)$$

We see that $E(t)$ depends on the frequency of the central mode (ω_0), the φ value, the resonator length l and the frequency difference between two neighboring modes, $\Delta\omega$. If we adopt for simplicity a zero phase value for the central mode then the summation of the 2.3.2 equations gives:

$$E(t) = E_0 \frac{\sin\left[(2n+1)\frac{\Delta\omega t}{2}\right]}{\sin\left[\frac{\Delta\omega t}{2}\right]} \exp(j\omega_0 t). \qquad (2.3.3.)$$

A plot of this expression can be seen in figure 4. As we can see the synchronization process leads to the appearance of intensity peaks. In mathematical language pulse maxima occurs when the denominator in formula (2.3.3) vanishes. It happens when expression ($\Delta\omega t$) is equal 0, π, 2π etc. Time between two successive pulses will be connected with the

frequency difference, $\Delta\nu$, of two consecutive modes. We can write an expression for Δt – time which separates two successive pulses:

$$\Delta t = \frac{2\pi}{\Delta\omega} = \frac{1}{\Delta\nu}. \qquad (2.3.4.)$$

For t > 0 the first minimum of the light intensity, $A^2(t)$, occurs when the numerator vanishes. It happens when $2((2n+1)\omega t') = \pi$. Then the pulse width, τ_p, is approximately equal to $\delta\tau$ (figure 4) and we can write (2.3.5):

$$\tau_p \cong \frac{2\pi}{(2n+1)\Delta\omega} = \frac{1}{\Delta\nu_L} \qquad (2.3.5.)$$

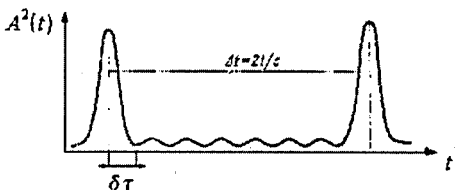

Fig. 4. Plot of the equation 2.3.3

2.4. Mode-locking techniques

During a long time now we've got two kinds of mode-locking methods: The first one, active mode locking, basing on external sources, and the second one, passive mode locking. The last one bases on non-linear optics effects and it is very popular in new researches in biology, chemistry and especially physics.

In active mode locking we distinguish:

- AM mode-locking – induced by an amplitude modulator
- FM mode locking – induced by phase modulator

In passive mode locking we distinguish:

- fast saturable absorber – uses saturation properties of a suitable absorber (dye molecule or a semiconductor) with a very short lifetime,
- Kerr lens mode locking (KLM) – exploits the self-focusing property of a suitable, transparent, non-linear optical material,
- slow saturable absorber – exploits the dynamic saturation of the gain medium,
- additive pulse (APM) – exploits the self-phase modulation induced in a suitable non-linear optical element inserted in an auxiliary cavity and coupled to a main cavity of identical length.

3. Basic features of photosystem I

3.1. Linear electron transfer

Under illumination with light at wavelengths shorter than approximately 700 nm photosystem I (PS I) carries out transmembrane electron transfer (Figure 5). The primary electron donor is a special chlorophylls pair called P700. From P700 electron goes through chain of intermediate electron acceptors to the terminal acceptor originally named P430. Now it is known that P430 is represented by one or both of two iron-sulphur clusters called F_A and F_B.

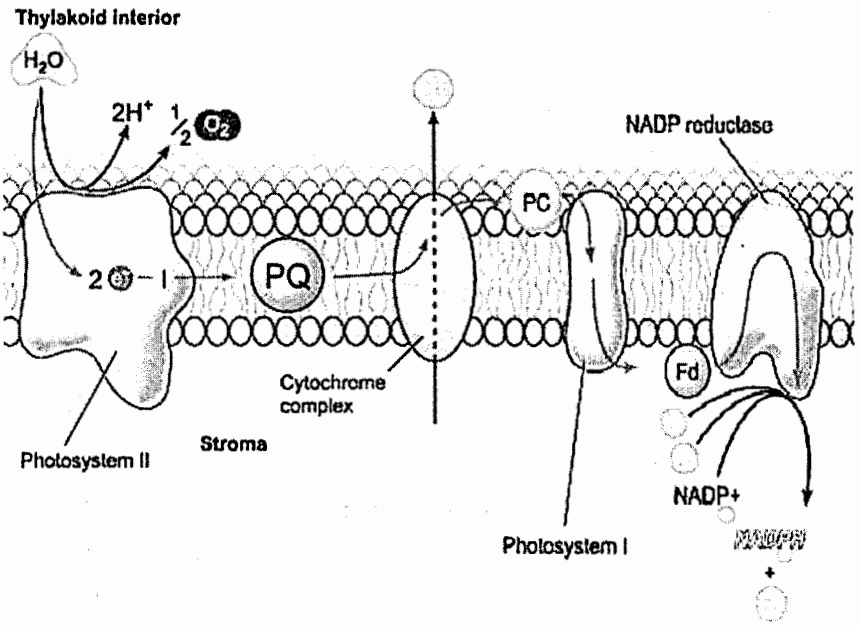

Fig. 5. Linear electron transfer from water to $NADP^+$ [13]

The reduced terminal acceptor is a strong reductant and donates its electron to $NADP^+$ via ferredoxin or in some cases, flavodoxin. Both these protein complexes are water soluble and are present on the stromal (outer) side of thylakoid membrane. The primary electron donor in its oxidized form, $P700^+$, is a strong oxidant and gets on electron from water oxidazing photosystem II via cytochrome b_6f complex and plastocyanin. Cytochrome b_6f complex is embedded in the thylakoid membrane whereas plastocyanin is a water soluble protein located on the luminal (inner) side of thylakoid membrane.

3.2. Structure of photosystem I

Nowadays the structure PS I from the cyanobacteria *Thermosynechococcus elongatus* is known at resolution 2,5 Å. This structure will be used here to describe an architecture of PS I. In cyanobacteria PS I exists as a trimer and in the higher plants, as a monomer. From now on the term PS I wil be used for its monomeric form.

Each monomer consist of 12 protein subunits and 127 cofactors (96 chlorophylls, 2 phylloquinones, 3 iron-sulphur clusters, 22 carotenoids, 4 lipids), an ion Ca^{2+}, and 201 water molecules. The biggest subunits, PsaA and PsaB, are homological and form the core of PS I. They bind large number of antenna pigments and almost all redox cofactors, except for F_A and F_B, which are bound to PsaC. The PsaC subunit is located peripherally on the stromal side of PS I. The other subunits are smaller and play rather structural role:

- PsaD and PsaE – dock ferredoxin or flavodoxin,
- PsaF – docks plastocyanin,
- PsaL and PsaI – are indispensable to form the PS I trimer in cyanobacteria,
- all of them ensure correct assembly and stability of PS I.

Some subunits seem to be specific for certain organism, e.g. PsaM was found only in cyanobacteria whereas PsaG, PsaH and PsaN only in algae and plants. A schematic presentation of PS I is shown in figure 6.

3.3. Antenna system

PS I (from *Thermosynechococcus elongatus*) contains antenna system formed by 90 chlorophylls *a* (Chl *a*) and 22 carotenoids. Seventy-nine chlorophylls are bound to subunits PsaA and PsaB. The smaller subunits and bind together 11 chlorophylls – directly, through water molecule or in one case through a lipid molecule. In plants and algae, PS I is also associated with another antenna complex called LHC I (light harvesting complex). In plants

LHC I contains 4 protein subunits which bound together about 60 chlorophylls - Chls *a* and Chls *b*, at a ratio of 3,5:1. The numbers of protein subunits and chlorophylls are larger in the case of a model alga *Chalmydomonas renhardti.*

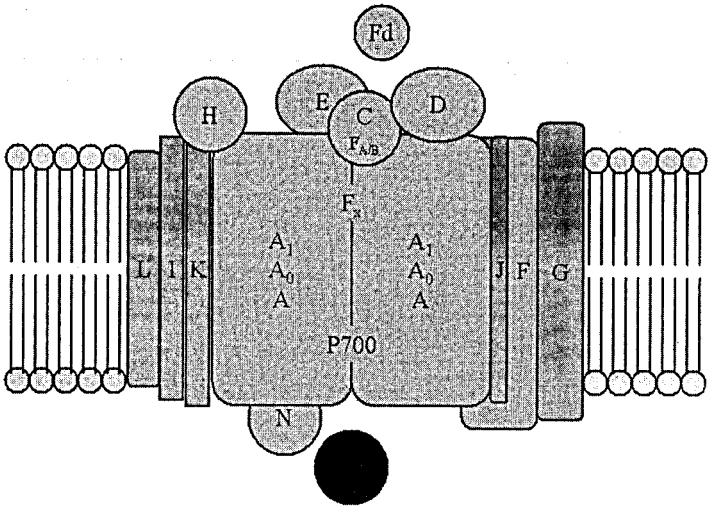

Fig. 6. Schematic presentation of PS I architecture [14]

Antenna system of PS I contains several spectral form of Chl *a* with absorption maxima between 666 and 693 nm and a few long wavelength chlorophylls called also "red chlorophylls". The latter ones have maxima absorption between 700 and 730 depending on species. It implies that their excitation energy is smaller than excitation energy of primary electron donor P700.

3.4. The electron transport chain

The electron transport chain is functionally most important part of PS I. It is formed by 6 chlorophylls, 2 phylloquinones and 3 iron-sulphur clusters Fe_4S_4. The structure of the electron transfer chain is shown in figure 7. Chlorophylls and phylloquinones are bound to subunits PsaA and PsaB in such way that they form two symmetric pathways A and B. The pathway A contains chlorophylls eC-A1, eC-B2, eC-A3 and phylloquinone Q_K-A whereas the pathway B contains chlorophylls aC-B1, eC-A2, eC-B3 and phylloquinone Q_K-B.

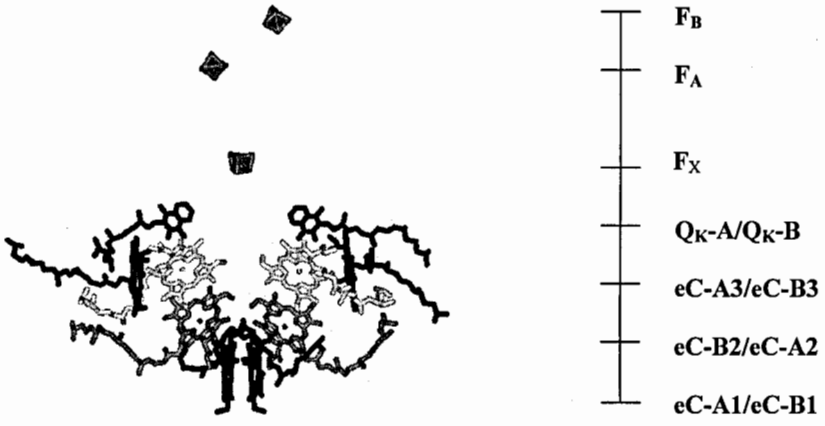

Fig. 7. The electron transport chain in PS I [15]

Charge separation is initiated at the primary electron donor P700 which is formed by chlorophylls pair eC-A1/eC-B1. Chlorophylls of the next pair eC-B2/eC-A2 are sometimes called *accessory chlorophylls* and their role in the electron transport is controversial. One or both chlorophylls of the third pair eC-A3/eC-B3 represents primary electron acceptor called A_0. The next electron acceptor, A_1, is one or both phylloquinones Q_K-A and Q_K-B. The iron-sulphur cluster F_X is the next electron acceptor and is bound to both subunits PsaA and PsaB. Two iron-sulphur clusters, F_A and F_B, bound to the peripheral protein subunit, PsaC, represent terminal acceptor of electron.

Upon excitation P700 to its lowest singlet excited state $P700^*$ electron is transferred to A_0 and next to A_1 on a picosecond timescale, then from A_1 to F_X on nanosecond time scale and finally to F_A and F_B also on nanosecond time scale. The controversial point is if one or both of two paths of electron transport chain are active.

4. Techniques applied to study dynamics of electron transfer in photosystem I

Three methods applied to measure kinetics of electron transfer in photosystem I will be considered: ultrafast absorption change measurements, transient electron paramagnetic resonance and photovoltage measurements. The first technique will be described in most detail, since it is most commonly used for measurements on photosystem I.

4.1. Ultrafast absorption change measurements

Time-resolved transient absorption spectroscopy is a sensitive technique to study time evolution of the excited and redox states and to determine the lifetimes and characteristic difference spectra of short living species.

In this method, there is used ultrashort laser pulse that is divided in two beams:

- pump pulse – which excites the sample,
- probe pulse – which is used to observe induced optical changes (that are monitored as a function of time) and is divided in two beams: first one goes through the excited part of the sample, and the second one (called reference beam) goes through not excited part.

The absorption of the reference beam is a background that is subtracted from the absorption of the probe pulse. To get the optical density of transient absorption signal, the spectral intensity of the probe pulse is measured directly in front of the sample and after passing through it. But using reference beam lets one to measure intensity only after passing trough the sample. The formula for optical density (OD) in this case is:

$$\Delta OD(\lambda,\tau) = \log\frac{I_0(\lambda)}{I(\lambda,\tau)} - \log\frac{I_0(\lambda)}{I(\lambda,\infty)} = \log\frac{I(\lambda,\infty)}{I(\lambda,\tau)}, \qquad (4.1.1.)$$

where $I_o(\lambda)$ is the spectral intensity of the probe pulse in front of the sample, $I(\lambda,\tau)$ is the spectral intensity of the probe pulse going through the sample measured at a time τ after excitation, and $I(\lambda,\infty)$ is the spectral intensity of the reference beam.

The change in optical dencity is received as a function of wavelength and delay time. Measurements of optical changes as a function of time are possible by using delay times between the pump and the probe pulses. Those delay times are received by using an optical delay line. 1μm optical path difference gives a time delay equivalent to 3.3 fs. What is the special advantage of this technique is that there is no necessity of using ultrafast detectors. What is more: accessible time window is very large (from sub-picosecond to second time scale).

4.2. Transient electron paramagnetic resonance

When the electron is knocked off from P700 to A_1, the spin-polarized radical pair appears, which is detected in transient electron paramagnetic resonance. In the absorption

change measurements a time scale from sub-picoseconds to second is covered and in transient EPR from 10ns to several microseconds is available. Transient EPR is also applied to characterize magnetic interactions in $P700^{+}A_1^{-}$.

4.3. Photovoltage measurements

Photovoltage technique allows measurement of the temporally resolved changes in the membrane potential in an oriented sample and provides kinetic information on electrogenicity of the individual reaction steps. While an electros is passing across the membrane, an electric dipole is formed in the direction perpendicular to the membrane plane. As a consequence, there is a possibility to measure an electric potential which increases during the movement of electron.

Advantages of this method are inherent selectivity for electrogenic events, high temporal resolution and excellent signal-to-noise ratio. Disadvantages is that electrogenic relaxations might contribute to a measured potential change.

References

[1] R. E. Blankenship, Molecular Mechanisms of Photosynthesis, Blackwell Science (2002).

[2] K. Brettel, Electron transfer and arrengment of the redox cofactors in photosystem I, Biochimica Et Biophysica Acta 1318 (1997): 322-373.

[3] P. Jordan, P. Fromme, H. T. Witt, O. Klukas, W. Saenger, N. Krauβ, Three-dimensional structure of cyanobacterial photosystem I at 2.5 Å resolution, Nature 411 (2001):909-917.

[4] R. Naskręcki, Femtosekundowa spektroskopia absorpcji przejściowej, Wydawnictwa Naukowe UAM, Poznań 2000.

[5] R. Naskręcki, Ultrashort laser pulses in physics and chemistry, Proc. 4Int. Workshop, Laser Spectroscopy on Beams of Radioactive Nuclei (2000): 182-192.

[6] I. Grotjohann, P. Fromme, Structure of cyanobacterial Photosystem I, Photosynthesis Research (2005) 85: 51 – 72.

[7] K. Brettel, W. Leibl, Electron transfer in photosystem I, Biochimica Et Biophysica Acta 1507 (2001): 100-114.

[8] A. Piekara, Nowe oblicze optyki, PWN, Warszawa 1968.

[9] H. Abramczyk, Wstęp do spektroskopii laserowej, PWN Waerszawa 2000.

[10] O. Svelto, Principles of lasers, Fourth Edition, PLENUM.

[11] http://micro.magnet.fsu.edu/primer/java/photosynthesis/javaphotosynthesisfigure1.jpg

[12] http://photoscience.la.asu.edu/photosyn/education/photointro.html

[13] http://www.biology.lsu.edu/introbio/spring/Spring%202005/1001/SMP/noncyclic-photosynthesis.jpg

[14] http://members.cox.net/chlorophyll/toon.htm

[15] http://members.cox.net/chlorophyll/images/PSI-RC.jpg

Pulsed Neutron Generator at the Henryk Niewodniczański Institute of Nuclear Physics Polish Academy of Sciences, Kraków

Maciej Grządziel

AGH University of Science and Technology,

Faculty of Physics and Applied Computer Science,

Kraków, Poland

Abstract

This paper describes the structure, operating principles and application of the 14 MeV pulsed neutron generator, which is working at the Institute of Nuclear Physics (IFJ PAN) in Kraków, Poland. A pulsed beam of fast neutrons produced by a pulsed neutron generator is the source of the decaying thermal neutron flux, which is investigated in a medium of interests.

Principles of operation

The 14 MeV neutron generator was built at the Institute of Nuclear Physics in the sixties. In the seventies it was turned into the pulsed regime, modernized in the last decade, and now is used for the thermal neutron transport research in bounded media, including applications for the nuclear geophysics. It consists of the ion source, linear accelerator, tritium target plate (Fig. 1) and is equipped with a sample camera with helium detectors.

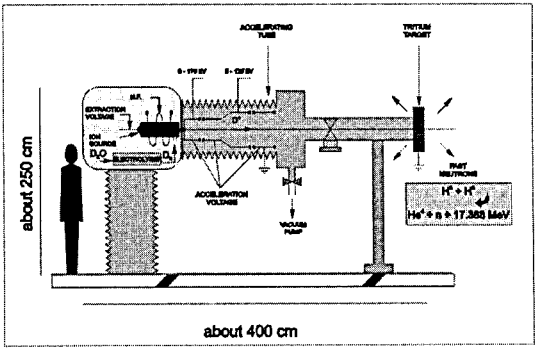

Fig. 1. Schema of The Generator

Neutrons are produced in the $^{3}H(d,n)^{4}He$ reaction. Deuterons are produced by ionization of the deuterium gas in the ion source quartz bulb (Fig 3). Gas deuterium is obtained from electrolysis of heavy water (D_2O) and dosed to the ion source through the palladium valve (Fig 2). The valve allows to control the deuterium gas yield by increasing or decreasing the temperature of palladium. The deuterium gas is ionized by a high frequency electromagnetic field. The ion plasma is specially formed at the output hole of a quartz bulb, which is connected to the input hole of the accelerator. The ions are periodically pushed off by positive extraction voltage pulses (amplitude 4 kV). The light intensity and colour of the glowing gas in the bulb provides us with important information about working conditions of the ion source (Fig 3).

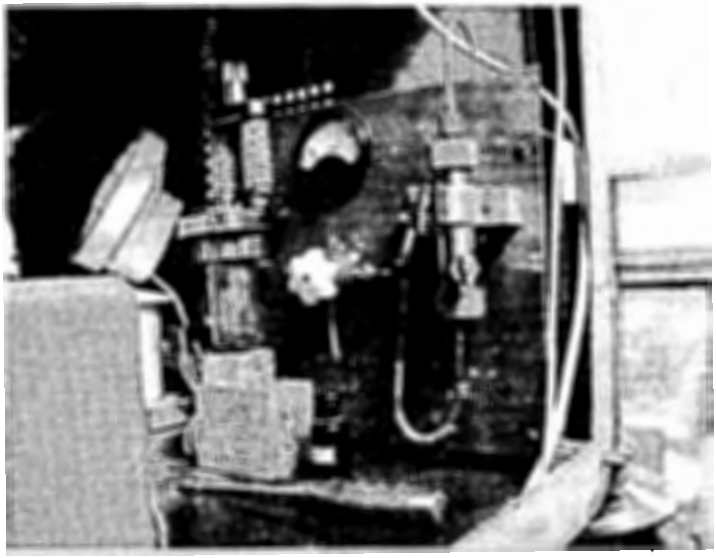

Fig. 2. Heavy water electrolyzer and palladium valve

The ions are accelerated and focused by a system of cylindrical electrodes, then they leave the accelerating section and travel through the straight section above 0,9 m long until they reach the tritium target plate. Deuterons hitting the tritium target plate cause the $^{3}T + {}^{2}D = {}^{4}He + {}^{1}n$ reaction. Neutrons created in this reaction are monoenergetic, 14 MeV.

Fig. 3. The ion source

Experiments

The thermal neutron flux is used for the thermal neutrons transport research in solid and liquid samples. Knowledge of the time decay constant of the neutron flux in a bounded sample gives information on thermal neutron diffusion parameters of the medium. The sample is placed inside the sample camera (Fig 4).

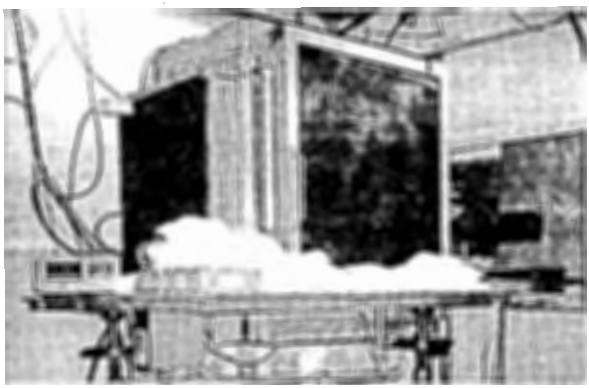

Fig. 4. Sample camera

The camera establishes proper physical conditions during the experiments. The camera is made of borated paraffin flat walls that form a nearly cube shape of the internal dimensions approximately 60 x 60 x 60 cm^3. Inside the sample camera Two ^3He detectors of thermal neutrons (Fig. 5) are placed symmetrically at the sample in the camera. The temperature inside the camera is automatically controlled and stabilized.

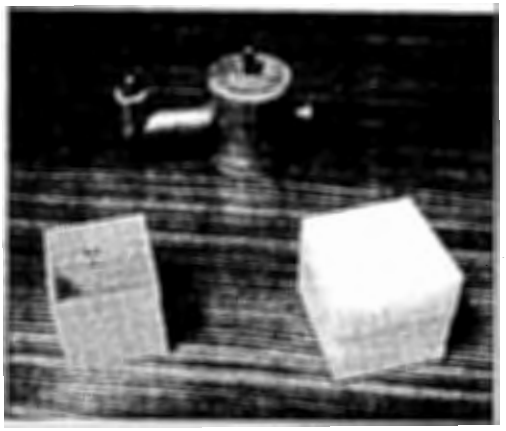

Fig. 5. Thermal neutron helium detector and two samples, plexiglas and polyethylene

Ackowledmements

The author wishes to thank doc. dr hab. Krzysztof Drozdowicz and mgr Barbara Gabańska (Laboratory of Neutron Transport Physics Department of Environmental and Radiation Transport Physics, Henryk Niewodniczański Institute of Nuclear Physics Polish Academy of Sciences, Kraków) for editorial assistance.

Americium Problem after Chernobyl Accident. Instrumental Methods of Am-241 Determination in Environmental Objects

O. Halochkina*, E. Khadzhinov

International Sakharov Environmental University, Minsk, Belarus

**e-mail: omiga@mail.ru*

The greatest contribution to effective dose after Chernobyl tragedy have brought Cs-137 and Sr-90. At the same time we should take into consideration the behavior of transuranic elements (TUE) in ecosystems because of their high radiotoxicity, long half-life period and kind of decay (because TUE are alpha-emitters).

After the accident on Chernobyl atomic power station in Belarus were 17 TUE, including uranium, neptunium, plutonium, americium. Now the most dangerous are Pu-238, Pu-239, Pu-240 and Am-241. At the moment on contaminated areas constant growth of americium content is observed due to beta-decay of Pu-241. Calculations show that the maximum level of pollution by Am-241 will be about the 2060^{th}. It will exceed a level of pollution by isotopes Pu-238 and Pu-240 in 2.7 times. About the 2086^{th} common alpha-radioactivity of soil on contaminated areas will be in 2.4 times above the initial period [1].

In line with these facts we have to consider the behavior of Am-241 in different ecosystems.

According to Belarusian laws zoning of territories depends on density of soil pollution by following radionuclides: Cs-137, Sr-90, Pu-238, Pu-239, Pu-240 and Pu-241. For today it is offered to use Am-241 instead of Pu-241 and to include Am-241 into the list of parameters for zoning territories.

Am-241 is one of the most dangerous radionuclides. First of all, it is alpha-emitter. Basic organs of americium deposition in organism are skeleton (up to 60%) and liver (30–40%). It's necessary to notice that from 10% to 40% of americium is removed with slow-removing fractions (48–1000 days). That's why it can lead such diseases as osteosarcoma, leukocythemia, tumor of lungs and so on [2].

Ecological danger of americium depends on its migratory properties in different parts of ecosystems. It makes researches in the area of "americium" problem very actual now.

For detection of Am-241 in soil following methods can be used:

- radiochemical: isolation of Am-241 from co-radionuclides (mainly alpha-emitting TUE), preparation of targets and measuring of alpha-radiation (E_α=5.49 MeV);
- incomplete radiochemistry: measurements of gamma-radiation are made after chemical procedures of concentrating and clearing from co-radionuclides (for example Cs-137);
- instrumental: based on registration of soft gamma-radiation without any preparations (E_γ=59.6 keV).

The last method does not require so much time and money as traditional methods of radio-chemistry. However the instrumental method demands a correct choice of gamma-detector.

In the modern situation of big variety of gamma-detectors, there are only few of them which have a good sensitivity for low energy gamma-radiation of Am-241. Within the task of zoning of territory it is necessary to choose the most suitable type. There are some criterions of "good" gamma-detector for Am-241: sensitivity, wide spread, mobility and, the last by order, but not by importance – price.

So, we have a task to classify existing detectors. As a base of classification may be comparison of the Minimum Detectable Activity (MDA) of Am-241. The MDA is a measure of the smallest activity, which could be detected by the device. The MDA is evaluated by the way of measurement of the corresponding isotope in a case of the real absence of this isotope in a sample [3].

Authors developed an algorithm of express-evaluation of the MDA of Am-241 in objects of an environment for scintillation and high pure germanium (HPGe) detectors. With this algorithm we save time on standard routine measurements, because we don't need for 20-50 of them, but the one.

Using the offered algorithm we checked the MDA of Am-241 for following devices:

- a gamma-spectrometer "NOMAD-PLUS" with the semi-conductor detector of type GMX;
- a gamma -spectrometer "NOMAD-PLUS" with the semi-conductor detector of type GEM;
- a gamma-beta-spectrometer EL-1315 with scintillation detector;
- a beta-gamma radiometer EL-1311 with combined scintillation block of detecting of type phosfich.

GEM and GMX detectors are HPGe detectors, they are produced by firma ORTEC, USA. The GMX detector differ by beryllium window. Such kind of detectors (especially the last with the beryllium window) allows to measure low-energy gamma-radiation.

The gamma-beta-spectrometer EL-1315 produced by Scientific and Production Enterprise ATOMTEX, Belarus and contains a crystal scintillator NaI(Tl). The crystal size is 63x63 mm. The beta-gamma-radiometer EL-1311 is produced by ATOMTEX too. It has phosfich detector. This kind of detector contains organic scintillator for beta-radiation (156x8 mm) and CsI(Na) for gamma-radiation (152x40 mm). We made measurement of different times and activities of co-radionuclide (K-40). The results of the measurements see in following table:

			EL-1311	EL-1315	NOMAD-PLUS GMX	NOMAD-PLUS GEM
m(KCl), g	A(K-40), Bq	t, s	MDA, Bq/sample	MDA, Bq/sample	MDA, Bq/sample	MDA, Bq/sample
–	–	7200	2.7	–	–	–
		10800	–	13.7	–	–
		25900	–	–	0.1	–
		55100	–	–	–	0.2
50	1700	3600	–	–	–	2.5
		5400	–	–	0.6	–
		7200	2.8	22.2	–	–
100	3400	3600	5.0	38.7	0.8	2.9
200	6800	3000	–	–	1.3	–
		3600	5.6	43.1	–	3.7
257	8738	3600	–	46.0	–	–
303	10302	3600	6.4	–	–	–

It is easy to see, the semi-conductor detectors have the best sensitivity. This result was rather predictable.

The most interesting are the results of beta-gamma radiometer EL-1311. The scintillator detector with a big crystal can give us the similar results, as some kinds of semi-conductor detectors. Considering cost of the equipment, operating conditions, prevalence, at

zoning territory of Belarus on a level TUE it is possible to assume an opportunity of use for the express-analysis beta-gamma radiometer EL-1311.

References

[1] The Scientific decision of Chernobyl problems (the basic results of 2001) // Committee on problems of consequences of accident on the Chernobyl atomic power station at Ministerial council of Byelorussia, Institute of radiology. - Minsk, 2002.

[2] V.A. Bazhenov, L.A. Buldakov, I.J. Vasilenko, etc., Harmful chemical substances. Radioactive substances. - Leningrad, 1990.

[3] V.A. Dementyev, Measurement small activities of radioactive preparations. - Moscow, 1967.

Spectrometry of Linear Energy Transfer Using TRACK-ETCH Detectors; Registration of Proton's Induced Heavier Secondary Particles

I. Jadrníčková, F. Spurný

Nuclear Physics Institute, AS CR, Na Truhlářce 39/64, 180 86 Praha 8, Czech Republic

Introduction

Risks from ionizing radiation depend both on the radiation quantity (absorbed dose) and the radiation quality (space and time distributions of dose and energy deposition distributions on the microscopic level). The radiation quality is characterized by the methods and procedures of microdosimetry. Current concept of radiation protection results from the connection between quality of concrete radiation and physical quantity – linear energy transfer (LET). For the purposes of measurements of LET spectra, there are several techniques. The tissue-equivalent proportional counter is probably one of the most used and accurate methods. However, in some cases its use can be compromised, for example at high dose rates and/or in the presence of very intense low LET component in the radiation field to be characterized. On the other hand, track etch detectors have some advantages, especially in situations where: dimensions and weight of detectors are important; high LET particles have to be characterized in low LET intense radiation beams and fields; and a long exposure time is expected.

Materials and methods

The spectrometer of LET based on a polyallyldiglycolcarbonate (PADC) chemically etched track detectors (TED) was developed in the Department of Radiation Dosimetry, Nuclear Physics Institute, AS CR [1, 2]. In the studies, three types of PADC materials are used: one available from Page (England) with a thickness of 0.5 mm, and another one available from Tastrak (Bristol) with thicknesses of 0.5 and 1 mm. After irradiation, the detectors are etched in 5 N NaOH at 70°C for 18 hours. To determine the LET value of a particle, the etching rate ratio V ($V=V_T/V_B$; where V_B is bulk etching rate and V_T is track etching rate) was primarily established through the determination of track parameters. They were measured by means of an automatic optical image analyzer LUCIA G. The V-spectra obtained were corrected for the critical angle of the detection and transformed into LET spectra using calibration curves based

on the heavy charged particles calibration. This LET spectrometer enables determining LET of particles approximately from 10 to 700 keV/μm. From LET spectra, dose characteristics can be calculated as:

$$D_{LET} = \int (dN / dL)\, L\, dL\,, \quad (1)$$

$$H_{LET} = \int (dN / dL)\, L\, Q(L)\, dL, \quad (2)$$

where dN/dL is the number of tracks in a LET interval, L is the value of LET, and $Q(L)$ is the ICRP 60 quality factor [1].

The detectors were irradiated by protons at Loma Linda University Medical Center (LLUMC) during experiment ICCHIBAN, and in the Joint Institute for Nuclear Research (JINR), Dubna. During experiment ICCHIBAN, exposure to monoenergetic protons with energies 70, 155, and 230 MeV was performed. Exposures to different doses (from 7 to 500 mGy) were made for all irradiation to study both proton dose registration efficiency and dose linearity. At Dubna, the detectors were exposed to 1 GeV protons and to two doses.

Results

First, it should be made clear the tracks of what particles are registered in PADC LET spectrometer. The LET threshold depends slightly on the choice of detector; it varies from 7 (Page) to about 22 (Tastrak 1 mm) keV/μm [3]. It follows that only tracks of protons with energy lower than about 6 (for Page) to 2 MeV (for Tastrak) [4] can be directly registered in a PADC LET spectrometer. Energies of protons used during experiments were higher; tracks observed correspond mainly to the secondary heavier charged particles created through nuclear interactions of primary protons with nuclei included in the detector and its surroundings.

The absorbed dose in the detector, D_{LET}, was calculated from the LET spectra and compared with ionisation collision dose of primary protons, D_{pic}. Good linearity of the response as a function of primary proton collision dose was observed. Further, the ratio of D_{LET} and D_{pic} was investigated. The values of D_{LET}/D_{pic} as a function of protons' energy are presented in Figure 1. Measured doses represent few percent of primary proton collision dose; their ratio varies slightly with proton energies.

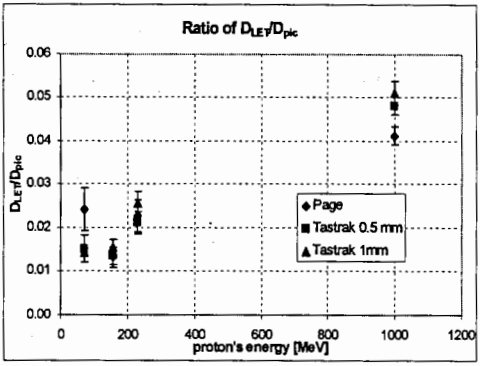

Fig. 1. Ratio D_{LET}/D_{pic}

The microdosimetric distributions of the absorbed dose *D(L)* in LET are presented in Figure 2. There are slight differences between PADCs in the spectra of *D(L)*: Page and 0.5 mm Tastrak show gradual growth up to about 200 keV/μm, while for 1 mm Tastrak one can see a plateau. With increasing energy of protons, the distribution of *D(L)* (related to 1 Gy) grows.

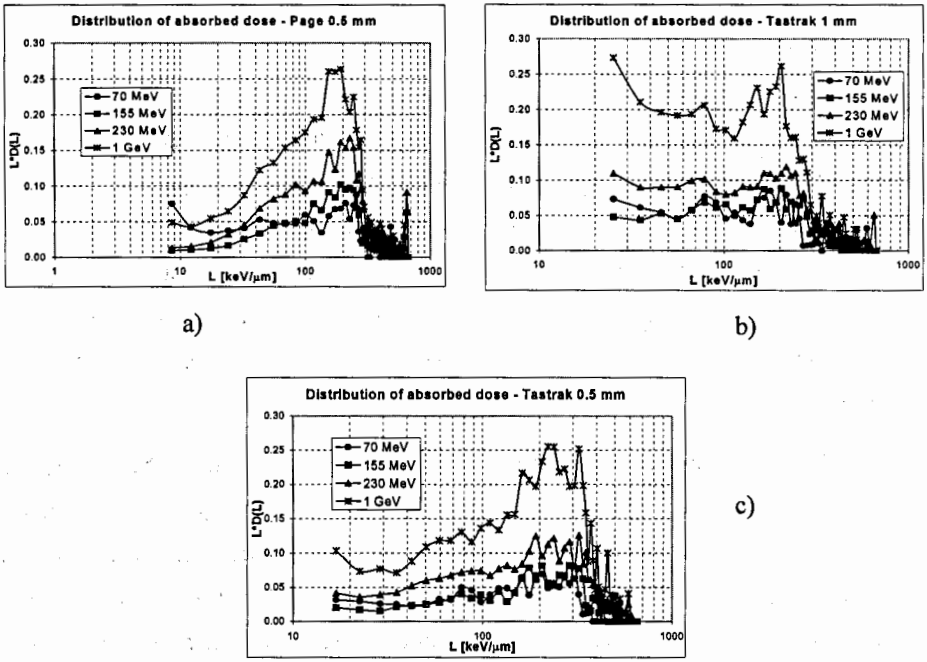

Fig. 2. Distribution of absorbed dose on 1 Gy as a function of LET for a) Page; b) 0.5 mm Tastrak; c) 1 mm Tastrak

Conclusion

The LET spectrometer based on the track-etch detectors have been developed. Some differences among individual materials of PADC have been observed, especially for lower energies of protons (70 MeV). Measured dose represents few percent of nominal dose; its ratio increases slightly with proton's energy.

References

[1] J. Charvát, LET spectrometry with polymer SSNTD's, PhD Thesis, Univ. of Prague, 1986.

[2] F. Spurný, J. Bednář, L. Johansson, A. Satherberg, LET spectra of secondary particles in CR 39 track etch detector, Radiation Measurements 26, 645-649, 1996.

[3] F. Spurný, I. Jadrníčková, A.G. Molokanov, V.P. Bamblevski, Upgrading of LET track-etch spectrometer calibration, Radiat. Measur.; to be published, Ref.: RM 2535, 2004.

[4] ICRU Report 49: Stopping Powers and Ranges for Protons and Alpha Particles, ICRU, Bethesda, 1993.

Nuclear Methods in Analytical Chemistry

Beata Jagucka, Justyna Jasińska

Faculty of Chemistry, Jagiellonian University, Krakow

Introduction

Nuclear methods are very useful in analytical chemistry. Nuclear techniques are complementary to non-nuclear methods. This techniques are fast, sensitive and provide a wealth of information, some of which is difficult or impossible to obtain by other means.

Nuclear chemistry methods are based on the measurement of isotopes. They use mainly properties of nucleus. This techniques deal with:

- nuclear excitations,
- electron inner shell excitations,
- nuclear reactions,
- radioactive decay.

In analytical chemistry all of following methods are being used:

- Neutron activation analysis (NAA),
- X-ray fluorescence spectrometry (XRF),
- Total reflection X-ray fluorescence spectrometry (TXRF),
- Particle-inducted X-ray emission spectrometry (PIXE).

Neutron activation analysis (NAA)

Neutron activation is an established analytical technique for determining trace elements in a wide variety of materials in solid, liquid, or gaseous states. Neutron activation analysis is the most sensitive analytical technique used for multi-elemental analysis. This method allows for qualitative and quantitative determination of major, minor, trace and rare elements. NAA is non-destructive technique.

Neutron activation analysis is based on the conversion of stable atomic nuclei into radioactive nuclei by irradiation with neutrons and subsequent measurement of the radiation, released by these radioactive nuclei. Radioactive nuclei can emit several types of radiation, but gamma-radiation offers the best characteristics for the selective and simultaneous determination of elements [1,2].

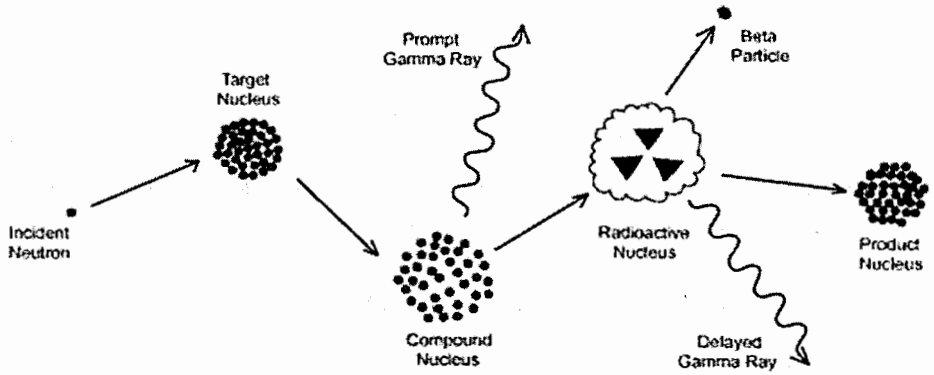

Fig. 1. Scheme of neutron activation [2]

X-ray fluorescence spectrometry

X-ray fluorescence is one of the oldest analytical techniques. XRF is a well established technique for qualitative and quantitative elemental analysis and it is fast, non-destructive, multi-elemental and requires minimal sample preparation. This method can be used to determine elements in solid, powdered and liquid samples.

When the sample is bombarded with appropriate energetic X-ray photons, characteristic radiation of the same nature is emitted by its chemical elements. This is X-ray fluorescence phenomena. Emitted X-rays are first collimated and then selectively separated

on the analyzing crystal by diffraction (energy-dispersive spectrometry works without a crystal). Number of emerging X-ray photons are measured with a proportional detector. Corrected intensities from inter-element effects are linearly correlated with certified concentrations of reference materials.

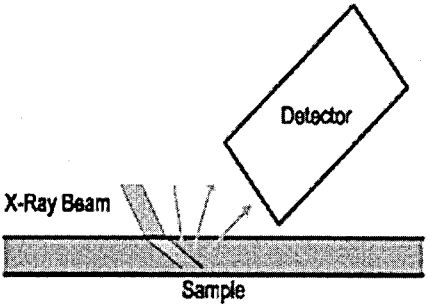

Fig. 2. Schematic of XRF [3]

The fluorescence X-radiation is characteristic for each element, what makes this technique very selective but less sensitive as NAA [1].

Total reflection X-ray fluorescence spectrometry (TXRF)

Total reflection X-ray fluorescence is a non-destructive surface analysis technique for ultra-trace analysis of particles, residues, and impurities on smooth surface.

Total reflection X-ray fluorescence spectrometry is a form of X-ray fluorescence spectrometry, that can be applied to very thin samples. TXRF is basically an energy dispersive XRF technique in a special geometry. An incident X-ray beam impinges upon a sample at angles below the critical angel for total reflection for X-rays, resulting of almost 100% of the primary beam photons. The background normally associated with XRF measurements is much reduced, leading to the higher sensitivity and lower detection limits. It is because only particles surface are excited giving rise to X-ray fluorescence emission.

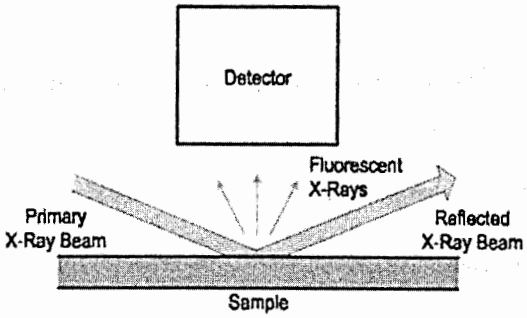

Fig.3. Schematic of TXRF [3]

Total reflection X-ray fluorescence spectrometry has many advantages. First of all the fluorescence intensity of the sample is doubled by excitation of both the direct and reflected beam. The background contribution from scattering on the sample is reduced. The detector can be mounted very close to the sample. This results in a large solid angle for the detection of the fluorescence signal [3,4].

Particle-inducted X-ray emission spectrometry (PIXE)

Particle-inducted X-ray emission is a sensitive, non-destructive, simultaneous elemental analysis of solid, liquid, thin film, and aerosol filter samples.

PIXE is a technique utilizing also X-ray fluorescence but without background. X-rays fluorescence is induced by bombardment of the target atoms with protons or charged particles with energies below threshold for nuclear reactions. When sample is bombarded with the beam, the protons interact with the electrons in the atoms of the sample, creating inner shell vacancies. The energy of the X-rays emitted when the vacancies are refilled is characteristic for the element from which they originated, and the intensity of X-rays is proportional to the amount of the corresponding element within the sample. The proton beam can be focused to a small cross-section (beam spot is in the order of 1 μm or less) and can also be deflected to produce a scan of the sample object. In this way, elemental maps can be created which can be superposed on an optical image from a microscope. PIXE technique has many advantages. It is very fast and sensitive analytical method especially for the lower atomic number elements [1].

References

[1] P. Bode, New horizons and challenges in environmental analysis and monitoring, Gdańsk, 18-29 August, 2003.

[2] http://www.elementalanalysis.com/naa/

[3] http://www.xos.com/txrf.htm

[4] http://www.gsinst.com/docfiles/Applications/pixe_application.htm

Statistic Analysis of Results from in Vivo Dosimetry in Radiotheraphy with the Use of Electron Beams

Aleksandra Kłos[1], Adam Konefał[2]

[1]*Department of Medical Physics,*

[2]*Department of Nuclear Physics and Its Applications,*

Institute of Physics, Silesian University, Katowice

The effect of radiotherapy depends on a precision of delivery of the planned dose to the target volume. The administration of a course of radiotherapy requires a whole series of steps starting from basic dosimetry over tumor localization, treatment planning, dose calculation, to patient immobilization. Malfunctions of apparatus, computer algorithms, human mistakes can contribute to a significant differences between the planned dose and received one.

The analysis of results of in vivo dosimetry in the electron beam radiotherapy is presented. The in vivo dosimetry measurements were carried out with the use of the EDE-5 semiconductor diodes in the Centre of Oncology in Gliwice. The detectors were linked to the DPD-510 electrometer (Scanditronix). The 0.6 cm^3 cylindrical ionization chamber (type NE 2571) and a tissue equivalent phantom composed of slabs with an area of 30 cm x 30 cm were used for the calibration of the applied detectors. The measurements were performed for 70 patients with cancers of the lung, chest and neck region. Total number of measurements was 208 (maximal 3 times for one patient). Patients were irradiated with the 9, 12, 15, 18 and 22 MeV electron beams generated by the biomedical accelerator Clinac Varian 2300 C/D. Detectors were positioned on the surface of the body at the centre of irradiated field. Results are shown on the histograms of percentage differences between the planned dose and received one (figures below).

Extremal values are -19% and 30% for the 9 MeV beam whereas -6%, 6% and -26%, 30% for 12 and 15 MeV, respectively. Analysis was not realized for 18 and 22 MeV because of only some cases. The extremal values were observed for single cases. The average of distribution is shifted to right side of histograms i.e. patients have given larger doses than the planned one. The differences do not exceed 5 % for majority of cases. That is in a good

agreement with the recommendation of ICRU. Deeper analysis showed that the main reason of the differences between the planned dose and delivered one is the algorythm of the planning treatment system CADPLAN.

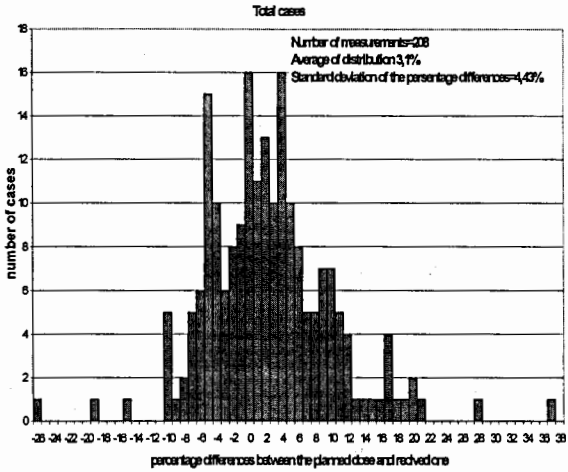

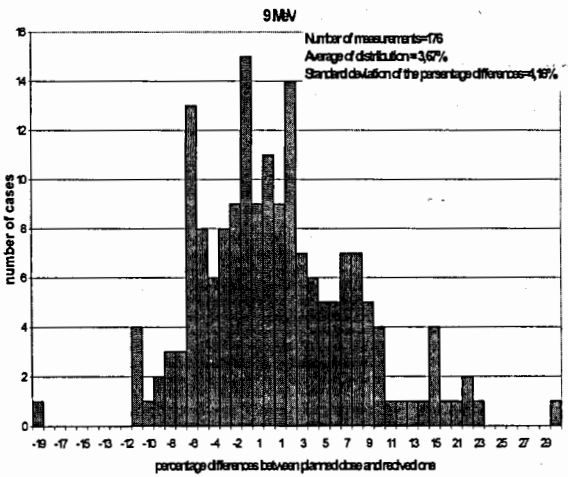

Radioactive Contamination of the Environment of Wood – Rings

Agnieszka Kluza, Grzegorz Bujnarowski

Institute of Physics, Opole University, Oleska 48, 45-052 Opole, Poland

Introduction

It is well known that the natural environment contains some amount of radioactive elements, originating from the natural sources present in Earth mantle and/or resulting from the interaction of cosmic rays with matter [1]. The radiation of the radioactive elements present in the natural environment forms some background level, harmless for the mankind, because of the adaptation in the evolution process. On the other hand, the radiation of the artificial radiation sources, with their intensity increasing with the civilization progress, may be imminent for the nature. Nuclear explosion tests, injuries to the nuclear power plants, and other radiation events stimulate the investigation of various aspects of the radioactive pollution on both the effects of the living organisms and on the inanimate matter.

The trunks of many kinds of trees display a grainy structure [2]. A new layer of a living tissue is built around the trunk of a growing tree. After few years this layer lignifies. In our climatic zone the layers of a new living tissue are growing in an annual cycle. The nourishing substances are transported only by the non–lignified peripheral part of the trunk composed from the last annual rings [3]. The wood-rings trap various chemical substances absorbed from the soil together with nourishing substances. If the area is polluted with radioactive elements, the permanent deposition of radioactive isotopes in annual rings of a tree is possible. Analysis of the chemical composition of annual rings is a source of information on climate and other changes in the environment, and, what is most important from our point of view, on the changes in the concentration of radioactive elements during the life of the tree.

Currently the changes in the pollution level in the annual layers of trees are widely carried on, depending on the age, kind and area where they are growing [4-7]. The purpose of this paper is to present the results of investigations of total β-activity as well as of spectrum of γ-radiation of a tree grown in Starkówek near Polanica in Poland.

Experimental

The tree chosen for the experiments was a 65 year old spruce (*Picea abies*) growing in the forest. From the trunk of the truncated tree a few centimeter thick slice, located about 70cm above the ground, was cutted of. After polishing its surfaces the slice was dried for few mount in a room conditions. After drying the slice was separated manually into subsequent annual rings. Chips of wood originating from indyvidual annual rings were burned in porcelain containers in an oven with free access of air. The combustion process was carried at temperature of 450^0C and lasted 4 hours. This way the wood was completely ashed. The combustion process was necessary to take away the carbon, strongly absorbing the β-radiation.

Thin layer of the obtained wood–ashes were located in standard measuring bowls and then the specific intensity of β-radiation was determinated using a standard detection system with a window–type Geiger–Müller counter. γ-radiation of some of the ashes, exhibiting an enhanced β-activity, has been investigated using a spectrometer equipped with a germanium detector. For the comparison purposes, the radiation of annual rings from the period before the years 1945 (first nuclear explosion tests) has been investigated, too.

Results and discussion

The experimentally determined dependence of the specific (per unit mass) intensity of β-radiation from individual annual rings on their age is represented on Fig. 1.

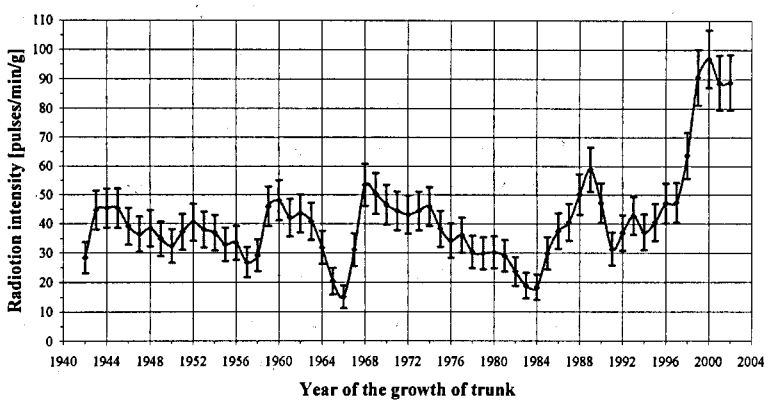

Fig. 1. Dependence of the intensity of radiation of ashed wood-rings

Few local maxima are clearly visible on this dependence, located at the years 1945, 1952, 1960–1963, 1968–1974 and 1989. The last maximum located at the year 2000 will not be interpreted in the present paper because of the lack of appropriate information about the nuclear explosion tests or injuries to the nuclear power plants. The remaining maxima of the β-activity correlate well with the periods of the intensive nuclear explosion tests [8].

This last statement is supported by the comparison of the age dependence of the intensity of β-radiation with the time dependence of the number of nuclear explosion tests (Fig. 2) and with the time dependence of total power of nuclear explosion tests (per year) – Fig. 3.

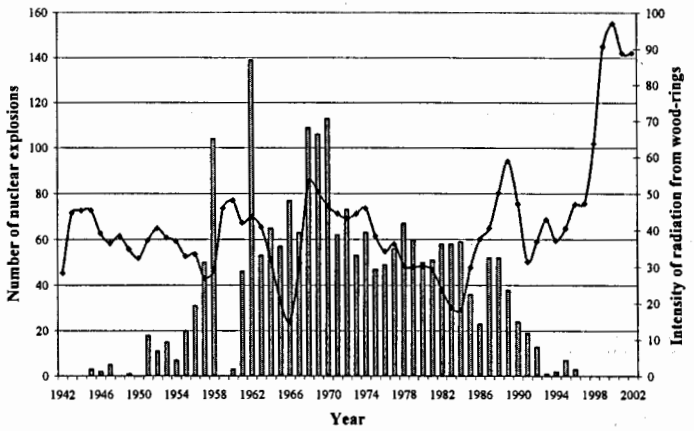

Fig. 2. Comparison of the changes of the intensity of β-radiation from ashes with the number of nuclear explosion in a year

As it seen from Figs 2 and 3, the positions of maxima of the intensity of β-radiation correlate well with the enhanced intensity of nuclear explosion tests. Increase in the intensity of β-radiation in the 1989 is, at least in part, caused by the damage of the Chernobyl nuclear power plant. There is some shift (tardiness) of the maxima of the intensity of β-radiation with respect to the maxima of the intensity of nuclear explosion test, resulting from the mechanism of transport of the radioactive elements to the trunk of the tree. Radioactive fall-out penetrates the soil with a velocity ranging from a dozen to several dozen centimeters per year. The tree begins to absorb the pollutants only after penetration at the depth of its rooting. Depending on that how deep the tree is rooted, it may last several years.

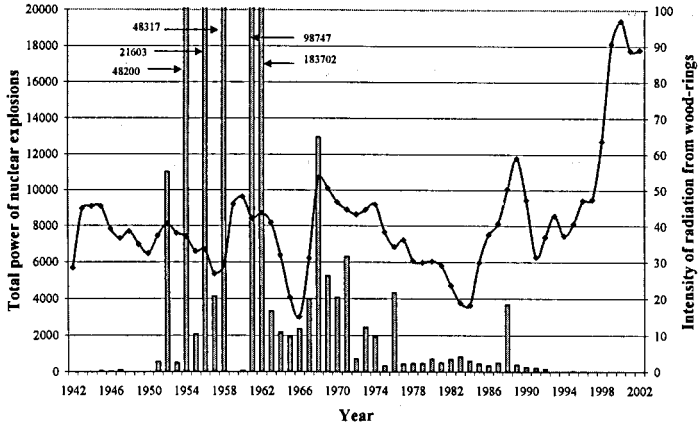

Fig. 3. Comparison of the changes of β-radiation from investigated ashes with the total power of nuclear test explosions in a year

Radioactive fall-out contains many different radioisotopes. The majority of them occur at slow concentration, or their decay is very fast. The main components of radioactive fall-out are ^{137}Cs, ^{90}Sr, ^{14}C, ^{144}Ce and ^{106}Ru. The remaining radioisotopes cause no serious threat because of their very short decay half-period. In our experiment, due to the application of the window–type Geiger–Müller counter as well as due to the sample preparation procedure, mainly the β-radiation of ^{90}Sr has been registered. Therefore, it can be stated that intensive radiation events (e. g. nuclear explosion tests or the consequences of the damages of nuclear power plants) cause an increase in the amount of ^{90}Sr radionuclide in the annual rings of growing trees.

For a better validation of this statement the spectrum of the γ-radiation for some ashes has been analysed. Basing on the results of these experiments the specific activity of several radioisotopes (^{40}K, ^{210}Pb, ^{211}Bi, ^{212}Bi, ^{214}Bi, ^{228}Ac, ^{231}Th and ^{235}U) has been determined. The age of dependences of the activity of these isotopes are shown in Fig. 4.

The activity of ^{40}K does not changes over the investigated period. It is easily understandable, because of its natural occurrence in the environment and long half-period amounting $1{,}28 \cdot 10^9$ years. For the remaining isotopes, belonging to the natural radioactive families, some changes in their activity are observed. This may suggest, that their presence in the wood does not result from the natural reasons. The possible reason may be artificial radioactive events. Similar investigations with similar conclusions are reported in [6].

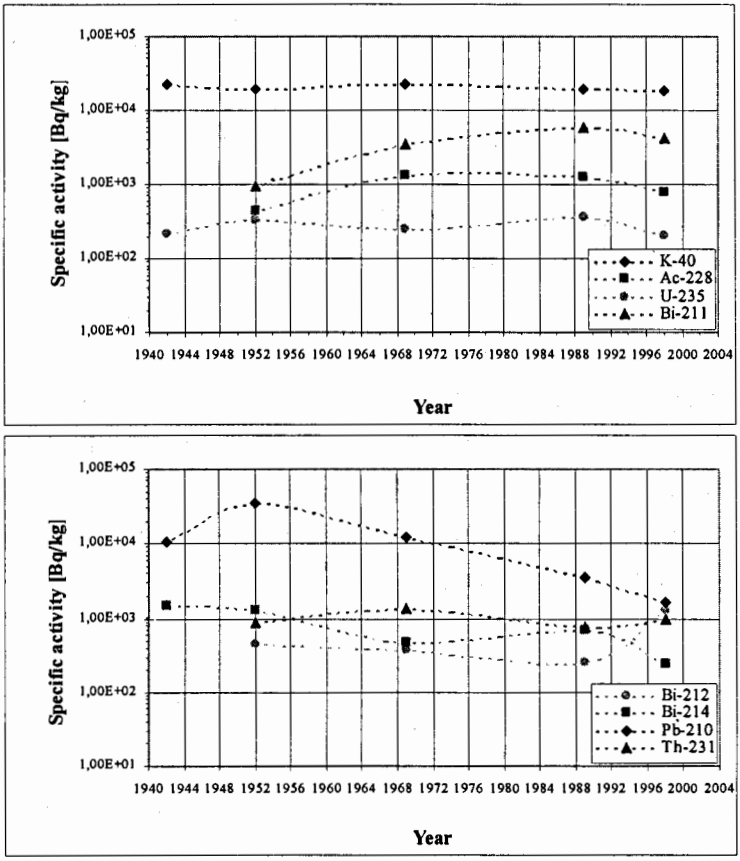

Fig. 4. Changes in the specific activity of chosen γ emitting isotopes in investigated ashes

The applied method permits to trace the occurrence of radioactive pollution in the area where the tree grows several years back. The method may be also used for preparation of maps of the areas contaminated many years ago. The method permits to verify the information

on the effect of nuclear explosion tests and damages of nuclear power plants on the environment as well as to reveal the hitherto unknown sources of the radiation pollution.

References

[1] A. Hrynkiewicz, ed. „Człowiek i promieniowanie jonizujące", Wydawnictwo Naukowe PWN, Warszawa (2001).

[2] A. Zielski, M. Krąpiec, „Dendrochronologia", Wydawnictwo Naukowe PWN, Warszawa (2004).

[3] A. Szwejkowska, „Fizjologia roślin", Wydawnictwo Naukowe UAM, Poznań (1998).

[4] G. Bujnarowski, A. A. Kluza, Z. Witkowski, K. Gąsiewicz, M. Dorociak, B. Białoń in „Młodzież akademicka a współczesna nauka", K. Jankowski, ed. Wydawnictwo Akademii Podlaskiej, pp. 31-35, Siedlce (2003).

[5] T. Majcherczyk, M. Wacławek, Chemia i Inżynieria Ekologiczna, T. 8, Nr 12, pp. 1269-1276, (2001).

[6] J. Pająk, M. Szuszkiewicz, A. Domagała, P. Krogul, Unpublished results, (1992).

[7] A. Kagawa, T. Aoki, N. Okada, Y. Katayama, J. Environ. Qual. 31, pp. 2001-2007 (2002).

[8] This information is compiled from unclassified Widley accepted sources – http://nuclearweaponarchive.org

Clinical Implementation of in-vivo Diode Dosimetry

Ondrej Koncek

Department of Dosimetry and Application of Ionizing Radiation

Faculty of Nuclear Sciences and Physical Engineering

Czech Technical University in Prague

Supervisor: Jan Hrbacek

In-vivo dosimetry is used as a Quality Assurance tool to measure the dose delivered to patients during radiotherapy. These dose measurements are compared with the target doses specified by the oncologist and calculated by the radiotherapy treatment plan.

In-vivo dosimetry in the University Hospital Motol is based on the entrance dose measurement, which is realized by using p-type and n-type semiconductor diodes (Isorad – Sun Nuclear Corp.) for all photon beams: Varian Clinac 600C (4 MV and 6 MV), Varian Clinac 2100C (6 MV, 18 MV). Each treatment room is equipped by 3 diodes for corresponding beam energy.

Diodes are a semiconductor analogy for ionisation chambers, which are too large and fragile to be used on patients. Diodes are used without external bias and only an electrostatic potential difference over depletion layer, which is created when diodes are doped, is used for minority charge collection.

Signal of diodes is influenced by following factors [1]:

a) **Photon energy:** A diode has a much higher atomic number ($Z_{Si} = 14$) compared to soft tissue ($Z_{eff} \approx 7$). Due to this difference the photoelectric effect is more important in the diode and it results in overestimation of the dose.

b) **Temperature:** With increasing temperature the energy of minority charge carries increases and probability of recombination decrease. And it leads in a higher response of diode per pulse.

c) **Accumulated dose:** As a consequence of accumulated dose is a progressive decrease in detector sensitivity. This is due to additional lattice defects, which are produced by the radiation and which act as recombination centers for the minority charge carries.

d) **Dose rate:** At higher dose rate the recombination centres are "occupied" which results in a relatively lower rate of recombination. This leads to a proportionally higher response at higher dose rates.

Due to these dependences the entrance dose measurement by diodes is also influenced by geometric parameters which could affect factors mentioned above. So set of correction factors has to be established to account for variations in diode response in situations deviating from the reference conditions. The factors influencing diode signal are mainly source to skin distance (SSD), field size, presence of a wedge because:

SSD: With increasing SSD is changing contribution of contaminating head-scatter electrons and also the dose per pulse.

Field size: Increasing field size results in a increase of number of scatter photons that come from flattening filter and that are not shielded by secondary collimators - so it is changing energy spectrum of the photons reaching the diodes.

Wedge: Inserting a wedge in the beam leads in a decrease of the dose rate and a hardening of the spectrum of the beam. Therefore, as the sensitivity of the diode depends on both dose rate and energy, a correction factor different from 1 is expected when using wedges.

The temperature dependence, should be accounted if a particular diode is used at different temperatures. This may be done by applying a temperature correction factor or by using a thermostatically controlled calibration phantom.

Beside the physical properties of the diode crystal, to the value of correction factors also contribute the fact that the measurements are performed with the diode located outside the patient or the phantom. The photon scatter conditions experienced by the diode are therefore different from those at the point of entrance dose definition, i.e. at the depth of dose maximum inside the patient or the phantom.

Our physical model incorporates corrections for field size, SSD, presence of a wedge and also temperature correction factor. Correction factors were measured by methods which are well described in numerous literatures and are not presented here (except temperature correction factor).

Temperature correction factor

When diodes are calibrated on a solid water phantom, they are in temperature equilibrium with room. But during clinical measurements, when diodes are placed on the patient skin, temperature of p-n junction increases and it results in a higher sensitivity of diode as was mentioned earlier.

To quantify this phenomenon diode was connected to a source of constant current according an arrangement on fig. 1. Then diode was put in a waterproof cap into a water phantom which temperature was measured by thermometer. Subsequent was measured voltage of p-n junction for several temperatures and calibration curve was gained. Note that for ideal diode this dependence (voltage on temperature) is linear in comparison with dependence of current on temperature, which is not linear. So it was possible to determine temperature of a p-n junction if the voltage on diode is known.

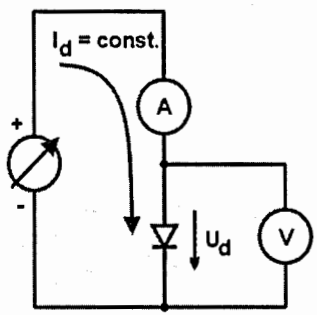

Fig. 1

But connection of diodes which is used in clinical mode does not allow determining temperature of p-n junction immediately. So correction for temperature may be done by applying a constant temperature correction factor.

Therefore were performed measurements on 15 patients for several parts of body to assign final skin temperature and also time which is necessary to reach temperature equilibrium.

Then was determined correction factor for a set of diodes as (1 - SVWT * Δt) where SVWT means sensitivity variation with temperature and Δt is the difference between room and average skin temperature.

SVWT was measured on a water phantom under reference conditions. Diodes were placed on the top of the phantom of a known temperature and were irradiated. This was performed for several temperatures (in a range from 20 °C to 40 °C).

Results

The database includes over 1690 records from measuring 230 patients. The overall average deviation from the prescribed dose is -0.70 % (SD = 0.07). The deviation less than ± 5 % (8 %) has been observed in 83.2 % (94.1 %) of all records (fig. 2). This includes also tangential field technique for breast cancer treatment with significantly wider spread deviations. In-vivo dosimetry proves to be a valuable tool for verification of delivery of prescribed dose and enables to discover major errors in the treatment planning process and patient's setup.

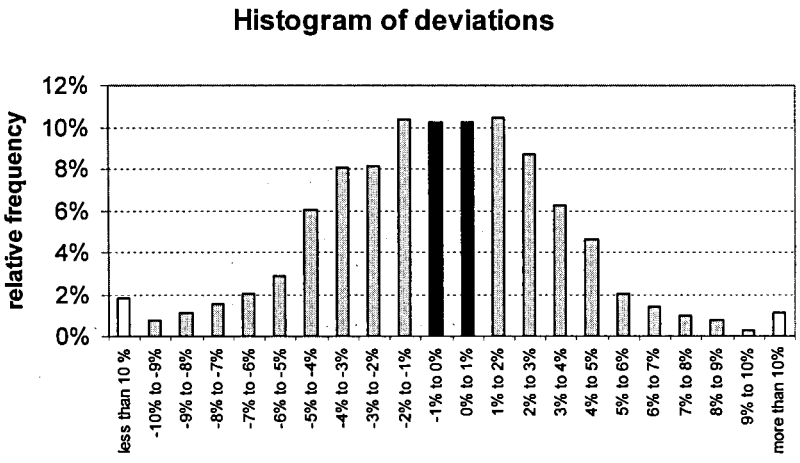

Fig. 2

References

[1] D. Huyskens, R. Bogaerts, J. Verstraete, M. Loof, H. Nystrom, C. Fiorino, S. Broggi, N. Jornet, M. Ribas, D. I. Thwaites, Practical guidelines for the implementation of in vivo dosimetry with diodes in external radiotherapy with photon beams (entrance dose), Physics for Clinical Radiotherapy ESTRO booklet 5, 2001.

The Detector Control System Board of the ALICE Experiment

Utilization of the DCS Board for status control of Silicon Drift Detectors of the Inner Tracking System

J. Kral, V. Petracek

Faculty of Nuclear Sciences and Physical Engineering, Czech Technical University

Prague, Czech Republic

ALICE and ITS

Work on a new accelerator and experiments is in progress at CERN. One of the recently build experiments is A Large Ion Collider Experiment. ALICE will focus on heavy-ion physics, proton-proton and lead-lead collisions at LHC energies (~5.5 TeV per nucleon). Main goal is to study quark-gluon plasma, which is expected to form in such density and temperature [1].

The experiment is composed of several detectors [2]. The innermost one, the ITS (Inner Tracking System), is ment to: determine primary vertex and secondary vertices necessary for the reconstruction of charm and hyperon decays, perform particle identification and tracking of low-momentum particles and participate on momentum and angle measurements [1]. The ITS is composed of six layers of silicon detectors; strip (SSD), drift (SDD) and pixel (SPD) detectors, each in two layers. This article deals with the SDD sub-detector.

Detector Control System

ALICE experiment is a complex device and requires a system, that provides synchronization with other devices, experiment status overview and ways to control the run of the experiment. Such a system is called the Experiment Control System (ECS). The Detector Control System is then a ECS's sub-system dealing with one detector only.It is a set of hardware and software components providing man to machine interfaces and configuration, process and operation control [3]. The DCS must provide complete supervision chain from field hardware to operator's screen and in opposite direction for carrying commands. For that, the DCS is composed of three layers: the supervising layer – the supervision and operation of

the detector; the controlling layer - the collection and processing of data; and the field layer - the connecting of the detector equipment to the DCS.

The field DCS layer can be also defined as a point, where commands from software part of system transform into device specific hardware communication. The supervising and the controlling layers of the DCS are realized on the software level. Field devices are simple, they do not and can not include any sophisticated computer to run programs to connect to the DCS. So arises a necessity of a device capable of working with software part of the chain and with device specific hardware part and carrying out the communication chain transition.

The DCS Board

A device meeting such needs has been under development at University of Heidelberg, the device name is Detector Control System Board (DCS Board) [4]. To connect to the software layers, the board incorporate a simple computer; processor, operation memory, flash memory and Ethernet controller. Programmable logic (FPGA) and various I/O controllers provide the board with ability to suite any specific device needs. The core of the board is the ALTERA Excalibur EPXA1F484C3 chip with integrated ARM922T standard 133MHz processor and FPGA [5]. The board is capable of running a Linux ARM architecture distribution. Any user software must be compiled for ARM architecture as well. Presence of a ordinary OS allows us to implement any software necessary for operation within the DCS. The board is completely manageable through the Ethernet network, once the OS and the FPGA image are loaded into flash memory by the JTAG chain for the first time. A RS232 interface is present for backup purpose.

The FPGA (user logic) is reprogrammed on every device boot according to the image stored in the flash memory. The user programmed logic registries are accessible for a kernel modules on defined memory addresses. The other side of user logic can be linked either directly to output pins or to LVDS (Low Voltage Differential Signalling) I/O units.

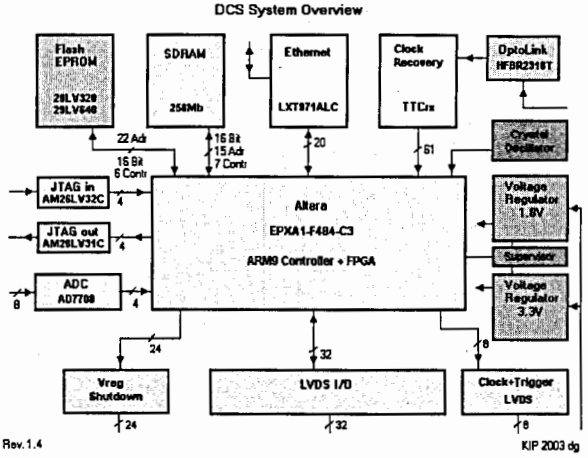

Fig 1. DCS Board block scheme [4]

Communication chain

The task we are working on is tosetup a chain, that will read temperature and low voltage data from the SDDs and make them available to the detector control system.

All the SDD wafers are mounted on a linear structures called ladders, each of them holding 6 or 8 detectors, depending on the layer [1]. Two front-end electronics modules (left, right) are attached to each wafer. The front-end modules on each ladder are connected to two low voltage half-module end-ladder cards. A DCU (Detector Control Unit) chip, capable of temperature and low voltage data readout, is present on each of the end-ladder cards. Two DCUs are operated by one control chip called Dilbert, which is then connected to the DCS Board.

The Dilbert chip provides a reset signals to both DCUs and possesses one additional ability. All three chips communicate by the I^2C bus protocol [6]. The realization of I^2C bus in between the DCUs and the Dilbert is not problematic because of the distances of several centimeters. The DCS Board is much farther from the Dilbert chip. The signal on I^2C bus would get lost in interference. For this reason a bus more stable to interference and capable of carrying the I^2C bus protocol communication is necessary in the Dilbert to Excalibur section, the "differential I^2C". The Dilbert is able to convert this differential signals back to standard I^2C. The same applies to the clock signal from the Excalibur chip.

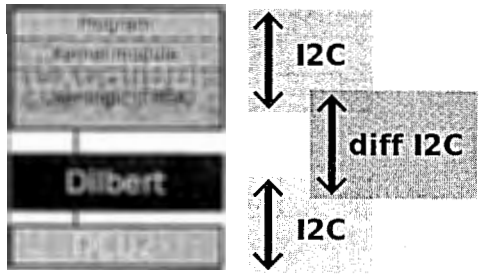

Fig 2. Communication chain scheme

$I^2$and differential I^2C

Nearly every electronic system includes a control unit coordinating work of task-specific units. This units are in need of some communication amongst them selves. To exploit this similarities, Philips developed a bi-directional 2-wire bus for efficient inter-IC control, the I^2C [6]. The bus is simple, requires only 2 lines (SCL serial clock line and SDA serial data line), yet powerful. Incorporates multi-master mode with collision detection and arbitration, 8-bit bi-directional data transfers up to 3.4 Mbits/s, units are software addressable and can be simply clipped or unclipped directly to the bus. The bus was meant to be used on PCBs and its bare bus design triggers problems while used for communication on longer distances, especially in environments with interference. Which is the case here. Both cores of the Excalibur and the Dilbert communicate using I^2C, but their distance is approximately 2.5 m. Modifications to the bus needed to be done, in order to increase its reach and make it more resistant to interference.

One way to achieve the goal is to encapsulate the I^2C communication by another bus, which already fits into criteria. The LVDS (Low-Voltage Differential Signaling) is a good choice. Its differential nature makes the LVDS resistant to interference and the communication distance ranges up to several meters. The downside of the LVDS usage is the wire count. The bus is uni-directional, thus requires separate line for each direction. The original necessity for 2 wires for the I^2C changes into necessity of 8 wires (SDA and SCL, each by 2 directions, each direction by 2 wires).

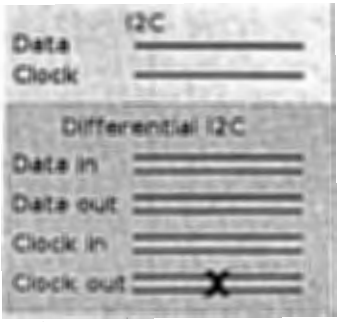

Fig 3. I^2C versus differential I^2C

Having so many wires inside the detector is always not comfortable because of space reasons. The nature of our Excalibur-Dilbert-DCU chain is that there is present one master chip only (Excalibur). The Dilbert and the DCUs will always behave as slaves (and will not generate clock pulses). This allows us to remove the SCL line in direction from the DCU to the Excalibur, which leaves us with 6 wires, but introduces deviation from standardized I^2C. The transition from the I^2C to the LVDS and backwards is realized on inputs of the Excalibur and the Dilbert chips, so their cores do not know of any LVDS and talk standard I^2C. Since the Dilbert and the DCUs are slaves always, there is no need to introduce any changes into the I^2C implementation because of the standard deviation either.

Software

The software portion of development consist of three parts. Primarily, the Excalibur's FPGA needs to be programmed for the I^2C to differential I^2Ctransition. Low-level part of the I^2C protocol support is also implemented in the FPGA. Code for the I^2C protocol support was taken from OpenCores [7] repository and modified to perform the transition.

Next step in software development is to create the device drivers (Linux kernel module), to provide connection between user programs and the FPGA. The code for the module was taken from Opencores repository again, but widely rewritten to exactly suite the needs of our chips. While the FPGA implements the low-level I^2C protocol support, such as clock and signal generation, the module provides the rest; addressing, acknowledge signals and device files.

Each of the DCU's or the Dilbert's registers is accessible via a device file. A user program just opens a corresponding file, reads and writes data and closes the file.

C function libraries were written to provide more comfort for following DCS development. Library functions include data loss, false read and write protection.

Conclusion

The system is planned to be operationalduring the year 2006 and will be used during the ALICE experiment initial testing and during conducting of experiments afterwards.

References

[1] ALICE, Technical Design Report of the Inner Tracking System, CERN, 1999.

[2] ALICE experiment website, http://aliceinfo.cern.ch/, CERN

[3] L.Jirdén, ALICE Detector Control System Project, http://alicedcs.web.cern.ch/AliceDCS/Documents/DCSProject.pdf, 2001.

[4] DCS Board Documentation Page, University of Heidelberg, Kirchhoff-Institut für Physik, http://www.kip.uni-heidelberg.de/ti/DCS-Board/current/index.html

[5] ALTERA, Excalibur Device Overview Data Sheet, version 2.0, 2002.

[6] Philips Semiconductors, The I^2C bus specification, version 2.1, 2000.

[7] The OpenCores project, http://www.opencores.org

Proton Beam Dosimetry in an Alderson Phantom

M. Mumot, G. Mytsin

Joint Institute for Nuclear Research

Since 1967, proton therapy research has been conducted at the Joint Institute for Nuclear Research (JINR). The described experiment involved a beam and routine equipment used in proton therapy and is closely connected with treatment performed at JINR's Medico-Technical Complex.

The experiment had the following two aims: to verify the dose distributions in a patient's body and to check the dosimetry methods used in an Alderson phantom. Measuring dose distributions in a patient's body in vivo is of course impossible; to avoid this difficulty, we used an Alderson phantom, which is an anthropoid, tissue-equivalent phantom and could be a good substitute of the human body (fig.1). This was the first experiment with this phantom in a proton beam, so we wanted to work out methodology for the routine usage of this phantom.

As a detector, we used radiochromic films and the TLDs (lithium fluoride made by Harshaw). We used these kinds of dosimeter putting them into the phantom (there are special holes for putting TLDs in every layer of the phantom).

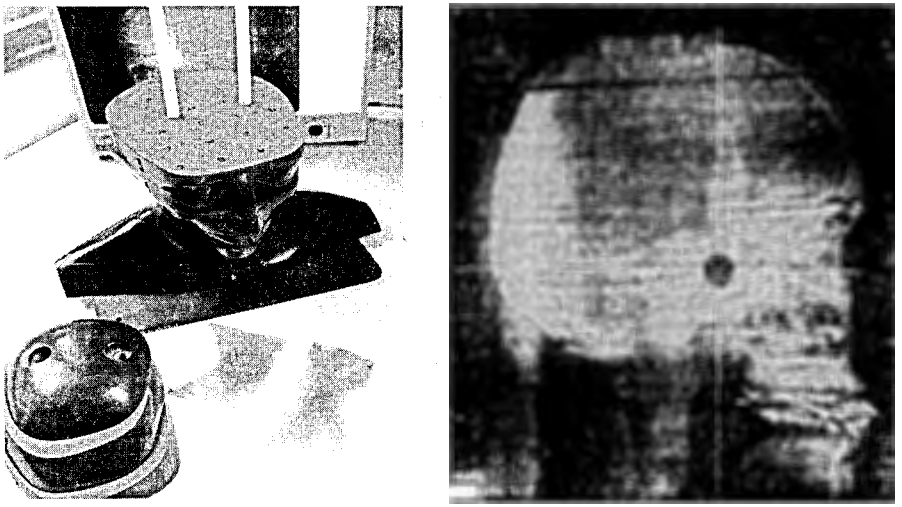

Fig.1. External appearance and internal structure of an Alderson phantom

The films consist of an active layer (an organic matter – for example, polydiacetylene), which is sandwiched between polyester layers (fig 2). Under the influence of irradiation, the active layers undergo polymerization producing polyconjugted polymer chains which exhibit the blue coloration.

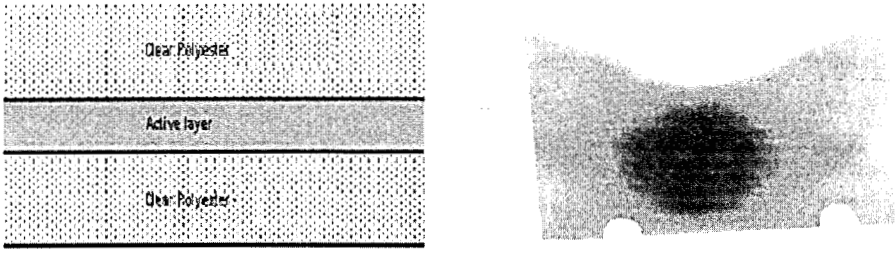

Fig.2. Structure and example of a radiochromic film

Three treatment plans were prepared for different clinical cases, and the CT scans of the phantom were done. The target was drawn on the scans; a physician determined the target, number of fields, and modifiers to get the best dose distributions for these cases. The maximum dose delivered to the phantom with the films was 60Gy; the maximum dose for TLDs was 2 Gy because of the dose range suitable for this kind of dosimeters. After 48 hours, the films were scanned; the obtained bitmaps were digitized into the dose matrixes using a calibration curve. The main isodoses were drawn and overlaid on the same isodoses from the treatment planning system. The results of this performance are shown on figures 3, 4, and 5. The next pictures present the dose profiles for all three cases (fig. 6, 7, and 8).

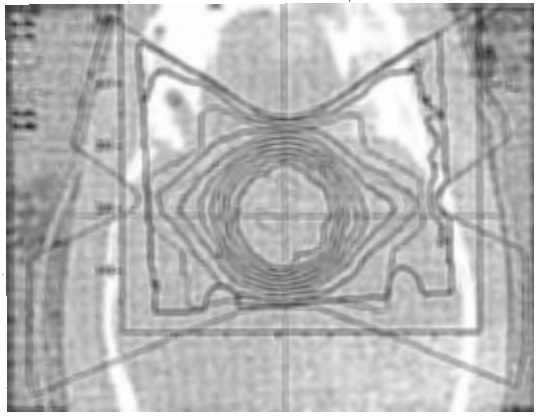

Fig.3. Isodoses from the treatment planning system (color) and measured using a radiochromic film for the first target

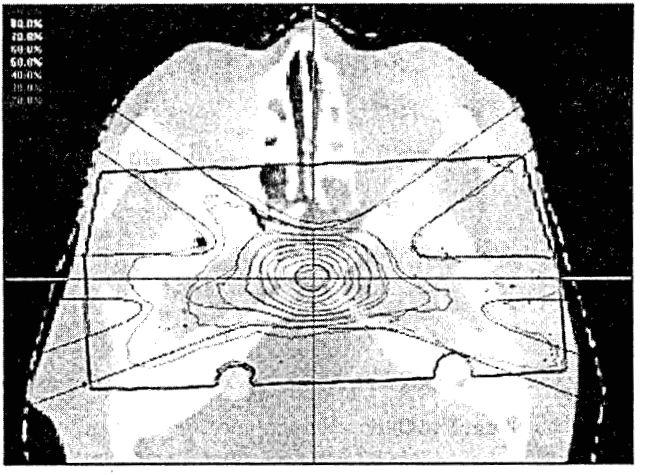

Fig.4. Isodoses from the treatment planning system (color) and measured using a radiochromic film for the second target

Fig. 5. Isodoses from the treatment planning system (color) and measured using a radiochromic film for the third target

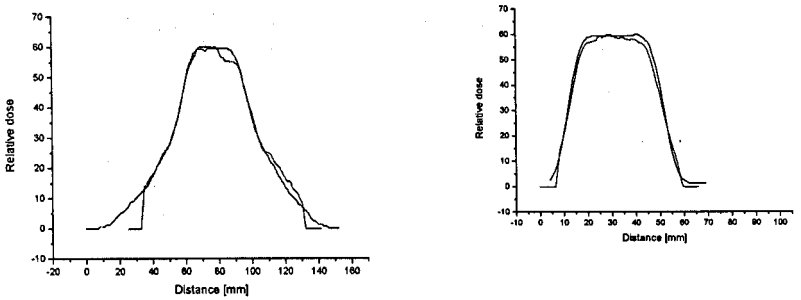

Fig. 6. Profiles along the x and y axes of target 1 (the red line is a profile from the film; the black line, from the treatment planning system)

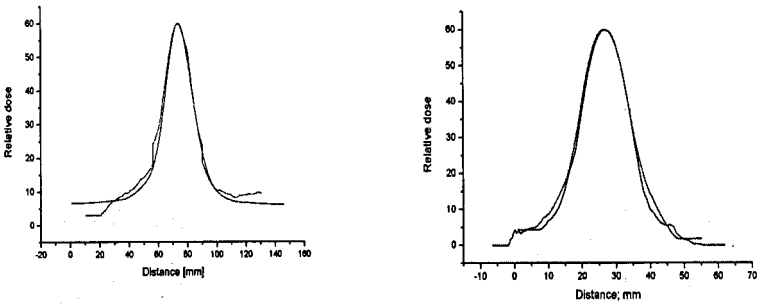

Fig. 7. Profiles along the x and y axes of target 2

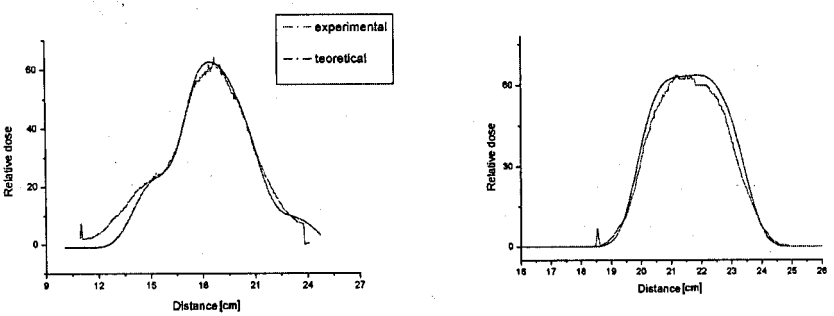

Fig. 8. Profiles along the x and y axes of target 3

We have no dose matrixes from the treatment plan, so we have done an analysis comparing the areas limited by isodoses from the plan and from films. The planned area was

taken as 100% and the area from measurements as respectively less portion (table 1). We can see that underdosage on the film is greater for higher doses near the Bragg peak. The differences in doses under 6% can be explained by RCF heterogeneity. We found that the films show greater underdosage in the Bragg peak region, which was also mentioned in other articles describing an experiment with radiochromic films in a proton beam (Vatinsky *et al* 1997; Piermattei *et al* 2000).

Table 1. Comparison of areas limited by isodoses measured using a film and from the treatment planning system

isodoses	**90%**	**80%**	**70%**	**60%**	**50%**	**40%**
Target 1	83%	91%	92%	94%	97%	99%
Target 2	97%	99%	98%	98%	99%	99%
Target 3	89%	90%	89%	89%	93%	94%

The TLDs were calibrated with Co60 and their individual coefficients were determined. A set of detectors was irradiated with a proton beam to a known dose to transform the individual coefficient for the protons. Taking into account all the coefficients, for 12 of 25 detectors the difference between the results obtained from measurements in the Alderson phantom and the planned dose is more than 5%. We checked the individual coefficients after the experiment and found that they had changed. It turned out that a number of detectors had mechanical microdefects and some of them had microscopic contamination with the phantom material. Concluding, we should propose another method for placing detectors in a phantom.

There is a good agreement between the plan and results obtained with radiochromic films, but we should observe their accurate response to proton radiation, especially near the Bragg peak. Further experiments are planned.

Dosimetry in Interventional Radiology

Jan Mužík

Faculty of Nuclear Sciences and Physical Engineering

Czech Technical University in Prague

Marcela Žáková

Na Homolce Hospital, Prague, Czech Republic

Interventional radiology is rapidly developing clinical specialization. There are new and more complex kinds of interventional procedures as a result in progress in medicine. Fluoroscopically guided interventions involve longer exposure than in other radiological diagnostics. Irradiations of both groups - the patients and clinical staff - may be thereby relatively high. On the other hand these techniques allow effective treatment of many diseases that could be otherwise treated only by surgical procedures under full anaesthesia which mean apparently higher risk for the patient. Therapeutic interventional radiology thus helps or replaces surgery and decreases the length of stay in hospital.

Interventional radiology represents image guided therapeutic procedures (interventions). These methods are usually performed under local anaesthesia. Image guidance is performed generally by fluoroscopy. Recently methods of US, CT and MR are employed as well for the localization and control of the result.

In general radiology various quantities and terminologies have been used (sometimes incorrectly) for the specification of dose on the central beam axis at the point at which X-ray beam enters the patient or a phantom. The same names for the different quantities are used. Conversely e.g. one abbreviation (ESD) is using for entrance dose in meaning to absorption in air (surface) and in skin (tissue). For each quantity it is necessary to provide the conditions of measurement, i.e. point of measurement and whether the back scatter contribution is included.

As a *direct dose measurement methods* are considered those in which the dose is determined by a direct measurement at or very near the skin during the procedure. Such a dose measurement could be done e.g. using TLDs placed directly on the patient. For patient

dosimetry in diagnostics and interventional radiology various types of films are used, too. The next dose measuring method is usage of real-time small detectors during the fluoroscopy.

Indirect or *calculation dose determining methods* are those in which the dose at the skin is inferred from dose measurement at other locations or from other equipment parameters. In case that the device is equipped with DAP meter, the dose can be determined from DAP quantity. In case that the system parameters and geometric setting with X-ray tube characteristic are known, the calculation of dose or dose rate in the point can be done.

Within the scope of diploma thesis the determination of patient doses undergoing the treatment of arterial aneurysms using endovascular replacement was performed. Two methods of indirect dose measurement have been used, determining from measurement of Dose-Area-Product and deriving from system parameters and radiation output. These methods were verified comparing the results with the values directly measured using thermoluminescence dosimeters (TLD). The thesis focuses also on radiation protection and possibilities of dose reduction.

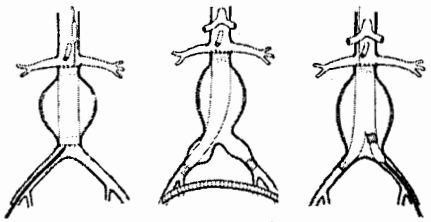

Fig. 1.Treatment of arterial aneurysms using endovascular replacement
A. Ferko, A. Krajina, et al. Arteriální aneuryzmata

The measurement ran on mobile X-ray machine OEC 9800 Mobile C-Arm with 1k x 1k WorkStation in Na Homolce Hospital (Czech Republic). Measurements in open beam were carried out using plane parallel ionizing chamber PTW type 77334 with the volume of 1 cm^3. Chamber was connected in dosimetric chain with electrometer PTW Unidos. Scattered radiation was measured using TOL/F device by Berthold Technologies. The patient was replaced during the measurement by phantom which attenuated the X-ray beam equivalently to 15, 20 and 30 cm of water. As a next replacement of the patient the anthropomorphic RANDO® phantom was used.

Fig. 2. OEC 9800 Mobile C-Arm and anthropomorphic RANDO® phantom

The values computed using DAP were higher in comparison with ionizing chamber measurements by c. 15 % at 80 kV (continuous mode). The manufacturer states the typical uncertainty ± 15 % and the total uncertainty (for the larger fields) ± 25 %. The results stayed in these limits, but they were conspicuously only at one side of the interval.

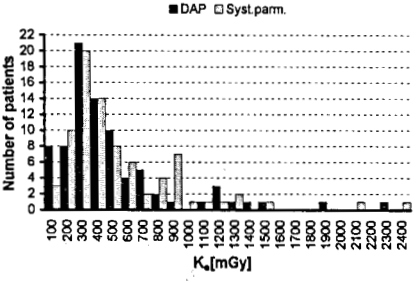

Fig. 3. Histogram of determined dose distribution

Continuous and pulsed mode of the X-ray tube was compared for the same attenuating material thickness. It was found out that the dose rate for the pulsed mode of general fluoroscopy (8PPS) is around one third in comparison with continuous mode.

Application of mobile shielding barrier provides extra protection in terms of one order. It results from the analysis of resulting values the most frequent value of entrance surface dose to be around 300 mGy. Cases exceeding the deterministic threshold value of 2 Gy occurred, too. The third quartile of the value group is determined to be around double of the most frequent dose, i.e. 600 mGy.

References

[1] S. Balter, et al., Techniques to estimate radiation dose to skin during fluoroscopically guided procedures. Skin Dose Measurement AAPM July 2002.

[2] A. Ferko, A. Krajina et al., Arteriální aneuryzmata. Základy endovaskulární léčby. Nakladatelství a grafické studio ATD Hradec Králové, 1999, 166 s.

[3] J. Muzik, Dozimetrie radiologických intervenčních výkonů: diploma thesis. Prague: CTU Faculty of Nuclear Sciences and Physical Engineering, 2005. 120 p.

[4] WHO Geneva. Efficacy and radiation safety in interventional radiology. Joint WHO/ISH Workshop on Efficacy and Radiation Safety in Interventional Radiology; 1996 October 9-13; Neuherberg, Germany. World Health Organization Geneva 2000.

[5] J. Zoetelief et al., Dosimetry in diagnostic and interventional radiology: ICRU and IAEA activities. Standards and Codes of Practice in Medical Radiation Dosimetry: proceedings of an international symposium held in Vienna, Austria, 25–28 November 2002 / organized by the International Atomic Energy Agency.

Effective Dose Evaluation in Diagnostic Radiology Procedures by Means of TL Dosimetry

L. Novak

Department of Dosimetry and Application of Ionising Radiation, Faculty of Nuclear Sciences and Physical Engineering, CTU, Brehova 7, 115 19 Prague 1, Czech Republic

National Radiation Protection Institute, Srobarova 48, 100 00 Prague 10, Czech Republic

Diagnostic procedures using X-rays are the most common application of radiation in medicine. The amount of radiation received by the population during X-ray examinations can be expressed in terms of a collective dose. To quantify the collective dose, typical effective doses per X-ray procedure must be known. The effective doses for X-ray examinations range between several microsieverts and several millisieverts. The effective dose is a weighted-organ dose quantity and therefore cannot be measured directly. To obtain a value for the effective dose, it is essential to know the absorbed doses in all radiosensitive organs. There are two approaches available to determine the organ doses for a particular X-ray examination. The first approach is to use a simplified mathematical model of a human body and a Monte Carlo simulation of radiation transport through this mathematical phantom. The second approach is to use an anthropomorphic phantom loaded with appropriate detectors and irradiate it in the same way as a patient. Thermoluminescent dosimeters (TLDs) are the most suitable detectors for this purpose. This method can verify the Monte Carlo model and also enables assessment of the organ and of effective doses for very complex and difficult X-ray procedures such us interventional examinations, for which computational models are not yet available. In this study, the organ and effective doses for four types of routine X-ray examinations were evaluated using the direct method with an anthropomorphic phantom and TLDs. The results were compared with two very widely used computational programs.

Before the phantom measurements, the whole TLD system was optimized. Major problems in dosimetry in diagnostic radiology are the very low doses applied to patients and also the wide range of energies in the X-ray emission spectrum. Moreover, photon energies in a spectrum range usually between 20 kV – 120 kV; TL detectors show strong energy dependence in this energy range. To avoid excessively high uncertainty due to energy dependence, and to detect doses in the microgray range, LiF:Mg,Cu,P was chosen as a TL

material, because of its tissue equivalence, and its very high sensitivity. This material also has excellent fading properties, its light sensitivity is negligible and the annealing procedure is very simple. As a reader, manual the Harshaw 4500 TL system with corresponding Winrems software was used to measure and evaluate the signal from the TL dosimeters. Physical form of the TLDs was a sintered chip with a diameter 4,5 mm and a thickness 0,9 mm.

Before each irradiation-readout cycle, oven-annealing was performed. The TLDs were annealed at 240°C for 10 minutes and then they were rapidly cooled down to room temperature. After the first oven annealing, the individual background and individual sensitivity correction coefficients were assessed for each of the TLDs. When corrected, the readout values show differences ±5% (2 SD) after a homogeneous irradiation. After these initial experiments, the energy and angular dependence of the TLDs were determined. Energy dependence of LiF:Mg,Cu,P does not exceed 20% relative to ^{137}Cs gamma radiation (see fig. 1). If calibrated in the corresponding energy range (similar voltage and half-value layer), the energy dependence does not exceed ±2% (see fig. 2). The angular dependence does not exceed 5% if the orientation of a TLD in a measurement field matches the orientation in a calibration field (see fig. 3). There was no need for fading correction during the experiments, because the measurement and calibration dosimeters were annealed, irradiated and read out together at the same time. Calibration of the TLDs was performed against a PTW DIADOS electrometer and the corresponding semiconductor detector with combined uncertainty 5% (2 SD). The combined uncertainty of dose assessment with TLDs is less than 10%.

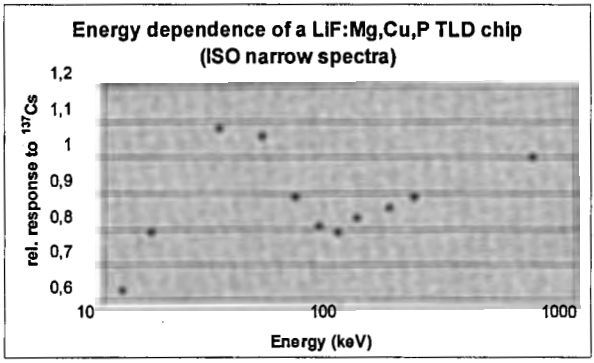

Fig. 1. Energy dependence of LiF: Mg, Cu, P (narrow spectra)

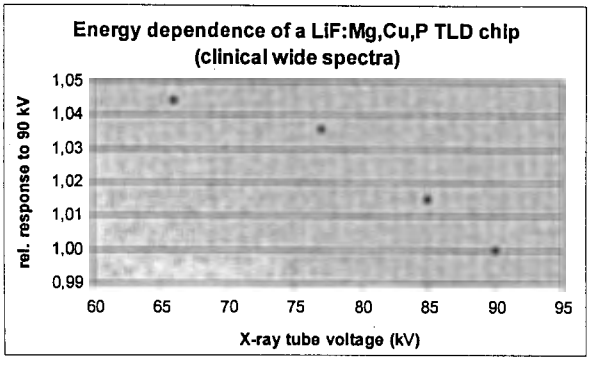

Fig. 2. Energy dependence of LiF:Mg, Cu, P (clinical spectra)

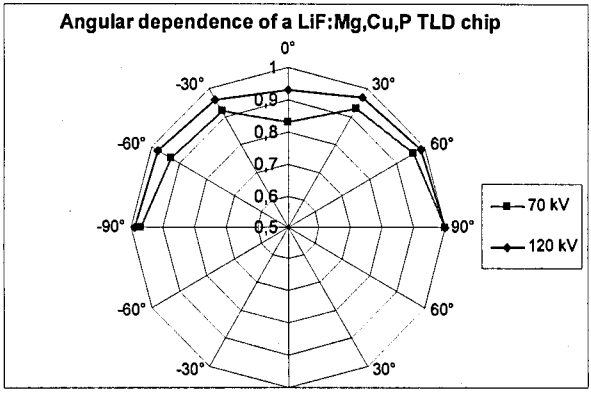

Fig. 3. Angular dependence of LiF:Mg, Cu, P

To obtain the doses absorbed to radiosensitive organs, an anthropomorphic RANDO phantom loaded with 100 TLDs was used for each type of examination. The RANDO phantom consists of a bone, lung and soft tissue equivalent material, and simulates the torso of a reference man. It is sectioned into 35 slices 2,5 cm in thickness. Holes 5 mm in diameter are drilled in a 3 x 3 cm array in each slice (see fig. 4 and 5). The correlation between the position of the radiosensitive organs in a human body and the holes in the slices of the phantom was made according to an anatomical atlas of CT slices [1]. Exposures of the phantom were performed using a Chirana MP-15 X-ray unit. A standard X-ray examination of a chest (low and high voltage technique), head, and abdomen were simulated. Calibration of the TLDs in terms of air kerma was made at the same unit. In the energy range of radiation used in diagnostic radiology, the air kerma and the absorbed dose in air can be considered

equal. In order to convert the dose in air to the dose in tissue or the dose to bone and bone marrow, the dose in air was multiplied by a factor of 1,06 or 1,1 respectively [2, 3].

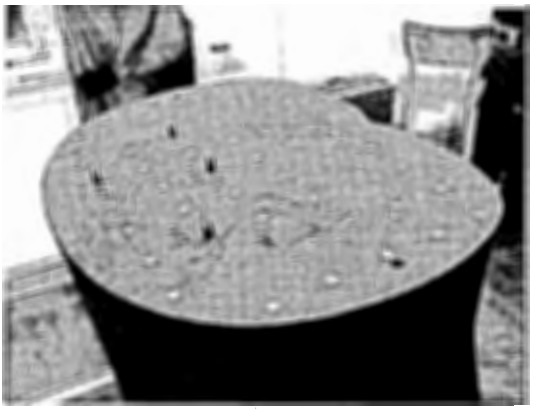

Fig. 4 and Fig. 5. Anthropomorphic RANDO phantom, general view and a slide with TLDs

The organ doses measured inside the phantom and the corresponding effective doses were compared with the doses obtained from two Monte Carlo based programs PCXMC and NRPB [3, 4]. Comparison of the results is shown in table 1.

Table 1: Effective dose estimated from TLD measurement and by MC programs

	Effective dose (mSv)		
	TLD	PCXMC	NRPB
Lung 117 kV (PA)	0,05	0,03	0,03
Lung 63 kV (PA)	0,06	0,04	0,04
Head (AP)	0,07	0,06	0,03
Abdomen (AP)	1,22	0,89	0,68

The results from the TLD measurements were systematically higher than the results from the computational models. The reason lies in insufficient coverage of the large organs (skin, bones, lung) with TLDs. Because of the small number of available TLDs, the

dosimeters were placed only into organ parts with the maximum dose. Quite good agreement was achieved in head examinations, where coverage of the head region of the phantom with TLDs was satisfactory. The second reason for the discrepancies is a difference in the organ position in mathematical and anthropomorphic phantoms and the setting of the X-ray field in the case of the phantoms. To achieve better agreement between the results, it is essential to perform the measurements with a greater number of TLDs and also to compare the results with other sources of available data.

References

[1] P. Fleckenstein, J. Tranum-Jensen, Anatomy in diagnostic imaging, Blackwell Publishing, 2001, pp. 262–350.

[2] M. Toivonen, C. Aschan, S. Rannikko, K. Karila, S. Savolainen, Organ dose determinations of X-ray examinations using TL detectors for verification of computed doses, Radiat. Prot. Dos. Vol. 66, Nos. 1-4, 199, pp. 289–294.

[3] M. Tapiovaara, M. Lakkisto, A. Servomaa, A PC-based Monte Carlo program for calculating patient doses in medical x-ray examinations, STUK-A139, 1997.

[4] D. Hart, D.G. Jones, B.F. Wall, Normalised Organ Doses for Medical X-Ray Examinations Calculated Using Monte Carlo Techniques, NRPB-SR262, 1994.

Detection of High Energy Cosmic Rays and Project CZELTA

Michal Nyklíček, Karel Smolek

Czech Technical University in Prague, the Czech Republic

Cosmic Rays

The study of cosmic rays began on the beginning of the 20th century. That time, there was a problem with spontaneous discharging of a well isolated electrosop. At first, scientists thought that it can be caused by radiation originated in the Earth. However, in the year 1912, Viktor Hess realized a balloon flight to the height of about 5 km and observed that the discharging of an electroscop was faster than on the surface of the Earth. In this way, it was proved that the source of the radiation must be outside the Earth and the history of studying of cosmic rays began.

In the year 1927, D. V. Skolbecin observed an electron with the energy of 20 MeV and in 1932 C. D. Anderson discovered a positron in cosmic rays. A few years later, in the year 1937, Anderson and Neddermayer observed a muon in cosmic rays. In the next year, Pierre Auger observed showers of secondary cosmic rays (Extensive Air Showers). In 1946, the first detector for detection of secondary cosmic ray showers was built. In 1962, the shower of secondary cosmic rays produced by a particle with the extreme energy of 10^{20} eV was detected.

What is the origin of cosmic rays? The presently accepted view is that ultrahigh energy cosmic rays are created and accelerated in active cosmic objects, like as supernovae, pulsars, galactic nuclei, quasars and radio galaxies. Because of the interaction with the relic photons, detected particles with the energy higher than $6 \cdot 10^{19}$eV could not be created farther than 150 Mly (Greisen-Zatsepin-Kuzmin cutoff).

And how are such energetic particles accelerated? In general, models for acceleration of cosmic rays fall into two classes: statistical or direct acceleration. In the case of statistical acceleration, the final energy is gained slowly over many decades of energy. The prototype of this kind of acceleration is the Fermi acceleration model. Fermi originally proposed that particles are accelerated by collision with the magnetic clouds in the galaxy; this picture can also be extended to acceleration by shock waves from supernovae, as well as in galactic

nuclei and radio galaxy hot spots. An advantage of statistical acceleration models is that the observed power law spectrum is achieved in a natural way. The acceleration is slow and occurs over an extended region of space.

Direct acceleration, on the other hand, assumes the existence of a strong electromagnetic field. The acceleration is fast, and is particularly applicable to systems such as pulsars with strong rotating magnetic fields producing an induced electromotive force.

There is a difference between solar rays and cosmic rays with the different origin. One way to understand this difference is to assume that cosmic rays have the same composition as solar matter at their origin. As they pass through interstellar space they interact with gas and dust particles, and the heavier nuclei spallate into lighter nuclei. On the other hand, in our solar system, there is not a possibility to accelerate solar rays into high energies and cosmic rays have higher energies of primary particles, if it reaches the Earth.

Primary cosmic rays (the particles traveling through the universe until they reach the Earth and until they interact with the atmosphere) are composed of 90% protons, 7% alpha particles, 1% nuclei (to uranium), 1% electrons and positrons and small fraction of photons.

The study of cosmic rays above a few PeV must be indirect because of the low flux involved. Experimental data comes from the detection and sampling of the shower of secondary cosmic rays (EAS - extensive air shower) produced by a cosmic ray as it interacts in the atmosphere. We study the characteristics of EAS that are important for the understanding of these experiments. EAS can be studied at the surface, beneath the Earth, and at various mountain elevations. The experimentally determined quantities are: the lateral distribution function, i.e., the particle density as a function of distance from the shower axis of the charged particles in the EAS; the lateral distribution of Cherenkov light produced by the EAS particles in the atmosphere; and the lateral distribution function of muons generated by pion and kaon decays in the EAS. The longitudinal development of the shower in the atmosphere can be determined in an indirect fashion from the study of the lateral distribution. The time distribution of particles arriving at the surface as well as the Cherenkov light pulse rise time and width also carry information about the longitudinal development of the shower. The hadronic component of the shower is concentrated very near the axis and is therefore difficult to study at high energies.

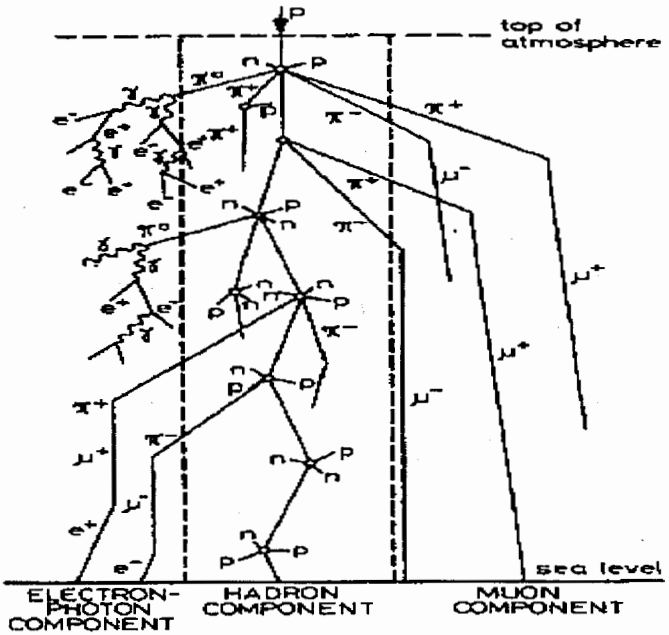

The flux of cosmic rays is depending on energy of primary particle. The flux decreases with higher energy. For example, the flux of the particles with the energy up 10^{16} eV is several particles per year on 1 m^2; one particle per year with the energy up 10^{19} eV on 1 km^2; one particle per century with the energy up 10^{20} eV on 1 km^2. There are unanswered questions at energies ~10^{15}eV and ~10^{18}eV. These regions are called "knee" and "ankle".

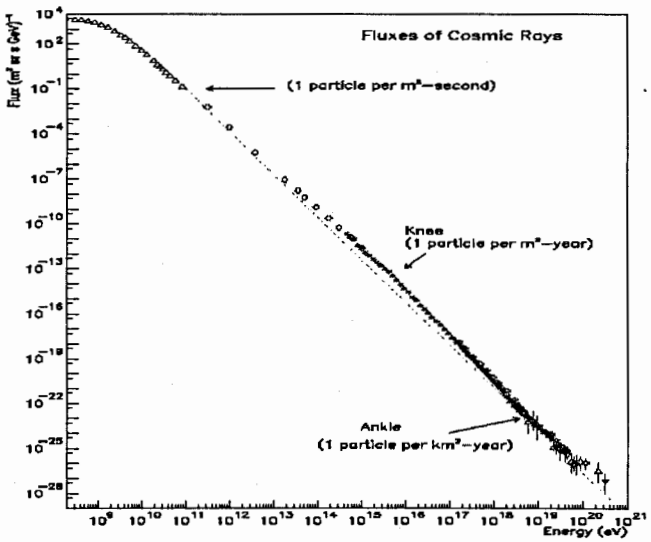

Detection of Cosmic Rays

There are some possibilities, how to detect cosmic rays – optical detection, particle detectors, large arrays, satellite experiments, underground experiments, experiments in the ice and balloon experiments.

At present, the biggest project to detection of cosmic rays is called Pierre Auger Project (Pierre Auger Observatory). It is place in West Argentina and it uses optical and large arrays detection techniques. For optical detection 24 telescops for the detection of fluorescent photons are used. The large arrays detection uses 1600 detectors (barrels with water, photomultipliers for detection of Cherenkov photons) on the total area of 3000 km^2. The distance between two neighbouring detectors is 1.5 km.

Project NALTA (North America Large-are Time coincidence Array), ALTA (Alberta Large-are Time coincidence Array) and many others similar are running now. This kind of experiments uses scintillation detectors placed at roofs of high schools (NALTA in the USA, ALTA in Canada). One scintillation detector (typical for ALTA project) is composed of 1cm thick scintillator, photomultiplier, plexiglas light guide, temperature monitor, outdoor casing and the electronics for the data acquision.

Project CZELTA

Institute of Experimental and Applied Physics (IEAP) of the Czech Technical University (CTU) in Prague realize project for the detection of high energy EAS, which will have not only scientific, but pedagogical impact, too. The aim of this project is to made relatively sparse net of detection stations, which will be placed mainly on the roofs of selected high schools in the Czech Republic. This project, which is called CZELTA (CZEch Large-are Time coincidence Array) is realized in cooperation with University of Alberta, that prepared a net of detection stations in Canada (project ALTA).

For the project CZELTA, optimal design in meaning of price and operation was chosen. Each station is composed from three scintillation detectors, which are placed into a triangle and uses the GPS signals for the time-labeling of the events. The distance between two scintillation detectors is 10 m. One scintillation detector has dimensions of 60cm x 60cm and is connected to a photomultiplayer, which detects photons originated from the passage of EAS through the scintillator. The detectors work in the coincidence – EAS must hit all three

scintilators to be stored. In such a case, the energy of primary particle is at least 10^{14} eV. For recognizing in which time the EAS was detected, GPS is used. It has accuracy of ~10 ns. From the time differences between the signal measured with the scintilators, the direction of EAS and primary particle flight can be determined.

Similar projects are running in other countries, too. In cooperation between Canada-USA a net NALTA (North America Large-scale Time coincidence Array) was made. It covers local nets in Canada and USA (ALTA, SALTA, WALTA, CHICOS CROP,...). Similar project is running in Japan (LAAS) and detection stations were made in the roofs in the high schools in Europe, too – in Sweden (SEASA), Germany (SkyView), Netherlands (HiSparc), Great Britan (Cosmic Schools) and in other countries.

The staff from IEAP CTU and from University of Alberta in 2004 installed the first station for the detection of EAS on the roof of IAAP and the project CZELTA started. To the end of the year 2005 two next stations will be build – on the roof of Silesian University in Opava and on high school in Pardubice. In the future, other stations on roofs of high schools in the Czech Republic will be installed.

Fig.1. The building of IEAP CTU with three boxes, which contain detectors

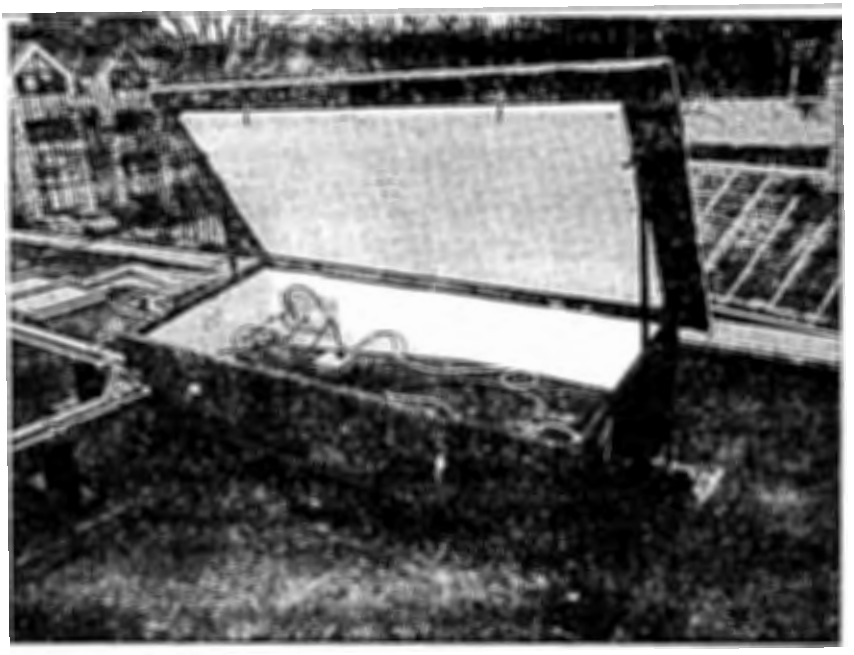

Fig.2. One of the scintillation detectors in the outer box

Fig. 3. The equipment for the data acquision

Quality Assurance in Conformal Radiotherapy

Irena Pavlíková[*,**], Ivana Horáková[*]

[*] *National Radiation Protection Institute, Šrobárova 48, 100 00 Prague 10, Czech Republic*

[**] *Faculty of Nuclear Sciences and Physical Engineering, CTU Prague, Czech Republic*

Abstract

The aim of this contribution is to inform about state-of-the-art in the field of quality assurance for conformal radiotherapy with photon beams in the Czech Republic.

Introduction

There are three workplaces in the Czech Republic, where intensity modulated radiation therapy (IMRT) is being used. This modern therapeutic technique is going to be implemented to other places. Nowadays, there are 14 linear accelerators equipped with multileaf collimator (MLC) in the Czech Republic and about half of them is convenient for IMRT. It is necessary to add tests for linear accelerators with multileaf collimator into the quality assurance (QA) programme. This extension should not be only the matter of technical assurance of the machine but it should be related to the whole chain of the dose delivery to the patient: treatment planning system, multileaf collimator (depending on the mode in which it is being used), electronic portal imaging device (EPID) etc. Clinically oriented tests, such as QA of individual treatment plans before and during treatment, are very important too. National Radiation Protection Institute (NRPI) shares these issues and also developes methods for independent checks of new items and techniques in the dose delivery chain to the patient.

Conventional versus conformal radiotherapy

In conventional radiotherapy, the treatment is provided with rectangular radiation fields and critical organs are shielded with custom beam blocks. The beam blocks are fabricated based on the patients treatment plan, using radiographic plane films or CT-scan data. Conformal radiotherapy uses multileaf collimators. MLC has movable, closely abutting leaves, arranged in pairs. By setting the leaves to a fixed shape, the fields can be shaped to conform to the tumour (this is called conformal radiotherapy). Special application is to use of the MLC to achieve beam-intensity modulation (IMRT).

Tests for MLC, IMRT and EPID

National Radiation Protection Institute has developed a questionnaire about MLC, EPID, and conformal radiation therapy. Workplaces with linear accelerators and multileaf collimator were requested to fulfill it. Results imply that 7 other workplaces propose to use IMRT in the future. It is necessary to broaden the quality assurance programme in workplaces for new techniques and equipment. In the Czech Republic, State Office for Nuclear Safety has published series of Recommendation for Quality Assurance in Radiation Therapy (among others for linear accelerators), where tests for current device are described. It is necessary to renew the Recommendation and to add tests for linear accelerators with multileaf collimator that are not described in the old version. For multileaf collimators, accuracy and reproducibility of leaf positioning should be regularly checked in conformal radiotherapy. Except these, there are other important parameters for IMRT: Dosimetric leaf separation, Average leaf transmission, Energy stability for IMRT fields, Sweeping gap for output at multiple gantry and collimator angles, Homogeneity, symmetry, and reproducibility for IMRT fields, Stability during discontinuous irradiation. Clinically oriented tests include independent MU check (measurement with ionization chamber in the tissue-equivalent phantom) and verification of relative dose distribution (film dosimetry, EPID, 2D-array of ionization chambers or semiconductor detectors). Electronic portal imaging device can be used for patient positioning accuracy verification. It is important to carry out checks of Contrast, Signal-to-noise ratio, Spatial resolution, Image quality. If EPID is used for verification of relative dose distribution, calibration must be done as well.

For QA for treatment planning systems (TPS), special phantoms were developed (Fig. 1). National Radiation Protection institute owns them and workplaces can borrow them. QUASAR Multileaf collimator beam geometry phantom serve as an instrument for verification of TPS geometric accuracy. QUASAR Body Phantom can be used for evaluation of the target volumes within the phantom inserts, CT number to relative electron density conversions and nondosimetric parameters of TPS.

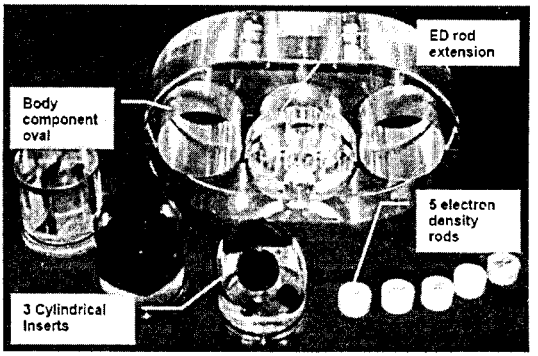

Fig. 1. QUASAR phantoms for quality assurance tests of treatment planning systems

Independent checks of therapeutic equipment

National Radiation Protection Institutes provides independent checks of therapeutic equipment, mainly newly put into the operation, as a part of the state supervision. It consists of regular TLD postal audits and on-site audits. On-site audits enable a comprehensive evaluation and comparison of geometric and dosimetric parameters of radiotherapy equipment: gamma beam therapy equipment (Co+Cs), electron accelerators (linear accelerators and betatrons), therapeutic X-ray equipment and brachytherapy afterloading equipment. They are performed after every acceptance test and then once per 5 years.

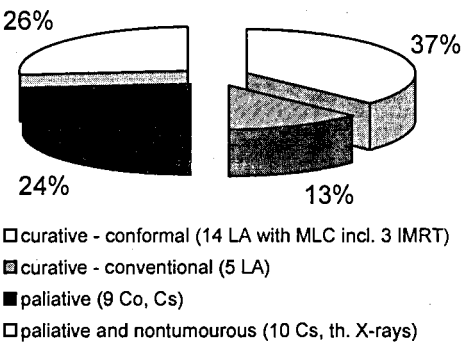

Fig. 2. Distribution of workplaces: External radiotherapy in the Czech Republic till June 2005

Measured values are compared with values given by the hospital, from treatment planning system for dosimetry parameters. If deviation exceeds the tolerance, results are carefully investigated. Remedial action or in-depth measurement by licensee can be recommended. Some components (e.g. applicators) or some practices can be prohibited.
In the end of 2003, MLC checks were added. Accuracy of leaf positioning and output factors for MLC shaped fields were tested. In the near future, methodology of on-site audit for IMRT will be finished.

Ministry of Health of the Czech Republic is acknowledged for financial support granted to the project NC7393-3/2003.

References

[1] Standards for Quality Control at Canadian Radiation Treatment Centers, Electronic Portal Imaging Devices, Canadian Association of Provincial Cancer Agencies, February 2004.

[2] M.G. Herman, et al.:, Clinical use of electronic portal imaging: Report of AAPM Radiation Therapy Committee Task Group 58. Med. Phys. 28 (5), May 2001. pp 712 – 737.

[3] Memorial Sloan Kettering Cancer Center, Department of Medical Physics: A Practical Guide to intensity-modulated radiation therapy. Medical Physics Publishing, Madison, WI, 2003.

[4] I. Pavlíková, I. Horáková, Kontrola jakosti řetězce dodání dávky při IMRT. Proceedings of Ist Conference of Society for Radiation Oncology, Biology, and Physics, Hradec Králové, February, 2005, 76 – 80.

[5] I. Pavlíková et al., Ověření nedozimetrických parametrů 3D plánovacích systémů pomocí QUASAR fantomů. Radiační onkologie (accepted for publication).

[6] G.A. Ezzel et al., Guidance document on delivery, treatment planning, and clinical implementation of IMRT: Report of the IMRT subcomittee of the AAPM radiation therapy comittee. Med. Phys. 30 (8), August 2003. pp 2089 – 2115.

[7] A. Boyer et al., Basic applications of multileaf collimators: Report of Task Group No. 50 Raiation Therapy Committee. AAPM Report No. 72. July 2001. pp 30 – 32.

Investigation of Plasma Turbulence on CASTOR Tokamak Using a Full Poloidal Ring of Magnetic and Langmuir Probes - 1st Results

Jana Sentkerestiová

Faculty of Nuclear Sciences and Physical Engineering,
Czech Technical University in Prague, Czech Republic

Supervisor: Ivan Ďuran

Institute of Plasma Physics, Association EURATOM/IPP.CR, Czech Academy of Sciences, Czech Republic

The history of the mankind is also history of everlasting searching of new resources. So far, none of the discovered source is perfect. One of the perspective future energy sources seems to be the energy gained from fusion. To initialize and preserve reactions in thermonuclear reactor, the particles need to be heated to high energies in the range of keV to overcome the repulsive Coulomb force. Another state of matter, called plasma, is created under this temperature. *Plasma is quasineutral ionized system of charged particles large enough to behave collectively.[1]* Major characteristics of the fusion plasmas except high temperature are also very high particle densities ~ 10^{20} and confinement time ~ s. Up to now the most succesfull device to achieve plasma with such parameters is tokamak. On the other hand, tokamak plasma is also the source of many instabilities that deteriorate confinement of particles and energy.

On principle, tokamak, on the Fig. 1, is a toroidal vacuum vessel with strong toroidal and poloidal magnetic field. Plasma ring is used as a 1-turn transformer secondary coil. Current circulating in the primary coil induces plasma current I_P, which produces a poloidal magnetic field B_Θ. Solenoid coils wounded around the torus create a strong toroidal magnetic field B_Φ. The resulting magnetic field is hellicaly shaped. Additional quadrupole (Helmholtz's) coils that create vertical magnetic field B_V and horizontal magnetic field B_H are important for plasma position control. Precise control of plasma position is crutial because any contact of plasma with the material wall releases a large quantity of inpurities.

Plasma position can be measured by magnetic sensors; e.g. inductive loops (coils) or Hall sensors.

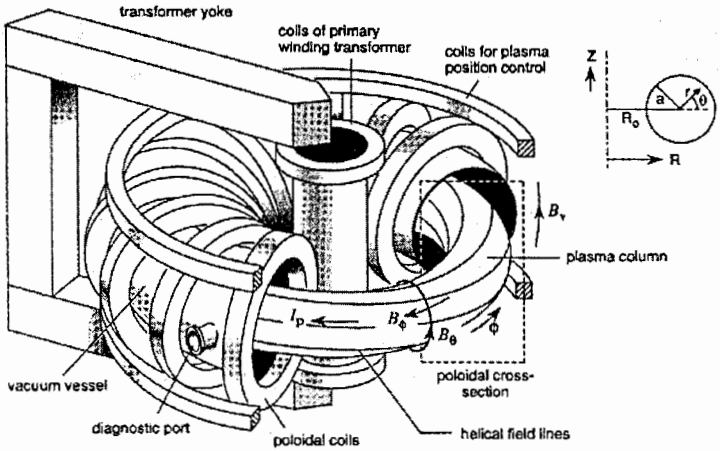

Fig. 1: Tokamak scheme

Diagnostisc based on magnetic coils are presently the standard methods for measuring the changes of magnetic field inside tokamak. According to Faraday law the voltage U is induced in coil proportionally to the time alternation of the magnetic field B passing through the coil's cross-section: $U = - d\Phi/dt = - A_{eff}\, dB/dt$; where A_{eff} is effective area of the measuring coil.

The function of the Hall sensor is based on the physical principle of the Hall effect. When a current I_H is flowing through a thin plate of conductor or semiconductor and is driven under angle α to the B, then free charge carriers drift due to Lorentz force. Across the plate a voltage difference appears, the Hall voltage $V_H = k_H I_H B \sin\alpha$.

On Castor tokamak the full poloidal ring (SK ring) of 16 coils, 16 Hall sensors and 96 Langmuir probes was constructed, see Fig. 2, to measure plasma position and properties of electrostatic and magnetic turbulencies. All sensors are uniformly distributed around the whole poloidal tokamak cross-section.

Calibration of the Hall sensors was performed. The simple calibration circuit consists of the high-frequency power source, Rogowski coil, Hall sensor and oscilloscope connected to the PC. With the help of the oscilloscope was measured the value of the magnetic field given by the Hall sensor. The effective value of the magnetic field was get from the equation $B = \mu_0 / 2\pi \; I/r$, where r is the distance between the conductor and the centre of the Hall sensor, μ_0 is the permeability of free-space and I is the current flowing through the conductor. The value of the current is gained from the known sensitivity (0.1 A/V) of Rogowski coil.

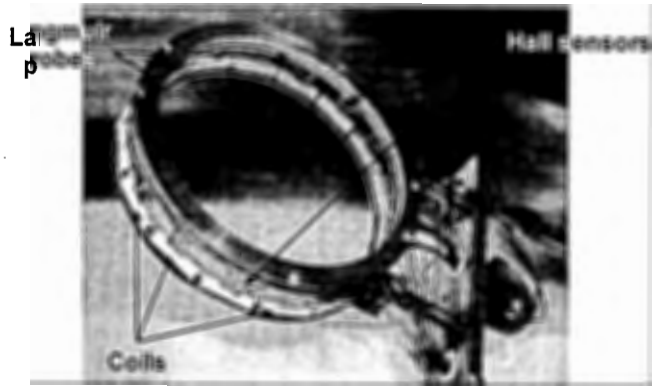

Fig. 2: Poloidal ring installed on CASTOR tokamak

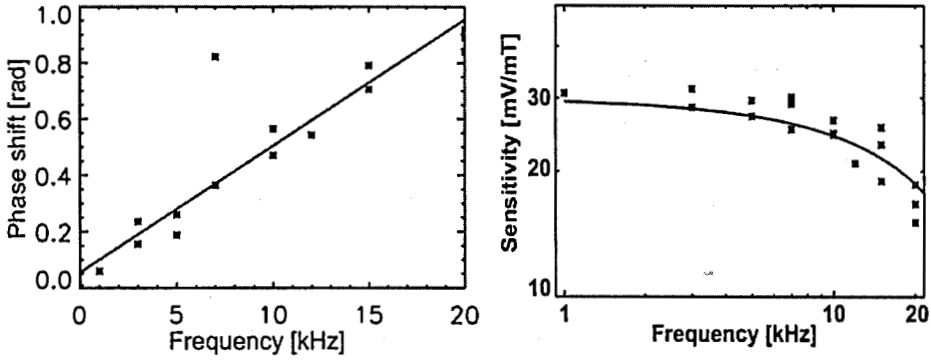

Fig. 3: Calibration results of the Hall sensors

The nominal sensitivity of the Allegro Hall sensors type A1322LUA is 31,25 mV/mT up to 30 kHz, the sensitivity from the calibration shown on the Fig. 3 is 30 mV/mT up to 10 kHz. Phase characteristics is also lineary increasing up to 10 kHz; phase shift between measured magnetic field and output signal is up to 10 kHz under 30°.

First tests of this diagnostics on Castor tokamak were performed. Basic agreement between magnetic field measurements using coils and Hall sensors was observed, see Fig. 4. But there are also seen vibrations of the coils in the later phase of the discharge. Because of that is planned to attached to the coils anti alliasing low filter at about 100 kHz frequency.

Another unexpected thing is that the Hall probes measured significant remaining magnetic field ~5 mT still 100 ms after termination of the discharge.

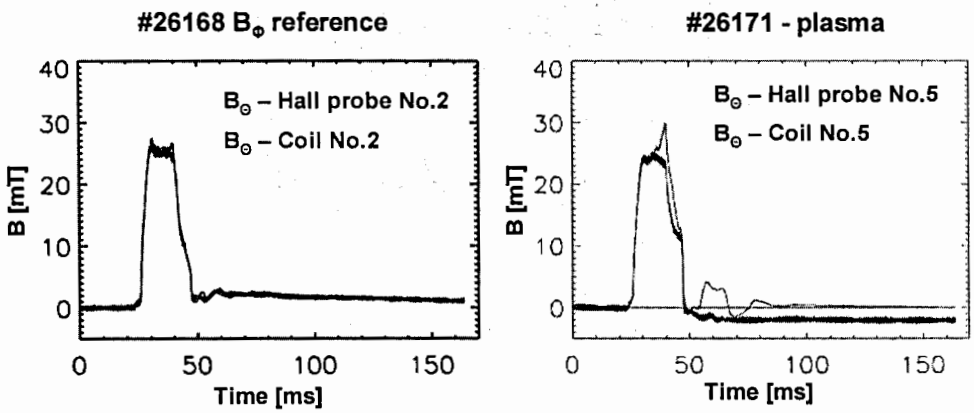

Fig. 4: Left panel - Record of B_Θ during the discharge #26168 with only toroidal field; Right panel – Record of B_Θ during the discharge #26171 with plasma

Good agreement between vertical position deduced from standard Castor diagnostics and from Hall probes mounted on SK ring was observed.

Briefly at the end, there is a lot of work before us, yet. Firstly, determination of the plasma position using the ring of the Hall sensors and coils employing the Fourier decomposition. Then study of the MHD instabilities and searching for the possible link between electrostatic and magnetic turbulancies.

References

[1] F.F. Chen: Úvod do fyziky plazmatu, Academia, Praha, 1984.

[2] Martin Valovič: Control of plasma position in the CASTOR tokamak, Czechoslovak Journal of Physics B 38, 1989.

[3] Scott Roleson: Field probes as EMI diagnostic tools, Conformity, November 2002.

Critical Comparison of Inhomogeneity Algorithms Used in Dose Calculation in Radiotherapy. Computer Simulation for NSCLC

Sebastian Szwarc[1], Tomasz Piotrowski[2]

[1] *Department of Physics, Adam Mickiewicz University Poznań,*

[2] *Greatpoland Cancer Center, Poznań*

1. Introduction

Conformal radiotherapy requires accurate dose calculation at the dose specification point and at other points in PTV (Planning target volume) and OAR (Organs At Risk). However , each patient is different and human body is unfortunately inhomogenious environment. Specialized software known as TPS (treatment planning system) provides many algorithms to calculate doses but due to tissue inhomogeneity we often get several errors in calculation. That's why additional correction algorithms are required. They convert calculations in homogenous water-like patient to the situation with inhomogeneities. Influence of inhomogeneities on the primary photon influence is generally well predicted, influence of inhomogenity on the dose delivered by scattered radiation is often aproximated in a crude way because most of correction algorithms are semi-empirical and accurate for only limited set of simplified geometries.

In our research we used Pencil Beam correction with three additional patches and we tried to answer if there are any significant differences between used methods and where these differences are located.

2. Analysis

Calculations were based on simumlation taken for female above 50 years old with none small cell loung cancer (NSCLC). Target dose was 60Gy in 30 fractions,we made simulation for 3DCRT with 3 beams irradiation on software Varion Eclipse. Short characteristic of used algorithms:

- eq TAR *(Tissed Air Ratio)*

Important feature is TAR dependance on area and depth of dose calculation, so the correction factor we may present as:

$TAR(d_{eff}, r)/TAR(d,r)$

- Batho Power Law

Improvement of eqTAR which include additional parameters such as build-up area, energy of radiation:

$$CF = k_N \cdot \sum TAR(d_m, S)^{(\mu_m - \mu_{m-1})/\mu},$$

where μ – is linear attenuation factor.

- Modified Batho

Use only „lower part" of TAR/TPR diagram. TAR/TPR value in build-up area is not so essential. The only difference is we change d_m to $d_m + D_{max}$.

The basic image used for transformation is CT scan (Fig.1). Then whole picture with initial dose calculation is exported as DIACOM file to ImageJ and converted to stack. Because rest of calculation was done in MS Excel picture had to be cuted to 250x250 pixels and rescaled as 1mm equals 1px. Each slice in stack is converted to text image and as result we get one square matrix for each correction patch filled with numbers related to percentage radiation doses. Comparing these numbers shows asymetry in dose difference diagram on the left side which means that patch curve is shifted to the right according to base curve (Fig.2), (Fig.3), (Fig.7). As we see algorithm patches represent dose calculations more accurately and somehow it may be for the patient matter of survival especialy when calculated target dose is near its critical value.

Interesting thing is that when we compare two patches curve together we see that area of huge differences dissapear. Why? It is unknown but probably is somehow related to algorithm feature.

Additional research was made to answer the questions : where these differences come from? Our hipothesys is that there is greatest probability to find differences in are of edges where the strongest gradient are located. To check it similar work was done as before with JPEG images transformed with edge detection filters (Fig.4). The results are shown on figure (5) and (6) and in fact the most probability of finding edge is in area of dose difference.

3. Conclusions

- Pencil Beam patches are quite effective in correction of dose calculation in very

inhomogenious organ e.g lungs.

- There are significant differences between patch and „none patch".
- Using patches provide more accurate dose planning.
- Base, „naked" algorithm has tendency to „get lost" in lungs.
- There is biggest probability to find dose differences in area where edges are present.
- Recent research cannot give straight answer to question: *which method is best for patient?*
- Future studies are needed to compare effectiveness of computer simulation with calculations taken from real man or phantom.

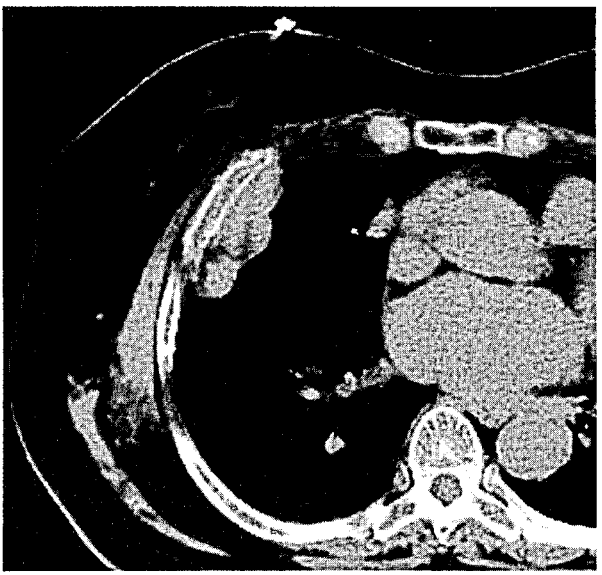

Fig. 1. CT scan of non small cell loung cancer

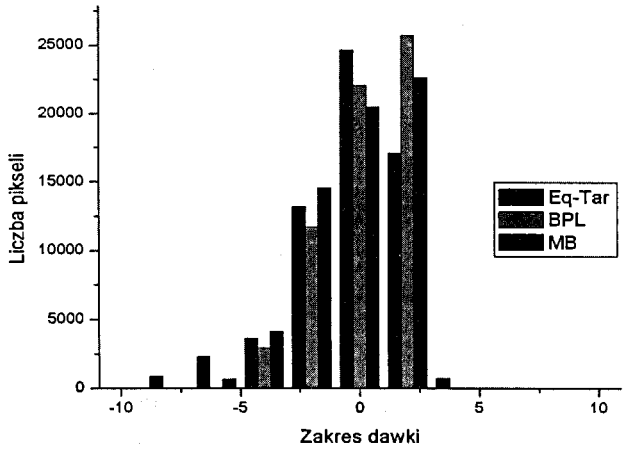

Fig. 2. Dose differences in body area (presented as number of pixels)

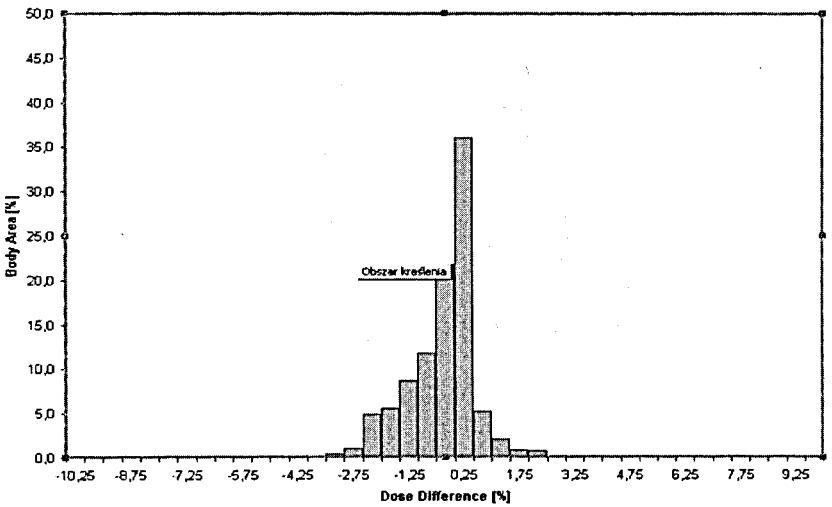

Fig. 3. Dose differences in two patches comapred together. As result area of big differences disapear

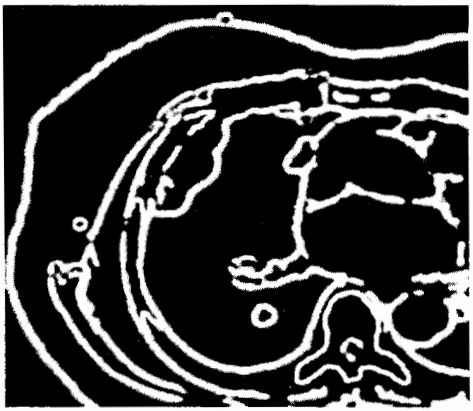

Fig. 4. Edge detection on basic CT scan

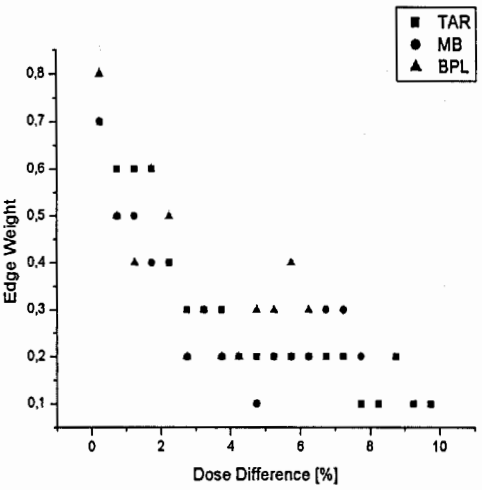

Fig. 5

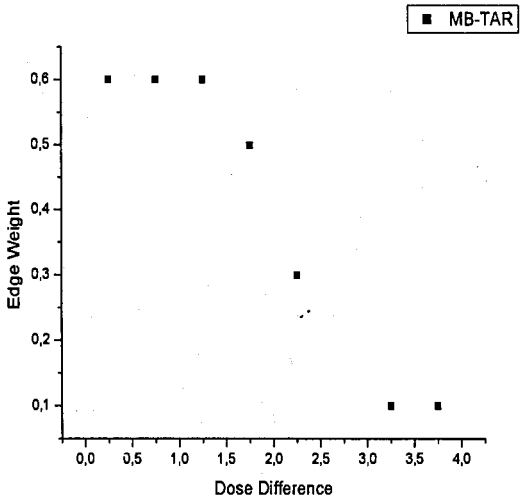

Fig 6. Comparing edge detection matrixes on two patches together. As before area of huge differences disapear

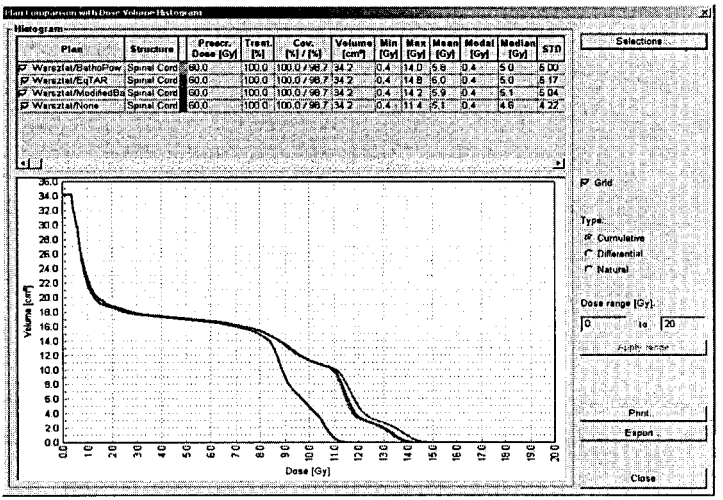

Fig. 7. Typical graph taken from Varion Eclipse. Curves representing patches algorithms are shifted to the right

Analysis of the Iron State in Iron Containing Medicines by Mössbauer Spectroscopy

P. Szalanski[1], R. Brzozowski[1], M. Pruba[1], P. Wierzbianski[1],
Yu.M. Gledenov[2], P.V. Sedyshev[2], A. Oprea[2]

[1] *University of Lodz, Poland*

[2] *Joint Institute for Nuclear Research, Dubna, Russia*

Abstract

An analysis of iron state in two commercial products of medicines containing ferrous gluconate (ASCOFER®, ESPEFA) and ferrous sulfate (HEMOFER®, GLAXOSMITHKLINE) was made by Mössbauer spectroscopy. Some ferric impurities were found in one sample.

Introduction

Iron is an essential metal and is an active site in hemoglobin, myoglobin, cytochromes, catalase, and other iron containing proteins that realize oxygen and electron transport and enzyme functions. Iron deficiency causes anemia and other pathological effects in the body and iron containing medicines, including oral iron containing vitamins and dietary supplements or injectable pharmaceuticals, are used in order to prevent and treat iron deficiency. A knowledge of the chemical states of iron in these products is very important because this may determine its effect and toxicity. For instance, ferrous compounds are more bioavailable than ferric ones for oral iron containing supplements [1,2,3].

Mössbauer spectroscopy

Mössbauer spectroscopy is a sensitive technique for determining the iron oxidation state. Numerous studies of the iron containing species demonstrated possibilities of Mössbauer spectroscopy in various fields of chemistry, biology and medicine. Mössbauer spectroscopy allows to observe the hyperfine splitting of the nuclear energy levels as well as changes of energies of the ground and excited states of Mössbauer nuclei (^{57}Fe in our case) in the absorption or emission spectrum of γ-rays. The typical Mossbauer parameters which can be obtained from Mössbauer spectra are isomer shift, IS, quadrupole splitting, QS, magnetic hyperfine field, H_{eff}, line width, Γ, intensity and area of the spectral lines [1,4].

The IS value is related to the electron density at the ^{57}Fe nucleus. The QS value is related to the electric field gradient tensor at the ^{57}Fe nucleus. The H_{eff} value is the effective magnetic field at the ^{57}Fe nucleus. The Γ value reflects information related to homogeneity of sample and dynamic processes. Intensity and absorption area are related to the mean square displacement of the ^{57}Fe nucleus and quantity of the ^{57}Fe nuclei. In general, isomer shift and quadrupole splitting give information about the iron electronic structure, valence and spin state while absorption area gives information about relative content of various iron compounds in the sample. Therefore, Mössbauer spectroscopy was applied in biomedical research, in particular for analysis of the iron containing pharmaceutical compounds [1].

A Mössbauer spectrometer has rather simple setup, and typically consists of a γ-ray source, the absorber (sample) and a detector. The source is moved relative to the absorber, shifting the energy spectrum due to the Doppler effect. For our study ^{57}Fe (14.41 keV transition, ~ 25 mCi of activity) was used. The radioactive isotope is usually incorporated in a host material such that its levels remain unsplit. The sources used for this work were ^{57}Co:Rh. All presented measurements were performed at the room temperature in transmission geometry.

Experimental results and discussion

Two different commercially available ferrous iron-containing samples were studied. The ferrous gluconate (ASCOFER®, ESPEFA) and ferrous sulfate (HEMOFER®, GLAXOSMITHKLINE) samples were used, first had the outer coating removed. Fig. 1-2 and Tab. 1 present our results. Tab. 2 presents comparison of our date and earlier measurements.

Table 1. Mössbauer parameters of ferrous gluconate (ASCOFER®, ESPEFA) and ferrous sulfate (HEMOFER®, GLAXOSMITHKLINE) samples measured at 295 K

Samples	IS [mm/s]	QS [mm/s]	Area (%)	Compound
ASCOFER®	1.23345(87)	3.1271(30)	64.39(18)	Ferrous gluconate (1)
	1.1921(44)	2.698(17)	25.48(21)	Ferrous gluconate (2)
	0.397(17)	0.803(30)	9.13(46)	Ferric high spin (3)
HEMOFER®	1.29307(56)	2.8214(11)	100	Ferrous sulfate (4)

Table 2. A comparison of the room temperature Mössbauer data

Samples	IS [mm/s]	QS [mm/s]	Reference
Ferrous gluconate			
70/20% Fe^{2+}	1.22/1.18	3.1/2.7	[5]
10% Fe^{3+}	0.45	0.7	[5]
Ferrous gluconate			
~ 65/25% Fe^{2+}	1.23/1.19	3.1/2.7	This work
~ 10% Fe^{3+}	0.40	0.8	This work
Ferrous sulfate	1.26	2.69	[5]
Ferrous sulfate	1.29	2.82	This work

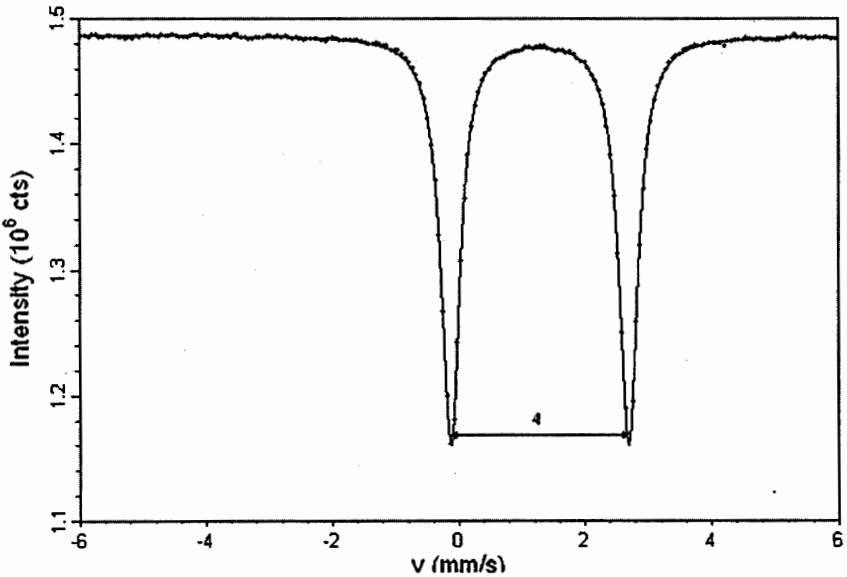

Fig. 1. Mössbauer spectrum of ferrous gluconate (ASCOFER®, ESPEFA). Components (1) and (2) are ferrous gluconate compounds, component (3) is ferric compound (T=295 K)

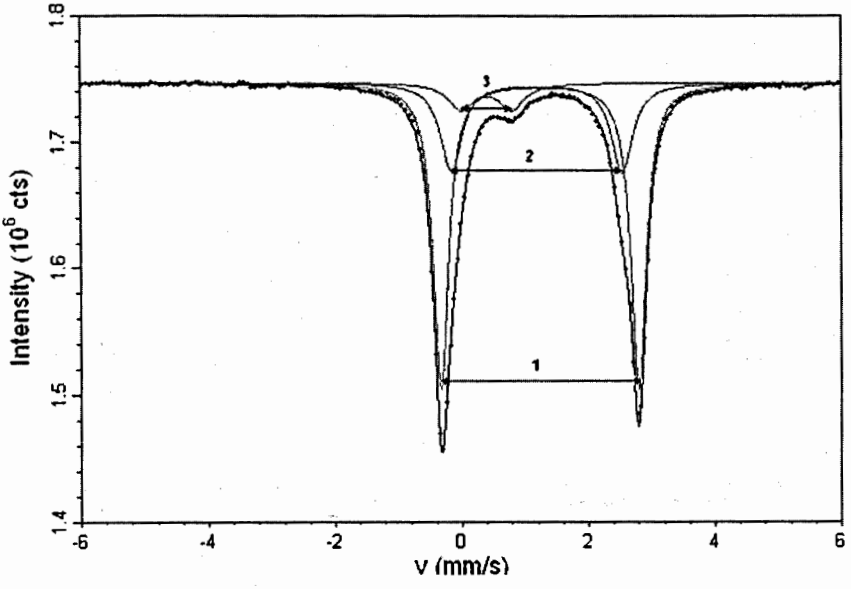

Fig. 2. Mössbauer spectrum of ferrous sulfate (HEMOFER®, GLAXOSMITHKLINE). Component (1) is ferrous sulfate compound (T=295 K)

Authors observed ~ 9% of ferric compounds in the sample containing ferrous gluconate that they attributed to ferric gluconate. Up to now we didn't received technical specification from manufacturer, but on the other hand the presence of ferric iron was not be higher than 2% according to international requirements. Thus, Mossbauer spectroscopy may be useful for the control of the iron compounds and their content in iron containing medicines.

Our date are in good agreement with the earlier measurements.

Conclusion

Measuements of the iron state in iron containing vitamins (ferrous sulfate, FALVIT®, JELFA and ferrous fumarate, MATERNA®, WYETH) are in progress.

Mössbauer spectroscopy demonstrates wide possibilities for analysis of the iron containing compounds, the iron electronic structure, valence and spin states and relative content of these compounds in the sample. This technique can be useful for studying various species including pharmaceutical and biological subjects and in biomedical research [6].

References

[1] M.I. Oshtrakh, O.B. Milder, V.A. Semionkin, Analysis of the iron state in iron containing vitamins and dietary supplements by Mössbauer spectroscopy, Analytica Chimica Acta, vol.506 (2004), 155-160.

[2] T. Bothwell, R. Charlton, J. Cook, C. Finch, Iron metabolism in man. Blackwell Scientific Publications, Oxford, 1979.

[3] M. Layrisse, C. Martinez-Torres, M. Renzy, I. Leets, Ferritin iron absorption in man. Blood, vol.45 (1975), 689–698.

[4] N. Greenwood, T. Gibb, Mossbauer Spectroscopy, Chapman & Hall, London, 1971.

[5] E. Coe, L. Bowen, R. Bereman, A Mössbauer and X-Ray Powder Diffraction Study of Some Ferrous Hematinics, Journal of Inorganic Biochemistry, vol.58 (1995), 291-296.

[6] M.I. Oshtrakh, Study of the relationship of small variations of the molecular structure and the iron state in iron containing proteins by Mössbauer spectroscopy: biomedical approach, Spectrochimica Acta Part A, vol.60 (2004), 217–234.

Radioisotope Diagnostics in Vitro – Radioimmunoassay Reactions

Ewa Szykowna

Faculty of Physics and Applied Computer Science

AGH University of Science and Technology,Cracow, Poland

Introduction

Radioimmunoassay is an in vitro measurement technique making use of specifity of the antigen-antibody reaction. It detects pathogens or signs of infection from blood, urine or tissue samples using radioactively labeled compounds.

Every substance inducing reaction of the organism's immune system is called antigen. Once an invading agent (such as for example virus, bacteria, toxicant) is recognized by the immune system as foreign the white blood cells called lymphocytes start producing antibodies against it. Antibodies bind antigens in order to neutralize them. There are two kinds of antibodies: *policlonal* (which can bind few kinds of antigens) and *monoclonal*. Monoclonal antibodies react specifically with antigens, which means that only one definite type of antigen can be attached to given antibody. This is the main idea of these methods.

Radioimmunoassay reactions may be used for:

- physical checkups
- diagnosis
- evaluation of drug potency

Classification of inspection is very wide and contains:

- biochemistry (enzyme, protein, sugar, lipid)
- immunology (tumor marker, serum protein, hormone, reagent, virus)
- hematology (computation, classification, coagulation)
- microbiology (bacteria identification, susceptibility)

The reation between antigen and antibody is held in vitro in plastic test tubes in which monoclonal antibodies are immobilized. They are monitored in quantitative manner by tagging a radioisotope to some component of the reaction.

The Competitive Radioimmunoassay (RIA) system

Limited fixed amount of antibody is immobilized in the tube. Then examined sample that contains fixed and known amount of radiolabelled antigen against which the antibody is addressed is added. Radiolabelled and not radiolabelled antigens compete for the binding places of the antibody and attache to them. After removing liquid layer from probe containing not attached antigens the activity of the attached antigens is measured. It is inversly proportional to the amount of antigens in the sample and can be calculated from the callibration curve shown below.

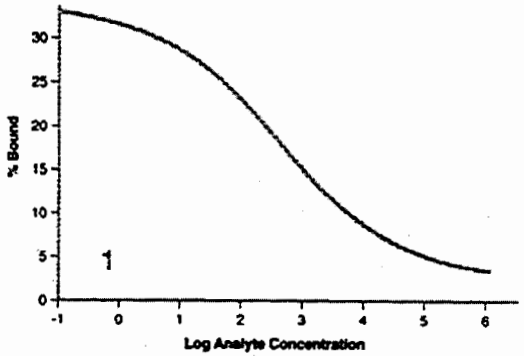

The Sandwich Immunoradiometric Assay (IRMA) system

This method is used for examinind bigger molecules. Two kinds of antibodies addessed against antigen are needed here. An access of one antibody is immobilized in the tube. Then, after adding the sample antigens attache to antibodies. After that the second, this time radiolabelled, antibody is added and it also attaches to the antigen. After removing the liquid layer from probe containing not attached radiolabelled antibodies the activity of the probe is measured. It is directly proportional to the concentration of antigen in the sample and can be calculated from tha callibration curve shown below.

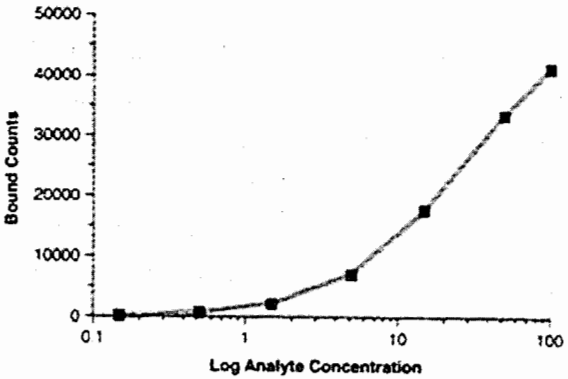

Isotopes

Isotopes that may be used for labelling are expected to have long enough half –life because changes in their concentration shouldn't influence the measurement which takes about 3 hours. They should be easily detected therefore β-emmiters like ^{3}H or ^{14}C are not very good. What is also important, radioisotopes built into the antigen or antibody can't affect stability of the molecule or it's ability to attach. Some of the radioisotopes used to labelling are shown below.

Radioisotope	Half - life	Energy	Detection method
^{3}H	12,26 years	β	Liquid scintillation
^{14}C	5730 years	β	Liquid scintillation
^{57}Co	270 days	γ	Scintillation crystal
^{75}Se	120,4days	γ	Scintillation crystal
^{125}I	**60days**	**γ**	**Scintillation crystal**
^{137}I	8days	β,γ	Scintillation crystal

Taking all the conditions into accaunt the best and mostly common radioisotope used is ^{125}I. It has sufficient long half-life, it is γ-emmiter (used with NaI scintillation crystal) and it acts well in the molecule.

Detection

Below you can see schematic block diagram illusrtating scintillation counter.

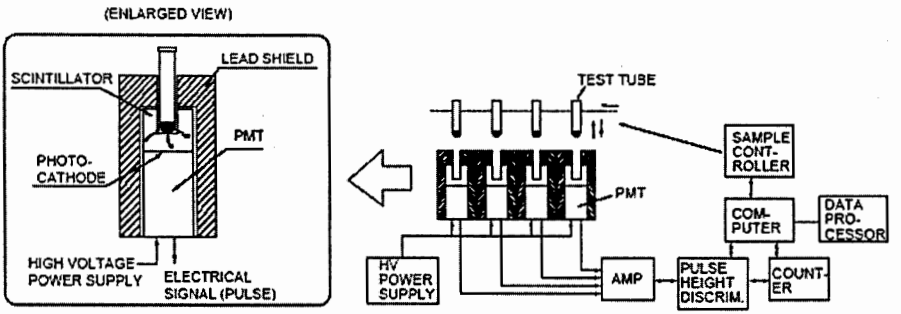

The tube is placed in a lead shield with scintillator (NaI) and photomultiplier. Photomultiplier is very important in the detection because tle level of the radiation is very low. Therefore it can't be noisy and it has to have high quantum efficiency at the peak emission wavelength which is 410nm for NaI.

Conclusions

Radioimmunoassay methods are very sensitive and convenient. Their detection limits are even pmol/l and you can get results in 3 hours, with minimal hands-on. They can indentify the carriers of infection, determine the infectivity of the disease, and predict response to treatment. Their role in the epidemiological study, management and prevention of a number of diseases such as malaria and tuberculosis is very important although they are being displaced by fluoroimmunoassays.

Aging and Biocomplexity:
Fractal Analysis in the Diabetic Retinopathy as a Model for the Study of Complex Physio - Pathological Structure

Ancuta Telcian[1], Annamaria Zaia[2]

[1] *University of Bucharest, Faculty of Physics, Romania*

[2] *Gerontologic and Geriatric Research Dept., INRCA, Ancona, Italy*

Abstract

Retinopathy represents the biggest cause of blindness in the industrialized world, with a high incidence for old people. It point's out all the consequent affection of the retina to systemic illnesses as: the diabetes (diabetic retinopathy), the hypertension (hypertensive retinopathy), other disorders of endocrine nature and local degenerative phenomenon or metabolic functional, connected with aging.

The main purpose of the project is to:

- develop a software able to qualify the abnormalities in the retinal vessel network, using highly sensitive parameters to pathology progression;
- deepen the employment of the fractal geometry within the identification and the qualification of the diabetic retinopathy;
- make an automatic method of segmentation of the vascular structure and to study the possibility to use it in substitution to the manual method;
- make a procedure for the extraction of the vascular retinal pattern and to follow the retinal vessel system modification using fractal dimension.

The current version of the method has been tested on several images differing for local retinal pattern view and ocular background.

The obtained results show that retinal vascular system is a fractal. The fractal dimension values are coherent with the analyzed figure complexity.

Introduction

Particular attention has been given to the study of two parameters: the angles between arteries and veins and fractal dimension of the vascular tree. In this study we will discus only about the second parameter. These parameters are under study and the methods developed for their evaluation use different procedures of segmentation to be applied: the construction of a

strong segmentation procedure to be used in the processing of retinal images; the segmentation method has been developed in such way that it can be also applied to retinal images acquired without fluorescence.

Retinopathy. Represents the biggest cause of blindness in the industrialized world, with a high incidence for old people. Three main types of retinal pathology have been identify (all are characterized by alteration of the vascular pattern): diabetic, hypertensive and senile.

For the prevention of loss of vision it is needed an early discovery of the retinal damage trough regular control and an qualitative evaluation of the retinal morphology.

With aging it is observed a progressive loss of the physiological abilities. To discriminate among healthy and ill subjects represents the priority objective for numerous studies influenced by the different modes of control.

In the evaluation of aging we must differentiate between physiological aging and pathological aging (a normal aging it is associated with one or more pathologies). A perfect distinction cannot be made between physiological and pathological aging.

The Diabetes. Provokes alteration of the vessels in the whole body and in particularly of the small vessels (capillary), which bring blood to the tissue and they exchange oxygen with them and nourishments. The capillaries are damaged by the interaction between the constituents of their wall and the excess of sugar in the blood.

Diabetic Retinopathy. Is an alteration of the retinal capillaries: becoming more week, they modify their morphology inducing a long time term alteration of the retinal tissue, which, not receiving enough blood and oxygen, degenerates. The organism is induced to stimulate the growth of new vessels to increase the oxygenation. The new vessels, however, are extremely fragile and subjects to repeated hemorrhages.

The Fractals. Latin "fractus"= "fragmented". The name of the fractals it is due to the technical characteristic to introduce irregularities, infinitely stratified, non observable fragmentations which can't be calculated without the computer. Fractals are geometric figures characterized by repeating themselves to the endless one of a same motive on it climbs more

and more redoubt. We find fractals in human body (neurons, nervous fibers, cardiac muscle, blood vessels and bowels) and also in nature (cauliflower, clouds, mountains and galaxy).

The fractal dimension. Is that fraction of area of a plan that is covered by a fractal curve, increased of a unity. The fractals have fractional dimension, not described, therefore from the integers 0, 1, 2, 3 to which it has gotten used us the Euclidean geometry.

Calculation of Fractal Dimension.

As example we consider a AB segment and we section it in parts with a scale factor s=1/2: we will get N=2 identical segments and similar to the original one. If we use a scale factor s=1/3, we will get N=3 identical segments similar to the original one, and so on.

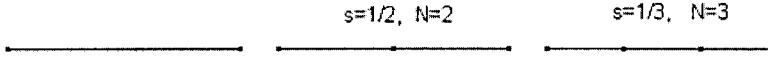

$d=-\log N/\log S$; $N=s^{-d}$; d - topological dimension of the object.

The retinograph. The retinography is performed through the retinograph, an ophthalmoscope with camera. For the visualization of the retinal capillary is used an fluorangiograph, in order to visualize the small vessels underlined through mean of contrast injected before the examination. The images are stocked in the camera and are transferred into the computer for being elaborated.

The automatic segmentation. The solution for the problem can be given as a binary image where the entrances of the corresponding matrix are fixed: 1 for the pixels that belong to the vessel and 0 for the remained pixels. To make a precise segmentation we have to consider the general characteristics of the structures that must be recovered:

Properties of the retinal vessels structure: a) every vessel almost has a continuous linear form; b) every vessel has a Gaussian form along the direction of the "cross-section"; c) the various vessels are connected in a network similar to a 'tree'.

Properties for the noise: 1) white noise of low intensity due to the process of acquisition; 2) ample zones with very different illumination; 3) small zones with non-linear properties.

The procedure of segmentation is based on:

Filtering phase. For the intensification of the objects characterized by the properties a), b) and for the attenuation of the objects that have the properties 1), 3).

Binary phase. It is bases on how the vascular tree it is separate from the background of the filtered image.

Connected components. The segmented image on the base of these components they have o big number of pixels that that conduced at a considerable reduction of the noise in the segmented images.

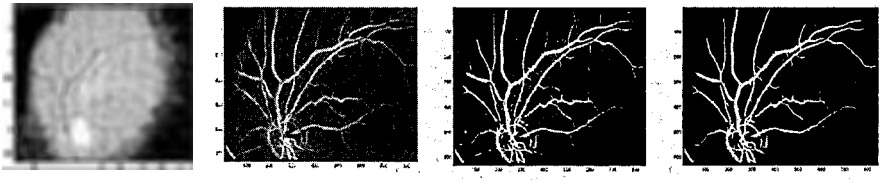

(a) (b) (c) (d)

Fig.1. Example of results of the procedure of segmentation: (a) an retinal colour image; (b) the filtered image obtained from the image (a) using sigma =3; (c) the binary image obtained from the image (b) with tau1 =0.01; (d) the segmented image obtained from the image (c) with tau2=500

We use three important parameters: sigma, tau1, tau2. Sigma characterised the length and the dependence of profile mentioned at point b) and tau1, tau2 represents the threshold (they can reduce or increase the noise). Using a large value for sigma we obtain a considerable smoothing effect and a significant enhancement of large vessels while thin ones are attenuated. Using a small value for sigma we obtain a significant enhancement of thin vessels while large ones can be damaged, and the global noise reduction is usually modest. Sigma is large when it's value is approximately equal to the half width of large vessels in the considered image and it is small when it's value is approximately equal to the half width of the thin capillaries in the considered image.

For this reason we have made some attempts to find the best combination of these parameters and to get am image with a good description of the whole vascular network, from the greatest vessels to the capillary.

The manual segmentation. Is made using the drawing pad.

The results of manual and automatic segmentation. The retinographic colour images (632 lines, 843 columns and with 256 levels of colour in every RGB channel). The images taken into account differ from the view of retinal network, in particularly we considere images with, optic disk and images with central or peripheral retina zones. Moreover, we also consider images with a different background.

Image 194

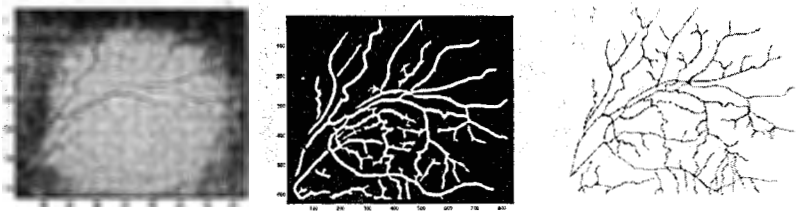

(a) *(b)* *(c)*

Fig.2. Example of results of the procedure of segmentation: (a) an retinal colour image; (b) automatic segmented image; (c) manual segmented image

The fractal analysis of the retinal vascular vessels. The calculation of the fractal dimension has been applied to the manual segmented images. For the estimation of fractal dimension it was tuned the Box Counting method implemented in Mat Lab.

Box Counting Method. It counts every box that contains at least a pixel of the skeleton of the vessels, departing from the smallest network (a pixel) and increasing to almost all the pattern. We put the results in a double logarithm graph having in ordered the logarithm of the number N (ε) of containing boxes at least a pixel of the figure and on the abscissa the logarithm of the length (ε), always in pixel, of the side of the box. The figure that is obtained is represented in central part by a straight line, whose inclination (negative) represents the value of the fractal dimension with changed of sign.

Fractal dimension of the vascular structure. The values of fractal dimension obtained from the fractal analysis of the isolated vascular structures with the method of the manual

segmentation. A very reduced value of the fractal dimension it shows a partial regression of the vessels and a very raised value of the fractal dimension - new vessels.

The values of fractal dimension obtained from the fractal analysis of isolatet vascular structures with the manual segmentation method:

Immagine	Fracttal Dimension DF
IMMAGINE 2	1.4291
IMMAGINE 10	1.3413
IMMAGINE 62	1.4298
IMMAGINE 194	1.3905

Conclusions

The obtained results show that retinal vascular system is an fractal.

The obtained value for the fractal dimension suggests that the applied method is good (valid).

The fractal dimension values are coherent with the analysed figure complexity.

For an evident ramification we have bigger value of the fractal dimension.

For a simple ramification we have a smaller value of the fractal dimension.

Perspectives

The improvement of the digital image acquisition and filtering techniques.

The improvement of the contrast and the best definition of the borders.

We must work at grey levels (the existence of another structure characterised by the same variation of the grey levels – microaneurisms).

The work time must be reduced (it is an important factor):

- Cleaning of the image 30 minutes;
- Filters 30 minutes.

The implementation of an algorithm able to distinguish between the micro aneurisms and blood vessels.

References

[1] T.J. Beckman, Regular screening in type 2 diabetes. A mnemonic approach for improving compliance, detecting complications. Postgrad Med. 2004. Apr;115(4):19-20, 23-7.

[2] S. Chaudhuri, S. Chatterjee, N. Katz, M. Nelson, M. Goldbaum, Detection of blood vessels in retinal images using two-dimensional matched filters. IEEE Trans. Med. Imag. Vol. 8, 1989: 263-269.

[3] A.L. Goldberger, D.R. Rigney, B.J. West, Chaos and fractals in human physiology. Sci Am. 1990 Feb; 262(2): 42-9.

[4] A.L. Goldberger, L.A. Amaral, J.M. Hausdorff, P.Ch. Ivanov, C.K. Peng, H.E. Stanley, Fractal dynamics in physiology: alterations with disease and aging. Proc Natl Acad Sci U S A. 2002 Feb 19; 99 Suppl 1:2466-72.

[5] G. Grassi, Diabetic retinopathy. Minerva Med. 2003 Dec; 94(6): 419-35.

[6] A. Grinvald, T. Bonhoeffer, I. Vanzetta, A. Pollack, E. Aloni, R. Ofri, D. Nelson, High-resolution functional optical imaging: from the neocortex to the eye. Ophthalmol Clin North Am. 2004 Mar;17(1):53-67.

[7] L.A. Lipsitz, A.L. Goldberger, Loss of 'complexity' and aging. Potential applications of fractals and chaos theory to senescence. JAMA. 1992 Apr 1; 267(13):1806-9.

[8] LA. Lipsitz, Physiological complexity, aging, and the path to frailty. Sci Aging Knowledge Environ. 2004 Apr 21;2004(16):pe16.

[9] A. Piantanelli, S. Serresi, G. Ricotti, G. Rossolini, A. Zaia, A. Basso, L. Piantanelli, Color-based method for fractal dimension estimation of pigmented skin lesion contour. In: Fractals in Biology and Medicine, Vol III, Mathematics and bioscience in interaction Series; Eds.: G.A. Losa, D. Merlini, T.F. Nonnenmacher, E.R. Weibel, Birkhauser Press: Basel, 2002; pp 127-136.

[10] A. Piantanelli, A. Zaia, S. Serresi, C. Pasquali, G. Ricotti, G. Rossolini, M. Balietti, A. Basso, R. Murri, Fractal dimension as a parameter for measuring complexity: an application on skin pigmented lesion images. Biogerontology 2002, 3 Supl. 1, 94-95.

[11] L. Piantanelli, G. Rossolini, A. Basso, A. Piantanelli, M. Malavolta, A. Zaia, Use of mathematical models of survivorship in the study of biomarkers of aging: the role of heterogeneity. *Mech.Ageing Dev.* 2001, 122, 1461-1475.

[12] Rishi R. Rakesh, Probal Chaudhuri, and C. A. Murthy. Thresholding in Edge Detection: A Statistical Approach. IEEE Trans. Image Proces., Vol. 13, Nr. 7, 2004: 927.

[13] S.W. Smith, Digital Signal Processing. Elsevier Science, London, 2003.

[14] A. Zaia, P. Maponi, M. Marinelli, A. Piantanelli, R. Giansanti, R. Murri, Image prcessing and retinopathy: a novel approach to computer driven tracing of vessel network. LNCS Computational Science and its Applications, vol 3045, 2004: 575-584.

Sito internet: http://www.oculistainrete.it.

Sito internet: www.oculistica.net -Corso di valutazione della Retinopatia Ipertensiva.

Short-term Instrumental Neutron Activation Analysis

Milan Tesinsky

Czech Technical University in Prague

Research project

The activation was carried out in the core of the training nuclear reactor VR-1 Sparrow at the Faculty of Nuclear Sciences and Physical Engineering of the CTU in Prague. The VR-1 Sparrow is a pool-type reactor with 36% enriched ^{235}U metal fuel in aluminium cladding. The core is equipped with a number of irradiation positions. For a short-term activation of examined samples, a vertical channel with pneumatic rabbit system was used. The transfer time of a sample from the rector core to the laboratory is approximately 3,5s. The laboratory is equipped with high-resolution gamma ray spectrometric system with a HPGe detector (FWHM 1,8 keV, relative efficiency 25%)

Experimental part of the research project is divided into three categories. First of them is devoted to non-point-configuration detector-sample, second to determination of hafnium in zircon samples and the last but not least one to neutron activation analysis of silver.

The aim of the first part is to discover the influence of non-point-configuration detector-sample and to suggest the optimal distance between the detector and the sample. Series of experiment were done in the following way. A point and an area γ-emitter were one after another given at the detector with an exact distance and the response of the detector was evaluated. The project concludes that the optimal distance is 80mm. On one hand, 80mm is enough, so the influence of the non-point-configuration is limited, and on the other hand, 80mm is not too far, so counts are not uselessly lost in the detector.

Determination of hafnium in zircon samples was based on analytical response of gamma line 214 keV of short-lived radionuclide ^{179m}Hf (18,67s). Cross section of the $^{178}Hf(n,\gamma)^{179m}Hf$ reaction is 52 barn. The optimal working regime was fixed: irradiation in the neutron flux $1x10^{9}$ $cm^{-2}s^{-1}$ during 180 s, decay time 20 s and accumulation of gamma-ray spectrum of induced activity during 90s. The abundance of hafnium in zircon was determined

by using the comparative mode (the net peak area of ^{179m}Hf in a sample is compared with the same net peak area of hafnium standard). The concentration varies from 0,2501% to 0,4756% depends on the area of origin of each single sample.

The aim of the last part was to find the best technique of neutron activation analysis of silver. The measurement was based on analytical response of gamma line 632keV of short-lived radionuclide ^{108m}Ag (2,4min) and line 657keV of short-lived radionuclide ^{110m}Ag (24,6s). The summary states that both lines can be useful for NAA, depending on working regime. While ^{108m}Ag needs higher power of the reactor and longer activation time, detecting of the ^{110m}Ag isotope is destroyed by detector dead time with such a technique.

X-Ray Fluorescence Analysis

Lenka Trnková

Czech Technical University in Prague,

Faculty of Nuclear Sciences and Physical Engineering, Department of Dosimetry and Application of Ionizing Radiation, Czech Republic

Supervisor: Tomáš Trojek

The goal of my research project is to compare characteristics of two apparatuses for X-Ray Fluorescence Analysis, which we have on our department. It involves the measurements of samples on the both apparatuses, determination detection limits, quantitative analysis of samples and comparison measured data.

X-Ray Fluorescence Analysis is an analytical surface method using ionizing radiation. It is based on excitation of characteristic X-ray. When a primary photon strikes a sample, it can be either absorbed by the atom or scattered. The process in which a photon is absorbed by the atom by transferring all of its energy to an innermost electron is called the „photoelectric effect". During this process electrons are ejected from the inner shells, creating vacancies. As the atom returns to its stable condition, electrons from the outer shells are transferred to the inner shells and in the process giving off. Energy of characteristic x-ray is the difference between the two binding energies of the corresponding shells. Energy of emitted X-ray is characteristic for each element. This property is described by Mosley law: $\sqrt{\frac{\nu}{R}} = \frac{Z - Sn}{n}$, ($\nu$ is frequency, R is Rydberg constant, Z is proton number, S_n is shield parameter and n is main quantum number.) The process of detecting and analysing the emitted x-rays is called „X-Ray Fluorescence analysis" or XRF [1].

Depending on the application, characteristic x-rays can be produced by using not only photons but also other sources like alpha particles, protons (PIXE method - particle inducted X-ray emission) or electrons (EMP method – electron micro probe). Each of them has some advantages and disadvantages. Advantages of using of charged particles are greater cross sections, so trace elements are easier identify and beam of charged elements are able to focus. The main disadvantage is a rise of braking radiation (bremsstrahlung) which represents

serious problem mainly in the case of electrons. Protons have a wider area of use, however requiment of an accelerator makes this technique less approachable. Alpha particles are not usually use in this method because of the problem with short range of these particles and with radiation danger.

There are two main ways how to detect characteristic X-rays, that is Wavelength-dispersive and Energy-dispersive method. Wavelength-dispersive is based on diffraction on crystal by Bragg law. Characteristic X-ray can either be detected by one detector (sequential method) detector or crystal is moving, or by more detectors placed around (simultaneous method). In energy-dispersive method the spectrometric detectors are used, whole spectra are obtained at once. The most used are semiconductor detectors (mainly Si(Li)), which have the biggest energy discrimination ability. Sometimes when a energy resolution is not so important and we need transferable and not so demanding device, scintillation or proportional detector is possible to use.

On department we use two devices for XRF. The first apparatus use a cathode heated X-ray tube as a source of primary radiation (Oxford instruments). It is operated at a voltage of 30kV and a maximum current of 100mA. The X-ray tube produce characteristic x-rays from molybdenum anode and bremsstrahlung. Semiconductor Si-PIN detector Amptek XR –100CR used for detection of characteristic X-rays It consist of 1mil thick Be window, active volume of 13 mm^2 of detection area and thickness of 300 μm. Its energy resolution (FWHM) is 190 eV [2]. Second apparatus applies radionuclide source, namely ^{55}Fe and ^{238}Pu as a source of primary radiation. To detection of characteristic x-ray we use Si(Li) detector SLP 06170 from ORTEC with 1mil thick Be window, with 28mm^2 detection area and a thickness of 5,67mm. The energy resolution of this detector is 170eV (measured 164eV).

For these two devices were measured different dependences and properties like: X-ray tube stability, dependence of peak area on current on X-ray tube, X-ray tube heating effect to intensity, measurement of wood (clean sample), determination of the origin of Ni peak in spectrum from apparatus with X-ray tube, measurements of radionuclides ^{238}Pu and ^{55}F, comparison spectra both apparatus. Device with X-ray tube was examined more, because it is relatively new apparatus on our department.

To evaluate a measured data program QXAS (Quantitative X-ray analysis System) is used. This program consists of many independent programs that can work separately. This program is able to do conversion of peaks areas to concentration based on Fundamental parameters method or Empirical parameters method, it allows qualitative analyses of spectra,

it calculates radiation absorption in sample with known composition, a part of program is a library of spectra which contain energies and intensities of spectral line and off course it can print and save results in different formats. For us is the most important part of QXAS algorithmic program AXIL (Analysis of X-ray spectra by Iterative Least-square fitting), which independent calculate area of selected peaks.

Limit of detection is a smallest amount of analyte that can be detected in a sample. The basic requirement of quantitative XRF analysis is firstly to prepare suitable sample. Detection limit we determine for given apparatus setup and for fixed or very close matrix. There have to be said confidence level. We can use for example the formula:

$$LLD = \frac{3 \cdot C_i}{I_p} \sqrt{\frac{I_b}{T_b}},$$

(I_b is the background count, I_p is the signal – number of counts, produced by the concentration C of the element and T_b is a measurement time) [3].

Quantitative analysis is a transfer of measured fluorescent intensities to concentration of analyte (measured data have to be corrected to background and overlap of spectral line). To make quantitative analysis is used AXIL. In this program there are more possibilities how to count the concentration of analyte.

Fundamental parameters method is one of used. The relation between the concentration c of an element x and the net count rate N of a characteristic line l can be written as $c_x = \frac{N_{xl}}{G\varepsilon(E_{xl})\sum_n I(E_n)[Q_{xl}(E_n)A'_{xl}(E_n)+H_{xl}(E_n)]}$, G is instrument constant, E_{xl} is energy of characteristic line l of element x, E_n is central energy of an energy interval n of the primary radiation, $\varepsilon(E_{xl})$ is relative detection efficiency for characteristic radiation E_{xl}, $I(E_n)$ is primary intensity at energy E_n, $A'_{xl}(E_n)$ is absorption correction factor for the line l of element x excited with E_n and $H_{xl}(E_n)$ is enhancement correction factor for the line l of element x excited with E_n.

In alpha coefficients method the following general formula describes the desired concentration as function of the measured net intensity and the concentrations of other elements in the sample $c_x = R_x \cdot \left(1 + \sum_j \alpha_{xj} \cdot c_j + \sum_j \sum_k \alpha_{xjk} \cdot c_j \cdot c_k\right)$, where c_x is analyte weight fraction (concentration), c_j, c_k is corresponding weight fraction of elements j and k, respectively, R_x is ratio of the net intensity of the analyte and the net intensity of the same line,

but from a sample consisting only of this element, α_{xj} is alpha coefficient and α_{xjk} is "crossed" alpha coefficient. The coefficient α_{xj} quantifies the effect of element j on analyte x [4].

References

[1] Musílek, Ladislav, Využití ionizujícího záření ve výzkumu, Praha, ČVUT, 1992, strany 23-39, ISBN 80-01-007669.

[2] www.amptek.com

[3] Richard M. Rousseau, Detection limit and estimate of uncertainty of analytical XRF results, The Rigaku Journal Vol. 18 No. 2 2001.

[4] QXAS manual, IAEA 1995.

Physical Bases of Using the Impulse Electrical Field for Hidden Damages of the Biological Membrane Diagnostic

E.K. Kozlova, A.P. Chernyaev, A.M. Chernish[1],
V.V. Moroz[2], M.S. Bogushevich[2], P.U. Alexeeva, U.A. Bliznuk
Physics department M.V. Lomonosov Moscow State University, Moscow, Russia
[1]*Department of Medical and Biological physics I.M. Sechenov Moscow Medical Academy, Moscow, Russia,*
[2]*Research Institute of General Intensive Care, Russian Academy of Medical Sciences*

Introduction

Pulse electric field, when acting on biological membranes can at certain conditions cause pore formation. This process is called electroporation. The purpose of membrane electroporation is to modify membranes, to change their qualities and to input various medicines and genes into the cell. Biological and artificial membranes are exposed to electroporation.

Various kinds of cells, such as erythrocytes, skeleton muscle cells, plant cells, bacteria, and especially cancer cells can be exposed to electroporation. In medical practice cardiomyocytes are exposed to electroporation during electric defibrillation. As a result of electric breakdown various biophysical phenomena occur: cell functioning modification and even cell death. The special interest is asymmetry of cell membrane electroporation from anode and cathode sides.

The combination of pulse electric field action on biological membrane and physicochemical phenomena can lead to alteration in electoporation results. Experimental facts show that not only electrical parameters of action (electric field strength, pulse duration) have impact on electroporation results but other factors capable of changing electroporation threshold as well. The electroporation threshold alteration of flat synthetic lipid bylayer under the surface-active substances is indicated. The electroporation threshold decreased under the combined action of pulse electric field and beam of accelerated electrons.

In clinical practice perflurocarbons are widely applied as blood substitute, for example perftoran. These compounds also make changes to membrane structure and alter characteristics of electroporation. Therefore studying of perftoran action on the erythrocyte membrane modified by an electric field is an actual theoretical and practical problem.

To study the action on the process of heart defibrillation by pulses of various shapes in clinical reumatology is an important practical task which is also related to the problem of alteration of electroporation characteristics. Defibrillation threshold and therefore electroporation threshold for byphasal pulse is lower than for monophasal. In number of cases during defibrillation it is necessary to use a few electric pulses. This process can be looked at as a combined action. It is indicated that the increase in number of pulses (1 sec between every two pulses) brought down the effective threshold of cell death.

The practical importance of electoporation and the diversity of biophysical phenomena during it determine the scientific interest for studying the mechanisms of membrane electric breakdown. At present there are basically two approaches of describing electroporation phenomenon: energy and kinetic.

The purpose of our experiment: 1. Getting experimental data on erythrocyte membrane electroporation under combined action of electrical pulses of various polarities on membranes with perftoran and surface-active substances. 2. Creation of mathematical model, describing the electroporation process and allowing estimating quantitatively the extent of influence of certain physicochemical factors on electroporation threshold, number of formed pores and their radii.

Materials and methods

The initial erythrocyte suspension out human blood was prepared immediately before the experiment in ratio 0,05 ml of blood in 1 ml of 0,9% sodium chloride solution. In 1 ml of initial suspension there are approximately 230 million erythrocytes and its optical density of 5 mm solution layer equals 1. It is known that suspension characteristics along with physical factors effect on it depend significantly on solution temperature. That is why there was held a series of experiments (140) in order to determine the optimal experimental method. As a result the experiments were held an hour from suspension preparation under 20^0C. The suspension was termostated in every experiment. Right before every step of the experiment the suspension was intermixed. During the experiment the initial characteristics of control suspension did not change.

Clinical defibrillator *Lifepak 7* (USA) was used as a source of pulse electric field. Field strength in the solution was determined with pulse energy set by defibrillator and solution resistance.

Exposure effect was evaluated by the rate of erythrocyte quantity decrease which was a result of hemolysis. The data for erythrocyte quantity at the certain moment in suspension was received by measuring optical density of the solution with photoelectrocolorimeter. Light wavelength is 760 nm, and for all these the permeability of light through the solution is mainly determined by scattering of light off erythrocytes. The decrease in erythrocyte quantity being a result of their hemolysis $n(t)$ led to decrease in suspension optical density $D(t)$. In the case of linear dependence: $D(t) \sim n(t)$. We well call dependence $D(t)$ - kinetic curve. The optical density of control suspension was controlled during every step of the experiment.

In our experiments we used the calibrated pulse of electric field was supplied (1700 V/cm) and kinetic curves were measured right after the exposure. There were estimated two parameters by the kinetic curve: 1) average rate of erythrocyte number decrease and 2) efficiency of pulse action.

Comparison of average rates of cell death resulting from electrical pulse and from its combined action with other factors gives information about intensity of these actions on membrane.

In experiment the suspension was exposed by both single electric pulse and two electric pulses, with second pulse having polarity in number of cases equal to the first one and in the rest of cases having it changed to the opposite. In Fig. 1 there is an outline of corresponding pulses. Symbol «1+» stands for the first pulse with positive polarity. Symbol «2+» stands for the second pulse with equal polarity and symbol «2-» stands for the second pulse with different polarity. In future perftoran will be labeled as PF, surface-active substance – as SAS, and electric field – as EF. In experiments the following combinations of pulse exposure on erythrocyte suspension were used:

1) One of (1+) and two pulses of EF (1+, 2+ or 1+, 2-),
2) PF and one pulse 1+, PF and two pulses (1+, 2+ or 1+, 2-),
3) SAS and one pulse 1+, SAS and two pulses (1+,2+ or 1+,2-).

There was conducted a total of 450 experiments under the combined action of physicochemical factors and pulse EF on erythrocyte suspension. The results of the experiments were processed with standard mathematical statistics methods.

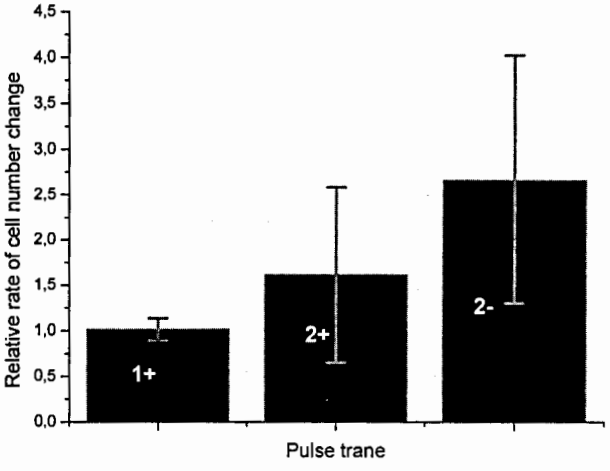

Fig. 1. Action of two electric field pulses on erythrocyte suspension.
Statistical representation of results of 95 experiments

Results

Combined action of two electric pulses on erythrocyte suspension

In Fig. 1 there are presented the results of experiments on exposure by first and second pulses on erythrocyte suspension. In every series of experiments the left column shows the rate of erythrocyte quantity decrease, which is a result of pulse 1+ exposure. This rate is assumed to be 1. We will consider that effectiveness of pulse exposure is determined by the rate of erythrocyte quantity decrease. It is shown that the effectiveness of the second pulse exposure is higher than that of the first pulse and the effectiveness of pulse 2- exposure is higher than that of pulse 2+. The combination exposure of first and second pulses results in unlinear phenomena.

Combined influence of PF, SAS and pulse EF on erythrocyte suspension

In Fig. 2 there are presented experiment results when adding PF in suspension before exposing it by pulse electric field. Kinetic curves of PF action (concentrations are 100 μl/ml of suspension and 10 μl/ml of suspension – curve 1) pulse EF 1+, pulse energy = 230 J (curve 2) and their combined exposure (curves 3 and 4).

When two pulses were acting on system "erythrocyte suspension – PF" the effectiveness of first and second pulses exposures was determined by PF concentration (Fig. 3). For concentration $C = 0$ the effectiveness of pulse 2+ exposure in these experiments

was always higher than that of pulse 1+. For pulse 2- exposure the effectiveness was even higher.

Accelerating effect of PF was expressed stronger for two pulse exposure than for single one. In Fig. 3 there is presented the data for relative change of erythrocyte number decrease rate depending on concentrations for one and two pulses. In the region of small concentration PF decelerated down the hemolysis of erythrocytes being a result of membrane electric breakdown, i.e. was slightly decreasing threshold potential. For concentration 10 μl/ml for pulse 1+ exposure decelerating effect made up about 10-12%, for two pulses 1+, 2+ exposure it made up about 30% and for pulses 1+, 2- - about 45%. This data shows the different alteration of effective electroporation threshold in system "erythrocyte suspension – PF" with various combinations of pulse polarities.

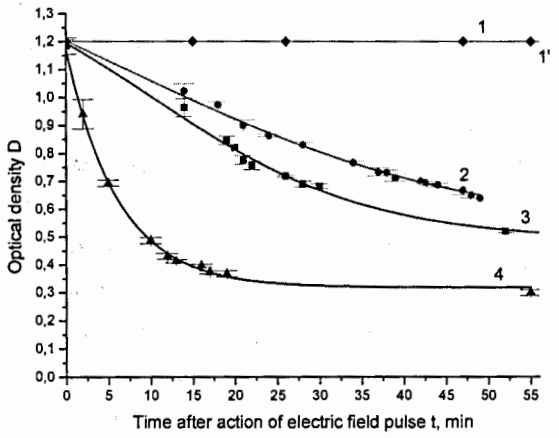

Fig. 2. Kinetic curves of erythrocyte quantity decrease under the influence on blood suspension of:
1, 1' - perftoran with concentration 10, 100 μl/ml of suspension,
2 – pulse electric field (pulse energy 230 J),
3 – combined influence of perftoran in concentration of 10 μl/ml of suspension and pulse electric field (pulse energy 230 J),
4 – combined influence of perftoran in concentration of 100 μl/ml of suspension and pulse electric field (pulse energy 230 J).

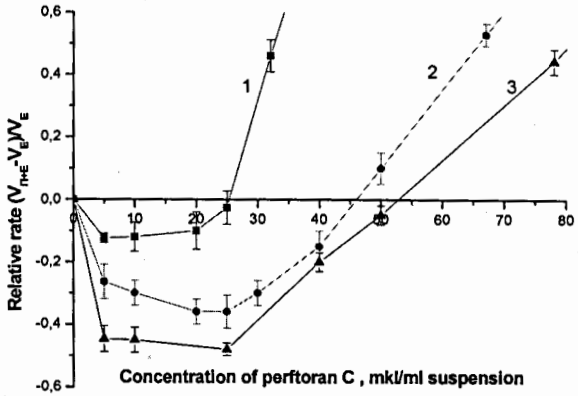

Fig. 3. The dependence of relative speed difference $(V_{P+E} - V_E)/V_E$ from the concentration of added perftoran for pulse 1+ (curve 1), for pulses 1+, 2+ (curve 2) and for pulses 1+, 2- (curve 3)

Thus it was experimentally demonstrated the following:

1) Action effectiveness of pulse 2+ on erythrocyte suspension was higher than that of pulse 1+ (in 70% of the cases). This indicates the electroporation threshold for second pulse was lower than that of the first one.

2) Action effectiveness of pulse 2- was higher than that of pulse 1+ in 92% of the cases. In the rest 8% effectiveness was the same.

3) Action effectiveness of pulses 1+, 2- was in 1,1 - 1,8 times higher then of pulses 1+,2+.

4) An addition of substances (PF C = 30...100 mcL/mL, SAS, ether C = 200 μl/ml) to the erythrocyte suspension brought down the electric breakdown threshold.

5) For small concentration perftoran increases electroporation threshold.

Discussion

Experimental data shows that the rate of cell quantity decrease during combined action of electric field and number of physicochemical factors does not equal to the sum of rates during action of each of these factors in separate. It is connected with electric breakdown conditions change. The number of pores and their radii are determined by induced transmembrane potential φ and electric breakdown threshold potential φ_{thr}.

Electric potential difference $\Delta\varphi_c$ induced on cell depends on field strength E in solution and cell radius r:

$$\Delta\varphi_c = 1{,}5Er\cos\theta\,, \qquad (1)$$

where θ is angle between vector E and radius vector of observation point on the sphere (in future we well omit symbol Δ). The electric transmembrane potential difference φ will be determined by ratio of membrane electric resistance R_m and cell solution resistance R_{sol}.

It is important to take into account that before the first electric field pulse, membrane resistance R_m is determined by initial membrane qualities and it is in its maximum in our experiments. For the second pulse (+ or -) R_m decreases because of pore formation, being a result of pulse 1+ exposure. The R_m for the second pulse will depend on quantity and radii of pores formed before its action.

Besides all that, the electric breakdown threshold φ_{thr} can change under the influence of physicochemical factors (chemical agents, ionizing radiation, pulse EF). As a rule action of these factors decreases the threshold, but in number of cases for small concentration of substances or low exposure dose there is a threshold increase. The degree of threshold change will depend on the first pulse energy and membrane qualities.

Model

We will single out membrane surface of unit area and will break down this area into N equal regions with every one of them having individual proper membrane qualities and in every one of them pore formation being possible. N is a high number. Pore formation in every region depends on proper qualities of this region. Proper qualities determine two parameters of electroporation: electric breakdown threshold potential and pore radius. It is assumed that there are at least two stages of pore formation during electroporation: pore appearance and the following increase in its size. For pore formation it is necessary that transmembrane potential exceeds threshold potential of electric breakdown in certain membrane region. In other words transmembrane potential determines on the cell level the topology of membrane surface where the appearance of electroporation is possible. Size increase of appeared pore depends on membrane condition and electric pulse duration. In the region where threshold potential is lower, the pore radius will be higher. The set of macroscopic membrane regions can be considered as Gibbs ensemble.

According this model it is possible to estimate the threshold change due to different physicochemical factors.

Depending on concentration perftoran can produce both strengthening and destructive effect on membrane without pulse electric exposure. Under the pulse electric field exposure the local PF concentration by the membrane can change. This will have impact on kinetics of pore formation during of the first pulse exposure. For small concentration dissolution of perftoroorganic compounds may strengthen the membrane by building into its defects. In this case the threshold potential increases and the pore radii decrease. This way the total pore area and hemolysis rate correspondingly might decrease. For high concentration PF building into membrane will increase the size of formed pores. This explains why hemolitic rate increases in 5-6 times (Fig. 2, 3).

The local change of PF concentration, which is a result of the first pulse exposure, will have impact on the influence of the second one. In fact, diameter of PF particle is in about 10 times higher than the membrane thickness. If (for high concentration) before the second pulse about 20-50% of membrane surface will be shut to the PF then electric field voltage in this regions will decrease in 10 times and electroporation won't occur. That is the first reason for effectiveness decrease of second pulse exposure. The other reason is reducing of induced transmembrane potential, being a result of pore formation from the first pulse.

We compare the effectiveness of pulse exposure on suspension with PF and without for various pulses (in brackets there is the decelerating effect of hemolysis). In fact, according to the model an establishing effect of PF for two pulse exposure was higher than for one. This effect is higher for the second pulse than for the first one and also it is higher for pulse 2- than for 2+.

Conclusions

In the model the possibility of electroporation of average erythrocyte (average age) is analyzed. In order to describe kinetic curves it is important to keep in mind various $\varphi_{m\,thr}$ for erythrocytes of various age: for old ones the average breakdown threshold reduces, for young ones – it is growing. Along with that in every statistical group of erythrocytes of various ages φ_{thr} *will* obey the normal distribution law. Thus the suggested approach can be implied to the whole ensemble of erythrocytes.

We are examining the spherical cell, though in reality erythrocyte has the shape of disk. In ensemble their radii obeys to the normal distribution law. It is assumed in the model that in the time between first and second pulses the cell location in the space didn't change.

This allows us to fix the erythrocyte surfaces L and R from cathode and anode side in our reasoning.

Our model allows considering the transmembrane potential distribution by cosine law, considering unequal alteration of transmembrane potential on the cell surface after the first pulse exposure and by that to calculate the pore distribution on the surfaces and pore radii more accurately.

The suggested mathematical model allowed describing the presented experimental results and numerically estimating the characteristics of erythrocyte membrane electroporation under the influence of various physicochemical factors. With the help of this model it is possible to calculate the influence degree for every factor separately at their combined action. The model allowed to numerically estimate the alteration of threshold potential for the various conditions of the experiment. It was shown that on different sides of the cell there are pores appearing of different size and their number can differ widely. The influence of perftoran of various concentrations on electroporation process has been analyzed. It was shown the strengthening effect for the low concentration of perftoran and destructive effect for high concentration. These phenomena are mathematically described. The various conditions and perspectives for the use of mathematical model in future studies were explored.

Abstracts of the lectures

The lectures in full are available at http://uc.jinr.ru/3SummerSchool/lecture.html

From Tissue Optics Study to Smart Laser Therapy

L. Avramov
Institute for Electronics of Bulgarain Academy of Sciences

Considered in detail are the basics of the laser interaction with biologic tissues. A review is given of experimental and series-produced laser systems. Featured are modern trends in laser equipment and methodology of medical applications of the laser; diagnostic and therapeutic laser applications; laser therapy computerization; telemedical networks for laser applications; and prospects for laser medicine.

Therapeutic Effects of Beta Radiation in Nuclear Medicine

M. Beran
Radiopharmaceutical Department
Nuclear Physics Institute of Czech Academy of Sciences
250 68 Rez near Prague, Czech Republic

Several β-radionuclides (^{90}Y, ^{166}Ho, ^{177}Lu, ^{169}Er, ^{186}Re) are being more and more frequently used in radiotherapy of various human diseases at present time. Their mean β-energies vary from 0.34 MeV (^{169}Er, T = 9.5 days) to 2.26 MeV (^{90}Y, T = 2.7 days) with a soft tissue range of a few millimeters (mean range 0.3 - 3.6 mm, maximum range 1 – 11 mm). These radionuclides provide curative effect through ablation (radiation necrosis) when targeted to the tissue involved (heavy arthritis/arthrosis, cancer etc.).

The radionuclides are usually incorporated within colloidal suspensions (e.g. ^{90}Y or ^{169}Er citrates, ^{166}Ho boromacroagregates) that are injected into diseased joint, or immobilized in a tumor (^{166}Ho chitosan complex) or introduced into isolated liver tumor through its nutritive capillary veins (e.g. ^{166}Ho or ^{90}Y polylactic microspheres).

Most promising therapeutic use of β-radionuclides consists in radioimmunotherapy, when selected monoclonal antibodies (Mab's) are labeled with ultrapure "carrier free" ^{90}Y radionuclide of high specific radioactivity. The labeled ^{90}Y-Mab conjugate is then targeted against appropriate antigens in the body, that are specifically expressed on the cancer cell. Even small metastases can be destroyed by this method.

Principles and some examples of β-radiotherapy are described in this lecture.

Isotopes in Medicine - Requirements, Production, Application and Future Prospective

G. Beyer
Prof.Dr.rer.nat.habil.(i.R.)
Geneva, Switzerland

A review of the history of nuclear medicine is presented. Considered are diagnostic and therapeutic uses of isotopes; nuclear medicine equipment (in particular, detectors); production of isotopes based on reactors and cyclotrons and in fission reactions caused by high-energy protons. Discussed are prospects for the application of isotopes (in particular, therapeutic uses of alpha and beta radiation and Auger electrons; positron emission tomography for in vivo dosimetry; and tissue, cell, and molecular surgery). Future demands for isotopes are estimated.

Modern X-ray Technique

N.N. Blinov
MEPhI, Moscow

Dramatic development of digital technologies in the end of 20 century resulted in new generation of x-ray units in all branches of medical radiology. The lecture is a review of digital x-ray imaging detectors and modern digital x-ray units based on these methods of x-ray detection. The concept and design of flat panels, CR systems, CCD & optics cameras, linear detector scanners and digital image intensifiers are given as well as description and analysis of their main features. Digital x-ray machines of different type produced by Russian and world industry are described.

Neutron Activation Analysis for Life Sciences

M.V. Frontasyeva
Department of Neutron Activation Analysis, Frank Laboratory of Neutron Physics, Joint Institute for Nuclear Research

In spite of competing non-nuclear analytical techniques (AAS, ICP-ES, ICP-MS, *etc*), reactor neutron activation analysis is continuing to be a most powerful multi-element analytical technique used in geosciences, life sciences and material sciences. Radioanalytical complex REGATA at the IBR-2 reactor for more than 20 years of operation has become a source of analytical data for a considerable number of international projects carried out with

specialists from JINR member- and non-member states. Supported by grants of JINR Plenipotentiaries (Bulgaria, Czech Republic, Poland, Slovakia, Romania), they all together are joined in the JINR project REGATA (2000-2004) dedicated to **air pollution studies** in the above countries and Central Russia, South Urals, Bosnia and Herzegovina, Serbia and Montenegro, Macedonia (FYROM), and Western Ukraine. The results obtained in Dubna are reported to the European Atlas of «*Atmospheric deposition of heavy metals in Europe - estimates on the basis of the analysis of mosses*» edited each 5 years under the aegis of the UNO Commission of transboundary transport of atmospheric deposition in Europe (UNECE ICP Vegetation). The next all-European moss survey will be in 2005. Several more researchers from Greece and Turkey, as well as from some Asian countries (Vietnam, Mongolia, and China) expressed their desire to joint our activity in this field. This led to a suggestion to prolong the JINR project REGATA for 2005-2007 with extension to Asian countries, besides Eastern Europe and Balkans. The other newly developing trend of applying NAA in life sciences is **food quality and safety**. IAEA Technical Cooperation (2003-2005) and IAEA Co-ordinated Research Programme (2002-2004) support these studies. The year of 2004 is the final one for our project in 5th Frame Programme of EU: «**Workplace monitoring and health-related studies** *at fertilizer plants in Russia, Poland, Romania, and Uzbekistan*». Our intense and productive cooperation since 1999 with the Georgian scientists in developing new pharmaceuticals (selenium- and chromium-contating) and sorbents of toxic elements (mercury, uranium, *etc*) based on blue-green micro-alga *Spirulina* platensis (**biotechnology**) resulted in two patents, the necessary prerequisites for production of *Spirulina derivatives* for food, perfume and medical needs.

Department of NAA serves a basis for **training young specialists** in nuclear analytical techniques. A special course «*NAA for studying the Environment*» and practicals at the radioanalytical complex REGATA are offered for graduate and undergraduate students from the universities of Dubna and JINR member-states. Every year 5-6 Master and Bachelor diploma are prepared, one Ph.D. thesis is defended (2003), and another three are in progress.

High-LET Radiation in Modern Oncology

I.A. Gulidov
Medical Radiological Research Center RAMS, Obninsk

Radiation therapy is necessary at least for 70% of oncological patients. Unfortunately, for 15-20% of them conventional low-LET radiation is uneffective. High-LET radiation has

some radiobiological advantages which allow using them effectively in modern radiation therapy. Among them: low dependence from phase of cell cycle; low dependence from oxygen tension in cells; low probability of repair of sublethal damages; small difference in radiosensitivity of different cell types.

Radiation oncologists use in clinical practice fast neutrons, thermal and epithermal neutrons, heavy ions. Physical and radiobiological features, clinical indications for use of different types of high-LET radiation, perspectives of further development of high-LET technologies, possibility of combination of high-LET and low-LET radiation will be discussed in this lecture.

Fast Light and Heavy Ions in Medicine, Materials Analysis and Materials Modifications

Heinrich Homeyer
Ion Beam Laboratory ISL, Hahn Meitner Institut Berlin

Fast ions exhibit unique features when they penetrate into matter, scattering from target nuclei, and electrons. The degree of ionization varies a lot depending on the ion charge mass and velocity. Thus, the different features can be used to cure cancer, to analyze thin or thick layers of materials, to modify materials. The different regimes will be discussed and specific examples, such as tumor treatment of ocular melanoma with fast protons, analyses of object d'art with high energy PIXE, thin layer analyses with ERDA and modification of materials due to high electronic excitations will be presented.

Treatment Planning for Radiotherapy

O. Jäkel
German Cancer Research Center (DKFZ), Dep. of Medical Physics in Radiation Oncology (E040) Heidelberg, Germany
e-mail: o.jaekel@dkfz.de

Treatment planning for radiotherapy is a complicated multi-step procedure, which involves a number of physical as well as medical aspects of radiotherapy. The overall procedure is outlined, beginning from the medical question what the aim of the treatment shall be, which treatment modality is chosen and what imaging is appropriate for this. The next steps in this procedure are then: image registration, definition of target volumes and organs at risk and the prescription of dose and definition of a fractionation scheme. After that, the

definition of treatment parameters, therapy simulation and numerical dose calculation follows. The procedure ends by the evaluation and optimization of the dose and finally the preparation of treatment including reporting and preparation of dosimetric verification measurements. The lecture will focus on modern computer assisted three-dimensional treatment planning techniques which are implemented in most commercial systems. Some aspects of recent developments in the field and their impact for treatment planning are reviewed, like the tools for stereotactic treatments, inverse treatment planning, intensity modulated radiotherapy, image guided radiotherapy and Hadron therapy.

Literature on the topic:

[1] Radiotherapy and Oncology Vol 73 (Supplement 2), 2004: "Proceedings of the Heavy charged particles in biology and medicine and ENLIGHT meetings held in Baden (2002) an Lyon (2003).

[2] Jäkel O., Schulz-Ertner D., Karger C.P., Nikoghosyan A., Debus J.: Heavy ion therapy: status and perspectives. Technology in Cancer Research and Treatment 2, 377-388, 2003.

[3] Suit H. et al.: Proton beams to replace photon beams in radical dose treatments. Acta Oncol. 2003;42(8):800-8.

Technical State of Hadron Therapy

O. Jäkel

German Cancer Research Center (DKFZ), Dep. of Medical Physics in Radiation Oncology (E040) Heidelberg, Germany

e-mail: o.jaekel@dkfz.de

In 2004 hadron therapy celebrated its 50th anniversary and between 1954 and 2004 nearly 40'000 patients were treated with protons and ~ 4500 with heavier particles (mainly helium, carbon and neon). Especially within the last decade, hadron therapy has gained increasing interest. In mid 2004, 22 proton facilities were operational and about half of all patients treated with protons received their treatment within the last 5 years. There are currently 3 facilities treating patients with carbon ions, two of them in Japan within a clinical setting and one in Germany at a heavy ion research center. In Germany, Italy and Austria new hospital based facilities for ion therapy are under construction or have been approved.

An outline of the current status of proton and ion radiotherapy is given with emphasis to the technical aspects of the respective facilities. This includes a description of the various

accelerators used for Hadron therapy, as well as the beam delivery using fixed beam lines and gantries. The design of different beam shaping systems, like the conventional used passive scattering technique and the recently introduced active scanning system for protons and ions will be described. The implications of the beam delivery system for treatment planning and dosimetry will also be discussed.

Literature on the topic:

[1] Radiotherapy and Oncology Vol 73 (Supplement 2), 2004: "Proceedings of the Heavy charged particles in biology and medicine and ENLIGHT meetings held in Baden (2002) an Lyon (2003).

[2] Jäkel O., Schulz-Ertner D., Karger C.P., Nikoghosyan A., Debus J.: Heavy ion therapy: status and perspectives. Technology in Cancer Research and Treatment 2, 377-388, 2003.

[3] Suit H. et al.: Proton beams to replace photon beams in radical dose treatments. Acta Oncol. 2003;42(8):800-8.

Modern State of Radionuclide Production and Usage in Russian Nuclear Medicine

G.Ye. Kodina

State Scientific Center - Institute Biophisics, Moscow

A systemized review is given of the current production in Russia of alpha and beta radionuclides for diagnostic and therapeutic applications. Considered are different stages of the production of specific radionuclides and special features of their application.

SPECT and NURSE-ECG Examination of the Heart Muscle

R. Krzyminiewski

A. Mickiewicz University, Poznan, Poland

The paper presents the main principles for obtaining enhanced signal resolution of standard ECG records, constructing of high-resolution vectorcardiogram and determining of activities of particular segments of the cardiac muscle. Standardized electric activities of the ventricles and septum in healthy people are given. Electric activities of particular fragments of the cardiac muscle were measured for a group of healthy and with ischaemia subjects and for people subjected to SPECT (single photon emission tomography)examination. A good

correlation was established between the results of scintigraphy examination (SPECT) and the decrease in electric activity of particular fragments of the cardiac muscle.

Mathematical Basis of Radiotherapy

P. Kukolowicz
Holycross Cancer Centre Kielce, Poland

It is shown that radiotherapy is a mixture of clinical experience and theory that is based on experience and developed by physicists and mathematicians. In radiotherapy, mathematical models should be used with great caution and only if there is no other choice.

Proton 3-D Conformal Radiotherapy and Radiosurgery of Intracranial Targets

Ye.I. Luchin
Joint Institute for Nuclear Research

Proton three-dimensional radiation therapy and radiosurgery is, at the present time, a powerful modality to decrease normal-tissue integral dose significantly while achieving a highly conformal dose distribution in the target area. Especially this is advantageous for many critically located and complex-shaped intracranial tumors and arteriovenous malformations. Purpose of this report is presentation of developed technique of 3D proton radiation therapy in Dubna and early results of clinical using.

Material and method: After difficulties during economic transformations in 1990, proton accelerator of the JINR (Phasotron) began to run more time that was enough to re-start proton therapy clinical program in Dubna. In-patient radiation therapy department has been organized in the local hospital. During 2000-2001 years one procedure room has been modified to satisfy requirements for precise stereotactic radiation treatments. Technological steps of the proton treatment are as follows. 1) Manufacturing of head immobilizing devices. 2) Imaging studies: high resolution CT with up to 99 2-mm slices on the "GE hi-speed" apparatus. MRI usually used as visually correlated image. 3) 3D treatment planning. We are using three-dimensional treatment planning system "TPN" that has been developed at the Loma Linda University Medical Center. This is early version of the "OptiRad-3D" system that is now presented at the market. The system was modified to incorporate the Dubna proton beams. Often treatment plans have been duplicated with local less sophisticated planning

system. 4) Manufacturing of beam modifying devices – individual cerrobend apertures, compensating boluses. 5) Realization of the treatment plans and beam position verification relatively to bone landmarks. Digital reconstructed radiographs (DRRs) with projection of target, isocenter and bone landmarks were calculated and printed. Alignment Rx-films were compared with DRRs during irradiation sessions. Alignment accuracy was about 1mm.

Early clinical experience: 143 patients with different intracranial targets received 3D-proton conformal radiation therapy or radiosurgery at Dubna since April 2001 till December 2004. Radiosurgery (1-3 fractions) irradiation applied for relatively small targets. Maximum total doses were 20-27 GyE. Hypofractionated regimen of 10-15 fractions has been used for larger size and critically located targets. Dose per fraction was 3-4 GyE with traditional for proton RBE=1.1. Total equivalent doses were calculated by the linear-quadratic formula and were equal to 56-60 GyE-a/b to the target margin. Some patients received conventionally fractionated (30-33 fraction) proton conformal radiation therapy.

Early clinical and imaging results demonstrated that developed technique of proton irradiation allow to deliver proton dose to the target volume precisely.

Hadron Therapy Complex at the Laboratory of Nuclear Problems, JINR

G.V. Mitsyn
Joint Institute for Nuclear Research

One of the promising ways to increase the efficiency of radiotherapy is to use new types of radiation, such as heavy charged particles and high-energy neutrons, produced at modern accelerators. These particles show pronounced advantages in the space distribution of the dose absorbed and favorable changes in some of their biological effects (relative biological efficiency and oxygen ratio).

To the date a seven-compartment Medico-technical complex based on a 660 MeV proton accelerator (Phasotron) has been constructed and now it is in operation at DLNP, JINR. It allows tumor treatment with wide and narrow beams of protons, negative pions, high-energy neutrons, and with their combinations. It is for the first time that one accelerator has provided a set like this of hadron beams for medical purposes. As a result, the most effective type of radiation can be individually selected for each patient, depending on the dose distribution features and biological characteristics of each sort of particles and on the size and clinical features of the tumor.

Unique dose delivery techniques, new methods of digital reconstructive X-ray, proton, and positron emission tomography have been developed and are used to treat patients. For the first time methods have been devised and equipment constructed for rotation irradiation of deep seated tumors and for simultaneous scanning rotation irradiation of a large target with several narrow proton beams, which ensures a high accuracy and fully computerized control over irradiation.

Physical and Technical Principles of the Stereotactic Radiosurgery and Radiotherapy with the Leksell Gamma Knife and Linear Accelerator

Jr.J. Novotny[a,b], J. Novotny[a]
[a]*Na Homolce Hospital, Prague, Czech Republic*
[b]*Charles University in Prague, First Faculty of Medicine, Institute of Biophysics and Informatics, Prague, Czech Republic*

Stereotactic radiosurgery represents a single session of a precisely focused radiation from external source to the stereotactically localized intracranial target. Stereotactic radiotherapy exploits stereotactic localization of the target but treatment is performed in fractionated scheme. Three-dimensional tomographic imaging such as computed tomography (CT) and magnetic resonance imaging (MRI) or positron emission tomography (PET) is especially essential to these activities.

To assure precise target localization a special stereotactic frame is attached by four fixation screws to the patient's skull or by a special plastic mask that is well shaped to a patient's face. This frame creates base of coordinate system that after three-dimensional brain imaging unequivocally defines intracranial target. Resulting images are transferred into treatment planning system (computer with software able to simulate irradiation of the target). Treatment planning procedure involves selection of a proper beam geometry and simulation and computation of relative dose distribution and absolute dose in terms of treatment irradiation time or monitor units. Treatment planning process is performed until the moment when simulated irradiation geometry assures sufficient target coverage and adequate saving of surrounding healthy tissue, especially important structures such as optic nerve, brain stem and etc. Then all data defining target irradiation are exported and treatment itself is controlled by computer.

The Leksell gamma knife contains altogether 201 ^{60}Co sources that are arranged in hemispherical geometry surrounding patient's head. Emitted energies of gamma photons are

1.17 MeV and 1.33 MeV, half-life of ^{60}Co is 5.26 years. All 201 beams are focused to a single point, which gives very high dose in this point and very steep dose gradient to surrounding healthy tissue. All beams are collimated by two fixed collimators. The final collimation is achieved by means of four interchangeable collimator helmets that produce 4, 8, 14 and 18 mm diameter fields at the focus. Individual plugs can stop-off beams from selected collimators if required to shield the eyes or to change the dose distribution.

Single high energy X-rays of bremsstrahlung photons are used for stereotactic radiotherapy with linear accelerator (typically 4-6 MV). Since only one beam is generated by linear accelerator different techniques must be used to simulate dose distribution that is obtained when high number of beams focused to a single point are used. These techniques include: non coplanar isocentric arcs, conformal static isocentric fields, conformal non coplanar isocentric arcs, dynamic conformal non coplanar isocentric arcs and techniques of intensity modulated radiation therapy.

Stereotactic radiosurgery or radiotherapy can be used for the treatment of following brain lesions: vascular diseases (mainly AVMs), benign tumors (mainly acoustic neuromas, meningiomas and pituitary adenomas), malignant tumors (mainly metastasis and glial tumors), functional disorders (mainly trigeminal neuralgias).

Principles and Application of Gel Dosimetry in Radiation Oncology Quality Control

Jr. J. Novotný[a,c], V. Spevácek[b], J. Hrbácek[b], P. Dvorák [b], J. Novotný[a], T. Cechák [b]

[a]*Na Homolce Hospital, Prague, Czech Republic*
[b]*CTU in Prague, Faculty of Nuclear Science and Physical Engineering, Prague, Czech Republic*
[c]*Charles University in Prague, First Faculty of Medicine, Institute of Biophysics and Informatics, Prague, Czech Republic*

Currently used techniques in radiation oncology allow tailoring of three-dimensional dose distribution to the treated target volume with high conformity and precision. By contrast there are not available dosimeters which can continuously measure three-dimensional absorbed dose distributions and which may be used for the verification of the treatment process.

The gel dosimeter and its use together with nuclear magnetic resonance (NMR) is a promising tool and attempt to satisfy the requirements of the ideal dosimetry system which

allows to measure three-dimensional dose distributions. Based on composition there are two types of such dosimeters at this time: Fricke-gel and polymer-gel dosimeter. Polymer-gel dosimeter eliminates some problems mainly related to ferric ion diffusion associated with the use of Fricke-gel and consequently is superior for clinical applications. Polymer-gel dosimeter is formed by acrylic monomers that are uniformly dispersed in a gel. Radiation-induced polymerization and cross-linking of acrylic monomers increases the NMR relaxation rates of neighboring water protons and thus NMR can be used for evaluation of three-dimensional absorbed dose distributions that are created in the polymer-gel dosimeter after its irradiation.

Several different polymer-gel dosimeter compositions have been presented. As an example typical composition of the dosimeter may be given (in weight fraction): 3% acrylic acid, 3% N,N'-methylene-bis-acrylamide, 5% gelatin, 1% sodium hydroxide and 88% distilled purified water. As an example of NMR evaluation sequence may be given protocol used in our center on Siemens EXPERT 1T scanner: multi-echo sequence with 16 echoes, TE 22.5 - 360.0 ms, TR 2000 ms, slice thickness 2 mm, FOV 255 mm, pixel size 1.0x1.0 mm^2. Many factors may influence dosimeter response. These factors include: dosimeter chemical composition and preparation history, time between dosimeter preparation and dosimeter irradiation, temperature during dosimeter irradiation, type of radiation and energy used (dosimeter energy dependence), dose rate used (dosimeter dose rate dependence), time from dosimeter irradiation to NMR evaluation, temperature during dosimeter NMR evaluation, sequence and other NMR parameters used during dosimeter NMR evaluation.

As an example of utilization of gel dosimeter in clinical practice measurements performed for Leksell gamma knife stereotactic procedures are presented. Altogether four applications of polymer-gel dosimeter were carried out:

1) head phantom with the polymer-gel dosimeter was used for verification of 4, 8, 14, 18 mm single isocenters irradiation,

2) head phantom with the polymer-gel dosimeter was used for verification of four different tumors treatment plans,

3) head phantom with the polymer-gel dosimeter was used for verification of six different eye lesion's treatment plans and

4) specially designed rat phantom filled by polymer-gel dosimeter was used for verification of experimental animal treatment plans. To compare measured and calculated dose distributions dose profiles in X, Y and Z Leksell stereotactic coordinates were calculated and compared.

Good agreement between measured and calculated dose profiles, by the Leksell GammaPlan treatment planning system, was observed. The maximum deviation in the spatial position of measured and calculated centers of dose profiles was 0.9 mm in the case of the head phantom and 1.0 mm in the case of the rat phantom. The maximum deviation in the width of the selected reference isodose of measured profiles was 3.0 mm in the case of the head phantom and 1.1 mm in the case of the rat phantom. It was demonstrated that polymer-gel dosimeter evaluated by nuclear magnetic resonance is effective tissue equivalent dosimetric tool that allows measurement of three-dimensional dose distributions with steep gradients.

The use of polymer-gel dosimeter for a verification of radiation oncology procedures has some unique advantages that can be summarized as follows: dosimeter itself is tissue equivalent, three-dimensional dose distribution can be measured, dosimeter allows simulation of the patient's procedures without any limitations.

This research project is supported by IGA MH CR grant NC 7460-3/2003.

Environment and Human Health

J. Stamenov
JNRNE BAS, Sofia 1784, boul. Tsarigradsko chaussee 72

The environment is characterized by the parameters of its components starting from aerospace, magnitosphere, atmosphere, hydrosphere, lithosphere, biosphere and finishing as well with the human society by itself. The correlations between the human health and different environmental parameters are more or less well known during the time. However, the relative high level of the information noises and the complexity of this multiparametric system make the investigations quite complicated. Nevertheless the essential improvement of the measurement accuracies of the environmental parameters, the correct studies of the correlations with different aspects of the status of the human health and its dynamic could provide reliable basis for the study of the relation human health – environment, treating it consequently as an inverse problem and trying to obtain by this way quantitative well defined estimations.

Modulation of Absorbed Dose Distributions by Magnetic Fields

S.M. Varzar, A.P. Chernyaev
Lomonosov Moscow State University Skobeltsyn Institute of Nuclear Physics

Considered is the application of the magnetic field in the proton and electron radiation therapy of oncological diseases for minimizing the radiation effect upon healthy tissues and increasing the dose absorbed by tumors.

Estimation of Effective Dose in Nuclear Medicine Diagnostic

Marta Wasilewska-Radwanska
AGH University of Science and Technology, Krakow, Poland

The principles of estimation of the effective internal dose due to radionuclides injected, ingested or inhaled will be presented. Methods of calculation will based on publications from the Medical Internal Radiation Dose (MIRD) Committee of the Society of Nuclear Medicine as well as from ICRP (International Commission on Radiation Protection) recommendations.

Biological Basis of Radiotherapy

A. Wojcik
Institute of Nuclear Chemistry and Technology, Warsaw, Poland

The lecture is concerned with the following issues: the development of a tumor from a mutated cell; the cell cycle and separation of chromatids during mitosis; the direct and indirect effect of radiation upon DNA; the fate of an irradiated cell; the chromosome radiation damage mechanism; the biological principle of radiotherapy, which is to use the difference between the tumor and healthy tissue with respect to the radiation-induced DNA damage; DNA reparation; radiation tolerance of cells irradiated during different stages of a cell cycle; the history of radiotherapy; and different schemes of radiotherapy (conventional, fractionated, and accelerated).

Lecturers and lectures at the International Summer Student School on Nuclear Physics Methods and Accelerators in Biology and Medicine 30 June – 11 July 2005, Dubna (Ratmino)

Bulgaria

L. Avramov

"From tissue optics study to smart laser therapy"
Institute for Electronics, Bulgarain Academy of Sciences

J. Stamenov

"Environment and human health"
JNRNE, Bulgarain Academy of Sciences, Sofia 1784, boul. Tsarigradsko chaussee 72

Czech Republic

M. Beran

"Therapeutic effects of beta radiation in nuclear medicine"
Radiopharmaceutical Department
Nuclear Physics Institute, Czech Academy of Sciences
250 68 Rez near Prague, Czech Republic

Jr.J. Novotny[a,b], J. Novotny[a]

"Physical and technical principles of stereotactic radiosurgery and radiotherapy with the Leksell gamma knife and linear accelerator"
[a]*Na Homolce Hospital, Prague, Czech Republic*
[b]*Charles University in Prague, First Faculty of Medicine, Institute of Biophysics and Informatics, Prague, Czech Republic*

Jr. J. Novotný[a,c], V. Spevácek[b], J. Hrbácek[b], P. Dvorák [b], J. Novotný[a], T. Cechák [b]

"Principles and application of gel dosimetry in radiation oncology quality control"

[a]*Na Homolce Hospital, Prague, Czech Republic*
[b]*CTU in Prague, Faculty of Nuclear Science and Physical Engineering, Prague, Czech Republic*
[c]*Charles University in Prague, First Faculty of Medicine, Institute of Biophysics and Informatics, Prague, Czech Republic*

Germany

H. Homeyer

"Fast light and heavy ions in medicine, materials analysis and materials modifications"
Ion Beam Laboratory ISL, Hahn – Meitner Institut, Berlin

O. Jäkel

"Treatment planning for radiotherapy" and "Technical state of hadron therapy"
German Cancer Research Center (DKFZ), Dep. of Medical Physics in Radiation Oncology (E040), Heidelberg, Germany
e-mail: o.jaekel@dkfz.de

Poland

R. Krzyminiewski

"SPECT and NURSE-ECG examination of the heart muscle"
A. Mickiewicz University, Poznan, Poland

P. Kukolowicz

"Mathematical basis of radiotherapy"
Holycross Cancer Centre, Kielce, Poland

M. Wasilewska-Radwanska

"Estimation of effective dose in nuclear medicine diagnostics"
AGH University of Science and Technology, Krakow, Poland

A. Wojcik

"Biological basis of radiotherapy"
Institute of Nuclear Chemistry and Technology, Warsaw, Poland

Russia

V.E. Balakin

"New generation of equipment for proton beam treatment of oncologic diseases"
Obninsk Branch of the Institute of Nuclear Physics,
Siberian Division of the Russian Academy of Sciences

V.N. Belyaev

"Positron annihilation and positron tomography"
MEPhI, Moscow

N.N. Blinov

"Modern X-ray technique"
MEPhI, Moscow

I.A. Gulidov

"High-LET Radiation in modern oncology."
Medical Radiological Research Center RAMS, Obninsk

G.Ye. Kodina

"Modern state of radionuclide production and usage in Russian nuclear medicine"

Federal Research Center – Institute of Biophysics, Moscow

E.K. Kozlova, P.U. Alexeeva, U.A. Bliznuk, A.M. Chernish[1]

"Physical bases of using the impulse electrical field for hidden damage diagnostics of the biological membrane"

Physics Faculty, Lomonosov Moscow State University
[1]Department of Medical and Biological Physics, I.M. Sechenov Moscow Medical Academy, Moscow, Russia

S.M. Varzar, A.P. Chernyaev

"Modulation of absorbed dose distributions by magnetic fields"
Skobeltsyn Institute of Nuclear Physics, Lomonosov Moscow State University

Switzerland

G. Bever

"Isotopes in medicine: requirements, production, application, and prospects"

Prof.Dr.rer.nat.habil.(i.R.)
University Hospital of Geneva, Cyclotron Unit, Geneva, Switzerland

JINR

V. Ye. Aleinikov

"Basic concepts of ionizing radiation dosimetry"

M.V. Frontasyeva

"Neutron activation analysis for life sciences"

Ye.I. Luchin

"Proton 3D conformal radiotherapy and radiosurgery of intracranial targets"

G.V. Mitsyn

"Hadron therapy complex at the Laboratory of Nuclear Problems, JINR"

Audience of the International Summer Student School on Nuclear Physics Methods and Accelerators in Biology and Medicine 30 June – 11 July 2005, Dubna (Ratmino)

Belarus

Aleksiayenak, Yuliya	*Sakharov International Environmental University, Minsk*
Galochkina, Olga	*Sakharov International Environmental University, Minsk*

Bulgaria

Arhangelova Nikolova-Todorova, Nina	*University of Shumen "Episkop Konstantin Preslavski"*
Borisova, Ekaterina	*Institute of Electronics, Bulgarian Academy of Sciences*
Ivanova, Galina Zhivkova	*Sofia University*

Czech Republic

Chudoba, Vratislav	*Czech Technical University, Prague*
Jadrnickova, Iva	*Czech Technical University, Prague*
Koncek, Ondrej	*Czech Technical University, Prague*
Král, Jiří	*Czech Technical University, Prague*
Maca, Pavel	*Czech Technical University, Prague*
Muzik, Jan	*Czech Technical University, Prague*
Myška, Miroslav	*Czech Technical University, Prague*
Novak, Leos	*Czech Technical University, Prague*
Nyklíček, Michal	*Czech Technical University, Prague*
Pavlikova, Irena	*Czech Technical University, Prague*
Sentkerestiova, Jana	*Czech Technical University, Prague*
Tesinsky, Milan	*Czech Technical University, Prague*
Trnkova, Lenka	*Czech Technical University, Prague*
Vins, Miroslav	*Czech Technical University, Prague*
Jaluvkova, Pavlina	*Silesian University in Opava*
Hladik, Jan	*Silesian University in Opava*
Kovacikova, Petra	*Silesian University in Opava*

Poland

Brzozowska, Kinga Maria	*Institute of Nuclear Chemistry & Technology/Dpt of Radiation Biology & Health Protection (Warszawa)*
Cybulski, Tomasz	*Krakow AGH University of Science & Technology*
Dziepak, Pawel	*Krakow AGH University of Science & Technology*
Gozdyra, Roman	*Krakow AGH University of Science & Technology*

Grzadziel, Maciej	*Krakow AGH University of Science & Technology*
Przybylowicz, Katarzyna	*Krakow AGH University of Science & Technology*
Szykowna, Ewa Karolina	*Krakow AGH University of Science & Technology*
Werschner, Dariusz	*Krakow AGH University of Science & Technology*
Jagucka, Beata Ewa	*Jagiellonian University, Krakow*
Jasinska, Justyna Patrycja	*Jagiellonian University, Krakow*
Pietrzyk, Mariusz	*Jagiellonian University, Krakow*
Siennicki, Jakub	*University of Lodz, Dpt of Nuclear Physics & Radiation Protection*
Wierzbianski, Piotr	*University of Lodz, Dpt of Nuclear Physics & Radiation Protection*
Giera, Wojciech	*AMU Poznan*
Kaszub, Wawrzyniec Emil	*AMU Poznan*
Pawlowska, Zuzanna	*AMU Poznan*
Smulski, Radosl'aw	*AMU Poznan*
Szwarc, Sebastian	*AMU Poznan*
Tomczyk, Karolina	*AMU Poznan*
Bujnarowski, Grzegorz	*University of Opole / Institute of Phyics.*
Kluza, Agnieszka Anna	*University of Opole / Institute of Physics*

Romania

Dontu, Simona	*National Institute of R&D for Optoelectronics, Bucharest / Faculty of Physics*
Telcian, Ancuta	*Bucharest University / Faculty of Physics*

Russia

Bakaev, Sergey	*Moscow Engineering Physics Institute*
Dorogush, Svetlana	*Moscow Engineering Physics Institute*
Agapov, Alexey	*JINR University Centre*
Deperas, Marta	*JINR*
Dyatlovich, Anna	*JINR*
Kolonuto, Petr	*JINR*
Mumot, Marta	*JINR*
Artamonov, Dmitry	*Moscow State University*
Bogdanova, Alexandra	*Moscow State University*
Filatov, Alexey	*Moscow State University*
Galinovskaya, Olga	*Moscow State University*
Gudkova, Olga	*Moscow State University*
Korshikova, Yulia	*Moscow State University*
Kornilov, Alexander	*Moscow State University*
Kutyakina, Vera	*Moscow State University*
Malyk, Alexandra	*Moscow State University*

Musaelian, Ivan	*Moscow State University*
Povolotskaya, Inna	*Moscow State University*
Umarova, Maria	*Moscow State University*
Voyskovich, Alexey	*Moscow State University*
Yungelson, Yevgeny	*Moscow State University*
Yastrebkova, Svetlana	*Moscow State University*
Zharova, Tatyana	*Moscow State University*
Bryzgunov, Maxim	*Novosibirsk Institute of Nuclear Physics, Siberian Branch of the Academy of Sciences*

Slovakia

Lovas, Lubomir	*Comenius University, Faculty of Mathematics, Physics & Informatics*
Lumtzerova, Eva	*Comenius University, Faculty of Mathematics, Physics & Informatics*
Nunukova, Vera	*Slovak Office for Standardization, Metrology, and Testing*

Научное издание

Nuclear Physics Methods and Accelerators in Biology and Medicine

Proceedings of the Third International Summer Student School

Ядерно-физические методы и ускорители в биологии и медицине

Труды Третьей Международной летней студенческой школы

E18-2005-195

Ответственная за подготовку сборника к печати *Е. А. Федорова.*

Фото *Ю. А. Туманова.*

Сборник отпечатан методом прямого репродуцирования с оригиналов, предоставленных оргкомитетом.

Подписано в печать 27.01.2006.
Формат 70 × 100/16. Бумага офсетная. Печать офсетная.
Усл. печ. л. 14,03. Уч.-изд. л. 11,63. Тираж 250 экз. Заказ № 55189.

Издательский отдел Объединенного института ядерных исследований
141980, г. Дубна, Московская обл., ул. Жолио-Кюри, 6.
E-mail: publish@pds.jinr.ru
www.jinr.ru/publish/